

Measuring the baryon fraction using galaxy clustering

Alex Krolewski* and Will J. Percival

Waterloo Centre for Astrophysics, University of Waterloo, Waterloo, ON N2L 3G1, Canada
Department of Physics and Astronomy, University of Waterloo, Waterloo, ON N2L 3G1, Canada and
Perimeter Institute for Theoretical Physics, 31 Caroline St. North, Waterloo, ON NL2 2Y5, Canada

(Dated: March 29, 2024)

The amplitude of the baryon signature in galaxy clustering depends on the cosmological baryon fraction. We consider two ways to isolate this signal in galaxy redshift surveys. First, we extend standard template-based Baryon Acoustic Oscillation (BAO) models to include the amplitude of the baryonic signature by splitting the transfer function into baryon and cold dark matter components with freely varying proportions. Second, we include the amplitude of the split as an extra parameter in Effective Field Theory (EFT) models of the full galaxy clustering signal. We find similar results from both approaches. For the Baryon Oscillation Spectroscopic Survey (BOSS) data we find $f_b \equiv \Omega_b/\Omega_m = 0.173 \pm 0.027$ for template fits post-reconstruction, $f_b = 0.153 \pm 0.029$ for template fits pre-reconstruction, and $f_b = 0.154 \pm 0.022$ for EFT fits, with an estimated systematic error of 0.013 for all three methods. Using reconstruction only produces a marginal improvement for these measurements. Although significantly weaker than constraints on f_b from the Cosmic Microwave Background, these measurements rely on very simple physics and, in particular, are independent of the sound horizon. In a companion paper we show how they can be used, together with Big Bang Nucleosynthesis measurements of the physical baryon density and geometrical measurements of the matter density from the Alcock-Paczynski effect, to constrain the Hubble parameter. While the constraints on H_0 based on density measurements from BOSS are relatively weak, measurements from DESI and Euclid will lead to errors on H_0 that are competitive with those from local distance ladder measurements.

I. INTRODUCTION

The flat Λ CDM model of cosmology is now constrained to such high precision [1] that it is not the values of the parameters that are of primary interest, but instead the consistency and details of the physical processes that lead to the observations. Thus, the most interesting questions in cosmology today are resolving tensions such as the Hubble tension and understanding the physics of dark matter and dark energy. The Hubble tension refers to the difference between recent measurements of the Hubble constant [2] using a local distant ladder formed from Cepheids and supernovae, which gives the measurement $H_0 = 73.04 \pm 1.04 \text{ km s}^{-1} \text{ Mpc}^{-1}$. This is in strong tension with the recent Planck measurement $H_0 = 67.37 \pm 0.54 \text{ km s}^{-1} \text{ Mpc}^{-1}$ from the Cosmic Microwave Background [1]. Likewise, the Baryon Acoustic Oscillations (BAO) standard ruler measures a low value of $H_0 = 67.35 \pm 0.97 \text{ km s}^{-1} \text{ Mpc}^{-1}$ when calibrating the sound horizon used as a standard ruler with Big Bang Nucleosynthesis (BBN) observations [3]. This difference is not currently understood: it either points to new physics, such as Early Dark Energy [4], or to an unknown systematic problem with one or more sets of data. New methods to measure the Hubble constant are important to help to distinguish between these options.

In a companion paper [5], we introduce a new method to measure the Hubble constant without including either CMB power spectra or calibrating the BAO standard

ruler with a known value of the sound horizon. This allows us to test modifications to the early expansion history such as Early Dark Energy, which change the sound horizon. The method is based on comparing the physical matter density $\Omega_m h^2$ obtained from measurements of cosmological abundances against geometrical measurements, which depend on the ratio of the matter density to the critical value Ω_m . Although the CMB provides a strong constraint on the physical density, the desire to solve the Hubble tension makes the importance of independent measurements paramount. We therefore consider measuring $\Omega_m h^2$ by combining BBN constraints on $\Omega_b h^2$ with a measurement of Ω_b/Ω_m obtained from the amplitude of baryonic features in the galaxy power spectrum. Note that we make a distinction between the BAO and the signature of baryons, which includes both the BAO and the change in shape of the power spectrum caused by the presence of baryons [6]. We use the full baryon signature to extract the baryon fraction from a galaxy redshift survey. The measurements are used in our companion paper to set constraints on the Hubble parameter.

The signature of baryons was first seen in the 2-degree Field Galaxy Redshift Survey (2dFGRS), using early data [7]. The analysis relied on using both the change in shape of the power due to baryons and the BAO, which both provide information about the baryon fraction. The BAO became clearer as more galaxy redshifts were obtained by the 2dFGRS [8] and the Sloan Digital Sky Survey (SDSS) [9]. The detection of BAO from galaxy redshift surveys passed the 5σ threshold with the Baryon Oscillation Spectroscopic Survey (BOSS) [10, 11]. For galaxy redshift surveys, the baryon signature is one of

* alex.krolewski@uwaterloo.ca

the cleanest physical signals. Traditionally (e.g. [12]), BAO observations have focused on measuring the projected BAO positions along and across the line of sight, which depend on D_H/r_d and D_M/r_d respectively, where $D_H(z) \equiv c/H(z)$; $D_M(z) \equiv (1+z)D_A(z)$ is the comoving angular diameter distance $D_M(z)$; and r_d is the comoving sound horizon at the baryon drag epoch. The sound horizon r_d has a complicated dependence on the baryon density, matter density and Hubble parameter, but it is extremely well-predicted given our knowledge of cosmological parameters and assuming the standard cosmological model. When comparing BAO at different redshifts (or to the CMB) the relative positions probe ratios of $D_A(z)$ and $H(z)$ removing the sound horizon dependence. BAO are either measured using a template fit or as a component of full model fits to the 2-point clustering signal. We now consider the extension of both methods to include measuring the baryon fraction.

The clustering of baryons and dark matter are traditionally described using transfer functions. These give the distribution of perturbations as a function of size and time, for any energy-density component in the universe. Fluctuations in the matter field can be described by the combined transfer function $T(k)$, combining baryon $T_b(k)$ and dark matter $T_c(k)$ transfer functions,

$$T(k) = \frac{\Omega_b}{\Omega_{bc}} T_b(k) + \frac{\Omega_c}{\Omega_{bc}} T_c(k), \quad (1)$$

weighted by their normalised average energy densities (where Ω_{bc} refers to the matter density excluding massive neutrinos). The dependence on the baryon fraction in Eq. 1 has a very simple physical meaning, and offers the chance to measure this quantity without relying on complicated physical models. Performing a full fit with galaxy clustering data and extracting the constraint on Ω_b/Ω_m from all physical processes that contribute to the clustering signal, would potentially bring in information from the location of the BAO feature, complicating the interpretation of the measurement. We instead parameterise the balance between transfer functions, isolating the split between energy-density components in this parameter, and marginalize over all other parameters required to model the power spectrum or correlation function.

The transfer functions are initially very different for baryons and dark matter, a consequence of the different behaviour before photon decoupling. The post-decoupling baryon transfer function can be modelled

$$T_b(k) = \alpha_b \frac{\sin(kr_d)}{kr_d} \mathcal{D}(\parallel), \quad (2)$$

in the limit $kr_d \gg 1$ [6]. $\mathcal{D}(\parallel)$ represents the effects of Silk damping, and α_b is a suppression factor arising from the adiabatic decrease in the sound speed, and the growth suppression between matter-radiation equality and the drag epoch before velocities decay due to cosmological expansion (see equations 14 & 15 in [6]). For cosmological models close to the Planck best-fit, α_b is primarily

determined by the baryon fraction, though with a small secondary dependence on $\Omega_m h^2$. We discuss this further in Section IV A 2.

Crucially, in this paper we find that the amplitude of the baryon signature can be recovered independently of the presence of Early Dark Energy. Fig. 1 shows this to be the case using phenomenological measurements from the linear power spectrum. Following Fig. 5 in [6], we measure the fractional change in $P(k)/P_{\text{sm}}(k)$ between the first BAO peak and first trough as a function of the baryon fraction and $\Omega_m h^2$. If Early Dark Energy were the correct model of the universe, the contours of peak-trough height would be shifted (solid to dashed contours in Fig. 1). However, if we analyze the data with a Λ CDM model (which has a different best-fit $\Omega_m h^2$ from EDE) the observed peak-trough height maps to the correct baryon fraction for the EDE model. This is clearly shown in the right panel, where we vary $\Omega_b h^2$ at fixed $\Omega_{\text{cdm}} h^2$ and h , and show that the relationship between the baryon fraction and BAO peak-trough height is the same in either Λ CDM or EDE.

As the Universe evolves, the baryon and dark matter fields both grow through gravity driven by the combined density of both components. While the transfer functions thus become more similar, the overall growth is scale-independent in the matter dominated regime without baryon velocity effects, so only the amplitude of the summed transfer function $T(k)$ changes, not the shape. The baryon fraction is expected to be constant in redshift in standard models. Thus, when we fit $T(k)$ to data to measure the relative amplitude of baryonic and dark matter components, there is a choice in the $T_b(k)$ & $T_c(k)$ we use in the fit: we can select these at any redshift, adjusting the amplitude, and still use Eq. 1. We therefore have an opportunity to optimise their difference and increase the fidelity with which we can measure Ω_b/Ω_m . Most of the signal constraining Ω_b/Ω_m will come from the amplitude of the BAO in the combined transfer function, which enter through $T_b(k)$, compared to the smooth broad-band signal that predominantly comes from the CDM transfer function $T_c(k)$. However, there is also some information from the different broad-band shapes of $T_b(k)$ & $T_c(k)$. This is discussed further in Section II A. In general, we measure f_b with larger statistical and systematic errors than the BAO position. The systematic errors arise because of degeneracies with other features in the transfer functions controlled by nuisance parameters with poorly-constrained posteriors. They will all be reduced by the inclusion of better data.

To compare with the measurement of the physical matter density, we also need a geometrical measurement of Ω_m . This can be obtained from the Alcock-Paczynski effect (AP; [13]). Consider a spherical object (or scale) that is sufficiently large that it expands with the expansion of the Universe. Along the line of sight to the object, we will measure a change in redshift Δz from front to back, and across the line-of-sight we will measure an angular extent $\Delta\theta$. If we know that the object is spherical (or

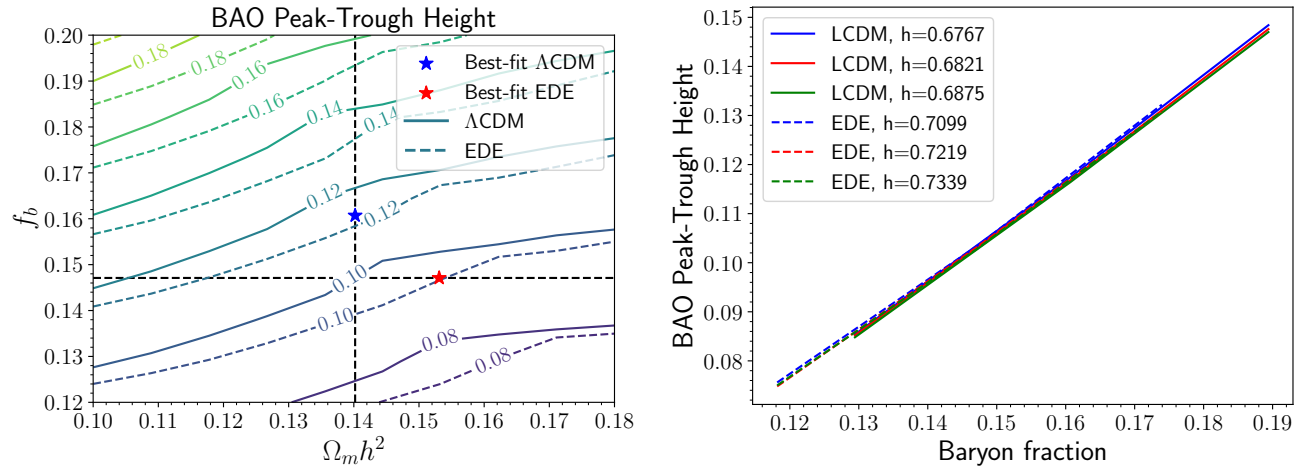


FIG. 1. The BAO amplitude can measure the baryon fraction independent of whether the true underlying cosmology is Λ CDM or Early Dark Energy. *Left*: Contours of the fractional first peak-to-trough height in the linear power spectrum as a function of the baryon fraction f_b and the matter density $\Omega_m h^2$ (following Fig. 5 in [6]), in both a Λ CDM (solid) and Early Dark Energy (dashed) cosmology. If the universe truly follows an EDE cosmology (red star, best-fit from [4]), we should expect a peak-to-trough height of 0.10. In our method, we fit the data with a Λ CDM model with Λ CDM parameters (best fit from [4]) shown with the blue star. The value of f_b that we would infer from our method is the intersection of the best-fit Λ CDM $\Omega_m h^2$ (vertical line) and the Λ CDM (solid) 0.10 contour. This lies exactly at the correct f_b of the EDE model (horizontal dashed line). *Right*: A further demonstration of this point, plotting the baryon fraction vs. the peak-trough height for Λ CDM and EDE cosmologies with a variety of different values of H_0 around the best-fit. Again the relationship is nearly identical, showing that the baryon fraction can be measured independently of whether Λ CDM or EDE is the correct cosmological model at early times.

isotropic), we can translate these measurements into a cosmological constraint on D_H/D_M . Such a ratio of distances does not depend on the Hubble parameter, and for a flat Λ CDM model only depends on Ω_m . We can use the BAO feature to provide the isotropic "object", or we can also use voids [14]. In general, these measurement will be correlated with the constraints on f_b , and so we will have to measure and fit these simultaneously.

After introducing the method, we fit to data from the Sloan Digital Sky Survey (SDSS; [15]) Baryon Oscillation Spectroscopic Survey (BOSS; [16]). We consider fits to the data both with and without reconstruction [17], a technique designed to sharpen the BAO features by moving overdensity in such a way as to remove non-linear motions. Using the correlation functions presented in [18], we are able to extract the baryon fraction with a systematic error that is larger than the BAO position, but still well within 1σ .

We discuss extracting the amplitude of the baryonic signature in Section II, introducing new methods for full fits and template fits in Sections II B & II C respectively. These are tested against mock catalogues in Section III with the results and a comparison of methods presented in Section IV. In Section V, we describe the galaxy redshift surveys we use and present the results of the fits. Finally we present our conclusions in Section VI.

II. MEASURING THE BARYON FRACTION

A. A parameterized power spectrum

In order to measure the baryon fraction we need to make some changes to the standard model for the power spectrum. We isolate the relative contributions of the component transfer functions by including an extra parameter γ_B designed to mimic the effect of changing the baryon fraction when combining baryon and dark matter transfer functions. γ_B enters into the linear power spectrum

$$P_{\text{lin},\gamma}(k) = A_s \left(\frac{kh}{0.05} \right)^{n_s-1} h^4 \frac{k}{2\pi^2} [\gamma_B T'_b(k) + (1 - \gamma_B) T'_c(k)]^2 D(z)^2. \quad (3)$$

where both k and the linear power spectrum are in units of $h \text{ Mpc}^{-1}$ and $h^{-3} \text{ Mpc}^3$, respectively.

We need to determine the functions T'_b and T'_c to use in this expression with care. For example, let's suppose that we model T'_b and T'_c as the low redshift baryon and CDM transfer functions that one would obtain from a Boltzmann code such as CLASS [19] or CAMB [20, 21]. The transfer functions include the growth of perturbations, which means that the BAO oscillations in $T'_b(z=0)$ are suppressed. They are also introduced into the CDM transfer function due to the growth of structure, as the

growth depends on both components. Thus, the low redshift baryon and CDM transfer functions are nearly identical, and will not work to split the baryonic and dark matter features. We instead need to use functions that maximise the differential features between the two transfer functions that can be used to measure the relative components, such as only having the oscillations in one of the terms.

We cannot simply use the transfer functions at very high redshift, for example at the drag epoch $z_d \sim 1060$, because the acoustic oscillations do not immediately stop travelling at z_d , but rather keep propagating outwards until $z \sim 600$, though at much reduced speed.¹ Consequently, at this epoch, the BAO have a different shape and position than at the lower redshifts that we want to model. An alternative approach would be to use the transfer functions at $z \sim 600$ when the baryon pulse finally stops travelling. However, by this epoch, the dark matter has already begun to clump around the baryon perturbations, polluting the CDM transfer function with a bit of the BAO signal, again diluting the oscillatory signal—the fit would not be optimal in terms of the information differentiating T'_b and T'_c .

Rather than using transfer functions directly from CLASS or CAMB at a particular epoch, we use the fitting function from Eisenstein and Hu [6] (section 3.1) for T'_c . We choose to use their CDM transfer function (their equation 17) rather than the zero-baryon transfer function (their equation 29). We define the baryon transfer function as the (appropriately scaled) difference between the density weighted sum of the baryon and CDM $z = 0$ transfer functions from CLASS and the Eisenstein and Hu transfer function T'_c

$$T'_b(k) = \left(T_{cb}^{\text{CLASS}}(k) - \frac{\Omega_c}{\Omega_c + \Omega_b} T_c^{\text{EH}}(k) \right) \frac{\Omega_c + \Omega_b}{\Omega_b}. \quad (4)$$

For our template fits, we use the transfer functions and densities for the fiducial cosmology at which the template is created. For our full fits we apply this equation to form the linear model used as the starting point for the perturbative calculations for each cosmology tested (hence T'_b and T'_c become cosmology dependent). The low-redshift baryonic signature is retained in T'_b , but with a split in signal between T'_b and T'_c as if we had taken high-redshift transfer functions where the two transfer functions are maximally different. This relies on the shape of the summed transfer function remaining invariant with time, as expected in the linear regime. We expect any deviations from this to be small. As shown in Fig. 3, this means that T'_c and T'_b differ in both their overall shape and the presence of oscillations in T'_b . Thus, their separation captures two physical effects: the oscillations from

the baryon-photon fluid, and the suppression of power on scales smaller than the sound horizon. This is because dark matter fluctuations can begin to grow at equality, whereas baryon fluctuations continue to oscillate until the pressure drops to zero at the drag epoch. In contrast, if we had set T'_c to the zero-baryon transfer function T_0 instead of T_c in [6], the T'_c - T'_b split would only capture the oscillations, not the effect of baryons on the shape. This distinction doesn't matter much for the template-based fits for the BAO position, but we achieve tighter constraints (and less degeneracy with the Λ CDM cosmological parameters) in the full-shape fits including the baryon amplitude with this approach (see Section II B).

Our analysis assumes that the bias of the galaxies that we observe is the same when comparing the galaxy density field to either the baryon or dark matter fields, such that we only have a single set of bias parameters relating galaxy and matter fields. This is common to all full-shape fits to date. In practice, the differential velocity and (more importantly) density of the baryon field compared to the dark matter field at early times could lead to a difference in the bias with these fields $b_{\delta_{bc}}$, $b_{v_{bc}}$ [22, 23], dependent on the physics of galaxy formation. We should expect such a bias to be scale-dependent and it could be removed in an analysis such as ours by including the appropriate template [24]. However, as there is currently no evidence that such a bias has an appreciable effect on the galaxies analysed and no preferred model for such a bias, we do not include it in our current analysis.

B. Full-shape fits

We first consider extracting the information on γ_B as part of a fit of a full model designed to model the shape of the power spectrum as well as the BAO component. Using Eq. 3 to model the linear power spectrum, we include γ_B as an extra parameter within full-shape Λ CDM EFTofLSS [25, 26] fits, extending the CLASS-PT code [27–32].² The power spectrum is modelled using one-loop perturbation theory supplemented by ultraviolet counterterms to account for short-scale non-local physics, a symmetry-based bias expansion, and infrared resummation to correctly capture long-wavelength modes and the shape of the BAO. CLASS-PT is similar to the methods of [33, 34] and was shown to give consistent results in a blinded mock challenge [35]. Treating the transfer function split and the non-linear correction separately is reasonable as we expect the transition from linear to non-linear to depend only on the matter (joint CDM+baryon) distribution.

¹ As seen in the animations at https://scholar.harvard.edu/files/deisenstein/files/acoustic_anim.gif, https://lweb.cfa.harvard.edu/~deisenst/acousticpeak/acoustic_physics.html

² We modify the publicly available likelihood, https://github.com/oliverphilcox/full_shape_likelihoods, which calls the CLASS-PT code itself <https://github.com/Michalychforever/CLASS-PT>.

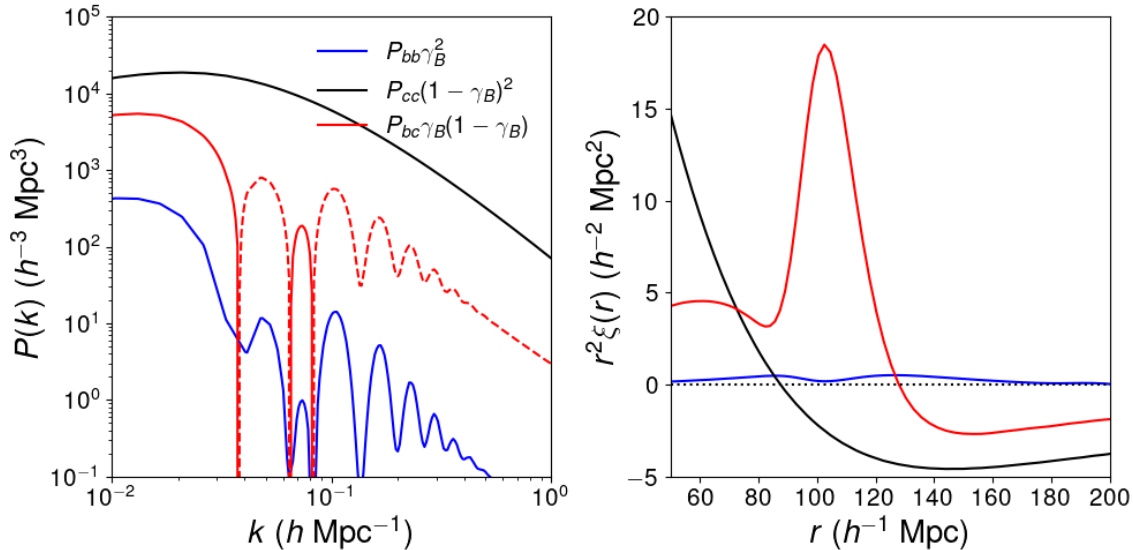


FIG. 2. Power spectra and correlation functions of the templates. Dotted lines indicate a negative power spectrum. The dominant oscillatory component arises from the baryon-cold dark matter cross power spectrum.

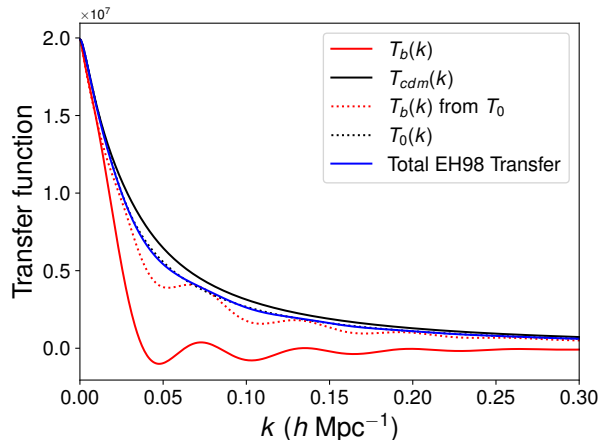


FIG. 3. Transfer functions from [6]. We show our fiducial choice (smooth transfer function from [6] T'_c , their Eq. 17, and T'_b subsequently generated to match the overall power spectrum) in solid black and red lines. In this choice, T'_b contains both the oscillatory component and the overall shape suppression from baryons suppressing the early growth of structure on small-scale modes that are within the horizon before recombination. An alternative transfer function would be T_0 ([6] Eq. 29; black dotted line) which matches the shape of the total [6] transfer function (solid blue line). However this choice leads to weaker constraints on the baryon fraction that are more degenerate with the other cosmological parameters.

Schematically, the power spectrum multipoles are the

sums of several terms

$$P_\ell(k) = P_\ell^{\text{tree}}(k) + P_\ell^{\text{1-loop}}(k) + P_\ell^{\text{counterterm}}(k) + P_\ell^{\text{stochastic}}(k) \quad (5)$$

where the tree-level power spectrum is the linear power spectrum with IR resummation for the BAO, the 1-loop power spectrum is an integral over products of linear power spectra, the counterterms scale as $k^2 P_{\text{lin}}(k)$ and the stochastic terms account for shot noise and scale as constants plus k^2 and $k^2 \mu^2$ corrections.

We modify CLASS-PT to insert γ_B into the linear power spectrum multipoles using Eq. 3 before the 1-loop integrals. CLASS-PT performs its own wiggle-no-wiggle decomposition of the power spectrum, by sine transforming the power spectrum and removing coefficients with frequencies within the BAO range [28]. This is necessary for IR resummation (i.e. exponentially damping the wiggle portion of the power spectrum), which is required to accurately model the BAO [36]. However, this split is done at the power spectrum level, whereas we prefer to split the baryon signal at the transfer function level; hence we do not use the built-in wiggle-no-wiggle split to model the BAO amplitude.

The model contains nuisance parameters accounting for galaxy bias (b_1 , linear; b_2 , quadratic; $b_{\mathcal{G}_2}$, tidal; b_{Γ_3} , third-order), counterterms (c_0 , monopole; c_2 ; quadrupole; c_4 , hexadecapole; \tilde{c} , Fingers-of-God), and stochastic terms (P_{shot} , a_0 , a_2) [37]. The stochastic terms are equal to

$$P_{\text{stochastic}}(k) = \frac{1}{\bar{n}} \left[1 + P_{\text{shot}} + a_0 \left(\frac{k}{k_{\text{NL}}} \right)^2 + a_2 \mu^2 \left(\frac{k}{k_{\text{NL}}} \right)^2 \right] \quad (6)$$

We adopt the following priors:

$$b_1 \in \text{flat}[0, 4] \quad (7)$$

$$b_2 \sim \mathcal{N}(0, 1^2) \quad (8)$$

$$b_{\mathcal{G}_2} \sim \mathcal{N}(0, 1^2) \quad (9)$$

$$b_{\Gamma_3} \sim \mathcal{N}\left(\frac{23}{42}(b_1 - 1), 1^2\right) \quad (10)$$

$$\frac{c_0}{(\text{Mpc}/h)^2} \sim \mathcal{N}(0, 15^2) \quad (11)$$

$$\frac{c_2}{(\text{Mpc}/h)^2} \sim \mathcal{N}(30, 15^2) \quad (12)$$

$$\frac{c_4}{(\text{Mpc}/h)^2} \sim \mathcal{N}(0, 15^2) \quad (13)$$

$$\frac{\tilde{c}}{(\text{Mpc}/h)^4} \sim \mathcal{N}(500, 250^2) \quad (14)$$

$$P_{\text{shot}} \sim \mathcal{N}(0, 0.5^2) \quad (15)$$

$$a_0 \sim \mathcal{N}(0, 0.5^2) \quad (16)$$

$$a_2 \sim \mathcal{N}(0, 0.5^2) \quad (17)$$

These priors are inspired by those used in [37] and [27], but not identical; in particular, the prior widths on the counterterms and stochastic parameters have been halved compared to the priors in [37] and [27].³ We modify the priors to reduce the dependence on the prior width and improve parameter recovery for the tests described in Section III A. The resulting narrower priors are more similar to the more restrictive ‘‘West-Coast’’ (WC) priors of [38] (see [39] for a comprehensive discussion of the impact of nuisance parameter priors on Λ CDM parameter constraints), especially for c_0 and a_2 . Translating the WC priors into the CLASS-PT parameter set [37, 39, 40], we find they correspond to priors of $\mathcal{N}(0, 12.97)$ on c_0 , $\mathcal{N}(0, 46.2)$ on c_2 , $\mathcal{N}(0, 56.0)$ on c_4 , fixing \tilde{c} to zero, $\mathcal{N}(-1, 2^2)$ on P_{shot} , fixing a_0 to zero, and $\mathcal{N}(0, 0.64^2)$ on a_2 .

We assume a Gaussian likelihood, with the covariance computed from the power spectrum multipoles and

post-reconstruction Alcock-Paczynski parameters measured on 999 Patchy mocks, using the publicly released covariances of [30]. Parameters entering the model linearly (b_{Γ_3} , c_0 , c_2 , c_4 , \tilde{c} , P_{shot} , a_0 , and a_2) are analytically marginalized [41]. The model is stretched by the distance ratio (Hubble parameter or angular diameter distance) between distances in the sample cosmology and the BOSS fiducial cosmology.

We vary and marginalize over the Λ CDM parameters controlling the shape of the power spectrum [h , $\ln(10^{10} A_s)$, Ω_m , n_s]. We impose flat and uninformative priors on all of these parameters, and fix $\omega_b = 0.02237$. We consider all of these parameters to be nuisance parameters, as we do not want any information about the full shape of the galaxy power spectrum. We then add three additional parameters ω_b^{dens} , Ω_m^{dens} and h^{dens} , using the superscript ‘‘dens’’ to indicate that the information comes from our density-based cosmological split. These parameters control the AP ratio $\alpha_{\perp}/\alpha_{\parallel}$ (Ω_m^{dens}), the amplitude of the baryonic signature ($\gamma_B = \omega_b^{\text{dens}}/(\Omega_m^{\text{dens}} h^{\text{dens}})$), and a simple Gaussian BBN prior centered at the true value of ω_b for Nseries (0.023) with width 0.00037. When there is no ambiguity, the quoted value of h refers h^{dens} unless stated differently. The neutrino mass is fixed, either to zero (for Nseries) or to the minimal value, $\Sigma_{m_\nu} = 0.06$ eV, on data.

C. Template fits

Standard BAO extraction methods using the correlation function or power spectrum multipole moments fit a model with terms that are designed to allow marginalization over broad-band shape and amplitude information. The idea is that we wish to isolate the BAO signal without having to model the broadband shape (allowing for a less model-dependent fit than the full-shape method). To add the baryon signature parameter, we follow a similar path to that adopted for full fits as discussed in the previous section, and simply replace the linear power spectrum in existing templates with Eq. 3. For example, consider the model used by [18] to isolate the BAO signal:

$$\xi_{0,\text{mod}}(s) = B_0 \xi_0(s, \alpha_{\perp}, \alpha_{\parallel}) + A_0(s) \quad (18)$$

$$\xi_{2,\text{mod}}(s) = \frac{5}{2} (B_2 \xi_{\mu 2}(s, \alpha_{\perp}, \alpha_{\parallel}) - B_0 \xi_0(s, \alpha_{\perp}, \alpha_{\parallel})) + A_2(s). \quad (19)$$

The parameters B_i sets the overall amplitude of the monopole and quadrupole (i.e. the combination of galaxy bias and power spectrum amplitude), while

$$A_i(s) = \frac{a_{i,1}}{s^2} + \frac{a_{i,2}}{s} + a_{i,3}, \quad (20)$$

is designed to isolate the BAO signal from broadband shape changes by fitting and removing any changes in the

³ Note that the stochastic priors in the publicly available likelihood https://github.com/oliverphilcox/full_shape_likelihoods have half the width of the priors reported in Eq. 12 of [27].

shape of the template. The bias parameters B_i and $a_{i,j}$, commonly called the polynomial parameters, are treated as nuisance parameters in the fit, allowing the model to:

1. fit smooth differences between template and data allowing for non-linear, bias and RSD effects,
2. fit smooth changes in clustering caused by observational systematics, such as the effects of stellar density,
3. fit any effects from reconstruction when the model is used to fit post-reconstruction data,
4. for different α , ensure that the smooth template (with potentially the wrong fiducial cosmology) is still able to fit the dilated clustering statistics, ensuring that the α are only constrained by the BAO.

We expect that these parameters will remove some of the smooth signal differentiating between baryon and dark matter clustering components.

In the standard BAO model [e.g. 42], ξ_0 and ξ_2 are linear models calculated by transforming the anisotropic power spectrum

$$P(k, \mu) = C^2(k, \mu) [\Delta P(k) D^2(k, \mu) + P_{\text{smooth}}(k)] \quad (21)$$

where $C(k, \mu)$ includes the Kaiser + Finger of God RSD term [43], $D(k, \mu)$ is the anisotropic damping, $P_{\text{smooth}}(k)$ is the smooth power spectrum model (in our case, calculated using the fitting formulae of [6]), and $\Delta P(k)$ is the difference between the linear power spectrum calculated using CAMB [20, 21] and the smooth power spectrum. Eq. 21 is then integrated over μ (weighted by Legendre polynomials) to calculate the power spectrum multipoles, Hankel transformed to real space, shifted by α_{\parallel} and α_{\perp} , and fitted to data.

In order to incorporate the new parameter γ_B introduced in Section II A in this model, we make the following changes. We refer to the model that includes all of these effects as the “new” model.

1. At the heart of the new model is using Eq. 3 when we calculate $P(k)$, giving a template that depends on γ_B . As in the standard template-based method, the terms do not need to be calculated for every model to be tested, but we need to store them in component form - three components corresponding to $T'_b T'_b$, $T'_c T'_c$ and $T'_b T'_c$, to allow for variation of γ_B .
2. We make use of the split of the linear power spectrum into transfer functions to isolate the BAO scaling, applying the scaling parameters α_{\parallel} and α_{\perp} to T'_b only. These therefore scale both the BAO and baryon shape change in T'_b , and consequently the physical interpretation is complicated, although we expect the nuisance broadband and polynomial terms to reduce the theory dependency such that it

is close to r_d as expected for the BAO. In our companion paper [5], we do not use the derived α 's, instead using the results from the literature.

3. We add two new broadband scaling parameters, $q_{\parallel, BB}$ and $q_{\perp, BB}$, which are distinct from α_{\parallel} and α_{\perp} . All other functions of k other than T'_b are shifted by $q_{\parallel, BB}$ and $q_{\perp, BB}$ (Fig. 4). This shifting must necessarily be performed in Fourier space, since the two transfer functions in the cross-term $T'_b(k) T'_c(k)$ are shifted by different parameters. These broadband scaling parameters are only sensitive to the distance scale.
4. γ_B is correlated with the broad-band polynomial terms, and we have to change these terms to accommodate this. We find that, in particular, the $1/s^2$ term is quite degenerate with the BAO amplitude. For the pre-reconstruction fits, we require a constant term for both the monopole and quadrupole, whereas for the post-reconstruction fits, we require a constant for only the monopole. These constant terms are motivated by the shape of the difference between the weighted and unweighted correlation functions (Fig. 6 in [18]), and by changes in the goodness of fit when adding polynomials in fits to the data. Future work will benefit from the new broadband marginalization introduced in [24].
5. We use the beyond-linear model of [44] for pre-reconstruction and post-reconstruction templates, with a more sophisticated treatment of the post-reconstruction damping and k^2 -dependent derivative bias (essentially, an EFT counterterm) to account for nonlinearities. Including the derivative bias allows us to marginalize over degeneracies between the BAO amplitude and nonlinear or higher-bias terms (which also scale as $k^2 P_{\text{lin}}$), although in an approximate way compared to the full EFT fits.
6. We vary the damping parameters Σ_{sm} (which sets Σ_{\parallel} and Σ_{\perp} in the limit of the linear model) and Σ_{fog}

We then proceed in the usual fashion: define the multipole moments $P_{\ell}(k)$; Hankel transform to $\xi_{\ell}(s)$, and fit ξ_0 and ξ_2 (noting the rather convoluted definition of B_2). We elaborate on the reasons for these changes in the sections below. We also carefully show how changing each assumption changes the results on the BOSS data away from the results found in [18]. We use the Nseries mocks to test the effect of the changes and whether they bias results.

1. Pre-reconstruction template fits

The pre-reconstruction beyond-linear “EFT1” model of [44] is very similar to the standard model of SBRS [42],

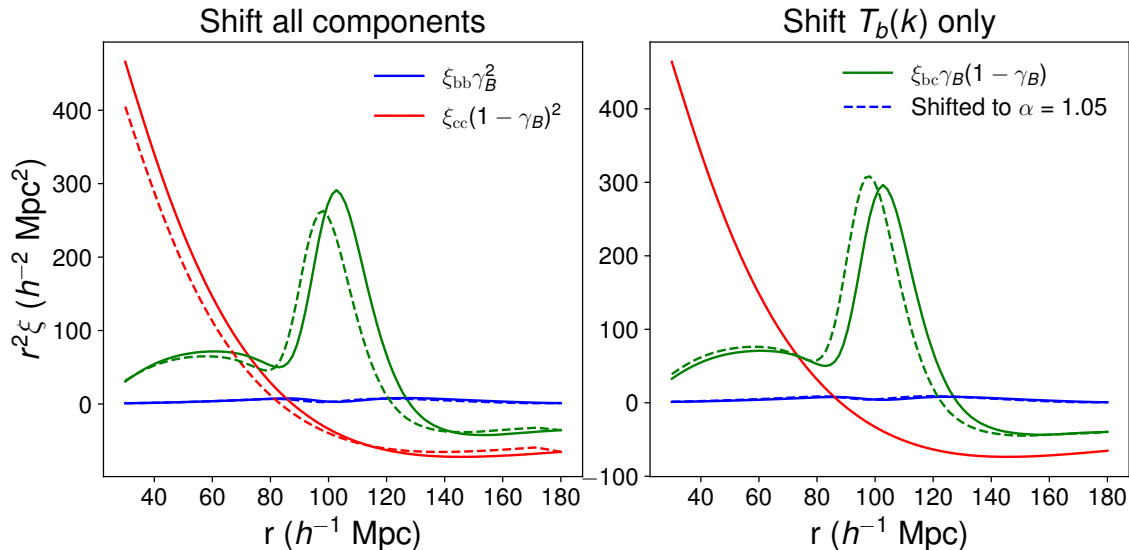


FIG. 4. *Left*: all components of the model are shifted by $\alpha = 1.05$ (except the polynomial terms, which are not shown). This is the default model used in previous work. *Right*: only $T_b(k)$ is shifted by α . Note that shifting only the transfer function $T_b(k)$ is not the same as shifting the wiggly component of the power spectrum, because $P_w(k)$ comes from the product of $T_b(k)$ (which is shifted) and $T_c(k)$ (which is not).

except for the extra derivative bias b_∂ . We use Eq. 21 with

$$C^2(k, \mu) = \left((b_1 + f\mu^2)^2 + b_\partial \frac{k^2}{k_L^2} (b_1 + f\mu^2) \right) \times \frac{1}{(1 + k^2 \mu^2 \Sigma_{\text{fog}}^2)^2} \quad (22)$$

and

$$D^2(k, \mu) = \exp \left[-k^2 (1 - \mu^2) \Sigma_{xy}^2 / 2 - k^2 \mu^2 (1 + f)^2 \Sigma_{xy}^2 / 2 \right] \quad (23)$$

We fix k_L to $1 h \text{ Mpc}^{-1}$. The damping term is very similar to the SBRS damping, except with Σ_{\parallel} and Σ_{\perp} explicitly tied together through the factor of $1 + f$. We allow b_∂ to vary within a uniform prior between -250 and 250. We find that a wider prior on b_∂ leads to poor recovery of the BAO amplitude and AP parameters when changing the input true cosmology (but fixing the fiducial template cosmology), but a narrower prior on b_∂ biases fits on the N -body mocks.

2. Post-reconstruction template fits

As for our pre-reconstruction fits, we use the ‘‘EFT1’’ model of [44] as our fiducial model. The post-reconstruction EFT1 model of [44] contains two key differences from the model of [42]. First, it models the power spectrum as the sum of contributions from the displaced galaxies, shifted randoms, and shifted randoms

cross-correlated with displaced galaxies. Rather than imposing a single damping on ΔP_L , the individual terms are separately damped. This effectively leads to two separate sets of damping parameters, transitioning from Σ_{ds} on large scales where the ds term dominates to Σ_{dd} on small scales where dd dominates. Second, the EFT1 model includes a derivative bias, in addition to the standard linear bias, to model nonlinearities and higher-order bias. That is, $b_1 \rightarrow b_1 + k^2 b_\partial$. This yields a term $\propto k^2 P_L(k)$, that is essentially identical to the counterterms in the EFT of Large-Scale structure (exactly equal for SPT [e. g. Eqn. 2.3 in 28], and nearly equal for LPT, where the counterterm $\propto k^2 P_{\text{zel}}(k)$ [33]). This model is not truly perturbative in that it drops the higher-order bias and 1-loop terms that contribute at equivalent order, but the amplitude of the derivative bias can be tuned to approximately match these contributions.

As in the linear model, we start by splitting the power spectrum into wiggle and no-wiggle components. The wiggle component is multiplied by the standard Kaiser RSD term (reduced by the ‘‘Rec-Iso’’ reconstruction scheme, i.e. reconstruction nearly eliminates the quadrupole) times a Finger-of-God term. The new element here is the additional derivative bias to encode beyond-linear physics. We fix $k_L = 1 h \text{ Mpc}^{-1}$. To conform to the notation of the standard method, we explicitly divide out all factors of the linear bias, b_1 , and will later scale the monopole and quadrupole separately by B_0 and B_2 . We therefore replace the divided b_1 by $B_0^{0.5}$. The Finger-of-God damping is only applied to the no-wiggle term, not to the oscillatory term, which is damped by $D(k, \mu)$.

$$P(k, \mu) = \left[C_{\text{nw}}^2 + \frac{b_\partial}{B_0^{0.5}} \left(\frac{k}{k_L} \right)^2 \left(1 + \frac{f\mu^2}{B_0^{0.5}} (1 - S) \right) \left(\frac{1}{1 + k^2 \mu^2 \Sigma_{\text{fog}}^2 / 2} \right)^2 \right] P_{\text{nw}}(k) + C^2 \Delta P_{\text{lin}}(k) \quad (24)$$

$$S = \exp(-0.5k^2 \Sigma_{\text{sm}}^2) \quad (25)$$

$$C_{\text{nw}} = C_{\text{Kaiser}} C_{\text{fog}} = \left(1 + \frac{f\mu^2}{B_0^{0.5}} (1 - S) \right) \frac{1}{1 + k^2 \mu^2 \Sigma_{\text{fog}}^2 / 2} \quad (26)$$

The BAO term then consists of three pieces, all scaling the wiggle power spectrum, each with their own damping:

$$C^2(k, \mu) = \delta P_{dd}(k, \mu) - 2\delta P_{ds}(k, \mu) + \delta P_{ss}(k, \mu) \quad (27)$$

$$\delta P_{dd}(k, \mu) = \exp \left(-k^2 (1 + (2 + f)f\mu^2) \Sigma_{dd}^2 \right) \left(1 - \frac{S}{B_0^{0.5}} + \frac{f\mu^2}{B_0^{0.5}} (1 - S) \right)^2 + \frac{b_\partial}{B_0^{0.5}} \left(1 - \frac{S}{B_0^{0.5}} + \left(\frac{k}{k_L} \right)^2 \frac{f\mu^2}{B_0^{0.5}} (1 - S) \right) \quad (28)$$

$$\delta P_{ds}(k, \mu) = -\exp \left(-k^2 (1 + f\mu^2) \Sigma_{sd}^2 \right) \left(\frac{1}{B_0^{0.5}} - \frac{S}{B_0} + \frac{f\mu^2}{B_0} (1 - S) + \frac{1}{2} \frac{b_\partial}{B_0} \left(\frac{k}{k_L} \right)^2 \right) S \quad (29)$$

$$\delta P_{ss}(k, \mu) = \exp \left(-k^2 \Sigma_{ss}^2 \right) \frac{S^2}{B_0} \quad (30)$$

The damping parameters are given by:

$$\Sigma_{dd}^2(q, z) = \frac{1}{3} \int \frac{dp}{2\pi^2} (1 - j_0(qp))(1 - S(p))^2 P_L(p, z) \quad (31)$$

$$\Sigma_{ds}^2(q, z) = \frac{1}{3} \int \frac{dp}{2\pi^2} \left(\frac{1}{2} (S(p)^2 + (1 - S(p))^2) - j_0(qp)(1 - S(p))S(p) \right) P_L(p, z) \quad (32)$$

$$\Sigma_{ss}^2(q, z) = \frac{1}{3} \int \frac{dp}{2\pi^2} (1 - j_0(qp)) S(p)^2 P_L(p, z) \quad (33)$$

They are calculated from a fixed template linear matter power spectrum, and evaluated with $q = 110 h^{-1} \text{ Mpc}$.

ΔP_{lin} is defined in a similar way as for the linear model. We explicitly write it in terms of the primordial power spectrum and the growth factor:

$$\Delta P_{\text{lin}}(k, z) = \left[(\gamma_B T_b(k) + (1 - \gamma_B) T_c^{EH}(k))^2 - (1 - \gamma_B)^2 (T_c^{EH}(k))^2 \right] 2\pi^2 h^4 \left(\frac{kh}{k_{\text{piv}}} \right)^{n_s} A_s D(z)^2 \quad (34)$$

allowing us to cancel the third term arising from P_{smooth} :

$$\Delta P_{\text{lin}}(k, z) = \left[\gamma_B^2 T_b^2(k) + 2\gamma_B(1 - \gamma_B) T_c^{EH}(k) \right] 2\pi^2 h^4 \left(\frac{kh}{k_{\text{piv}}} \right)^{n_s} A_s D(z)^2 \quad (35)$$

Finally, we scale k and μ following [45, 46]

$$k' = \frac{k}{\alpha_\perp} \left[1 + \mu^2 \left(\frac{1}{F^2} - 1 \right) \right]^{1/2} \quad (36)$$

$$\mu' = \frac{\mu}{F} \left[1 + \mu^2 \left(\frac{1}{F^2} - 1 \right) \right]^{1/2} \quad (37)$$

and allow for overall scalings of the monopole and quadrupole with free parameters B_0 and B_2 . We place a prior on these parameters following the same approach as [18]: first fitting B_0 from 50 to 80 $h^{-1} \text{ Mpc}$ (fixing B_2 equal to B_0 in this fit), and then putting a prior on $\log B_0$ and $\log B_2$ equal to the fitted value and with width 0.4.

III. MOCK VALIDATION TESTS

We conduct two sets of mock validation tests. For each test, we perform a full Bayesian analysis, deriving credible intervals for the cosmological parameters of interest after marginalising over nuisance parameters. First, we consider the results when fitting to realistic N-body mocks matching the parameters of the BOSS CMASS sample. Second, we test our sensitivity to the fiducial cosmology and priors imposed on nuisance parameters by creating a series of noiseless theory vectors from theoretical predictions with different parameters. The second set of tests directly gauges the dependence on the nuisance parameters and their priors by considering whether the true values lie within the credible intervals. The first set of tests allows us to test the dependence on noise, and helps us to understand the sensitivity to changes in the model. It also tests whether the model can account for

the nonlinear structure formation encapsulated by the mocks.

We use the 84 Nseries BOSS CMASS mocks presented in [47] to test our pipeline.⁴ Many different mocks have been created for BOSS, such as the Patchy mocks [48], QPM [49], and runA and runPB [46]. The QPM mocks were created to match LOWZ and CMASS as separate samples, rather than the final BOSS sample, which combines LOWZ and CMASS and then applies overall redshift cuts. As a result, the Patchy mocks match the combined sample better than QPM (e.g. due to QPM not properly matching redshift evolution within LOWZ) [48]. Moreover, both Patchy and QPM are approximate fast mocks created to measure covariance matrices from a large number of samples and therefore may not match the real Universe. Indeed, [46] finds that the BAO damping is too large in the Patchy mocks, which they attribute to the approximate nature of the mocks. As a result, (and following [46]) we favor using true N -body mocks to test our pipeline. The runA and runPB simulations used in [46] are only periodic boxes. Hence we use Nseries as the only N -body mock available in sky coordinates R.A., declination, and redshift.

The Nseries footprint matches BOSS CMASS NGC. Each mock covers $\sim 4 \text{ Gpc}^3$ effective volume (scaling by the sky fraction in NGC vs. the total sky fraction, and the effective volume from Table 3 in [50]). This is approximately the same effective volume as bins z_1 (3.7 Gpc^3), z_2 (4.2 Gpc^3), and z_3 (4.1 Gpc^3) (Table 2 in [11]).

These mocks were created from a single halo occupation distribution tuned to be consistent with the BOSS CMASS sample, and applied to 7 independent $2.6 h^{-1} \text{ Gpc}$ periodic boxes with the same cosmology at $z = 0.569$. Twelve different orientations were created out of each box, leading to 84 mocks. The boxes have high resolution, with 2048^3 particles and a mass per particle of $1.5 \times 10^{11} h^{-1} M_\odot$. The input cosmological parameters are $\Omega_m = 0.286$, $\Omega_b = 0.047$, $h = 0.7$, $n_s = 0.96$, $\sigma_8 = 0.82$, and no massive neutrinos. Galaxy catalogs have been created both before and after running BAO reconstruction.

We generate the noiseless theory vectors with a variety of different cosmological and nuisance parameters, including ΛCDM cosmologies, cosmologies with varying neutrino mass and numbers of relativistic species, and Early Dark Energy cosmologies. We describe these below in the subsection for each of the three types of fits.

The parameters that we are interested in are the baryon fraction $f_b \equiv \Omega_b/\Omega_m$, and the normalised Hubble parameter $h \equiv H_0 \text{ km s}^{-1} \text{ Mpc}^{-1}/100 \text{ km s}^{-1} \text{ Mpc}^{-1}$ determined using f_b , the BBN measurement of $\Omega_b h^2$ and the value of Ω_m from the AP effect (as described in [5]).

⁴ See also https://www.ub.edu/bispectrum/bispectrum_public/bispectrum_notes.pdf.

A. Full-shape tests

We test the credible intervals inferred for f_b and h derived from the posterior when fitting to either the Nseries mocks or synthetic data vectors from EDE and ΛCDM cosmologies. We fit the monopole P_0 , the quadrupole P_2 , and the hexadecapole P_4 , measured between $k_{\min} = 0.01$ and $k_{\max} = 0.20 h \text{ Mpc}^{-1}$. We use the BOSS z_3 NGC covariance, rescaled by the ratio of the effective volume of the total BOSS volume in bins z_1 and z_3 , to the effective volume of z_3 NGC (a factor of 2.6 using Table 2 in [11]). The volume rescaling allows us to compare the shifts between the truth and the credible regions relative to the statistical power of the entire BOSS dataset. We use the MontePython sampler [51, 52], run the chains until a Gelman-Rubin convergence criterion of $R-1=0.1$ is reached [53], and analyze the chains with GetDist [54].

In order to ensure that our geometrical constraint on Ω_m is uncontaminated by the sound horizon, we only include measurements of $\alpha_{\text{AP}} \equiv \alpha_{\parallel}/\alpha_{\perp}$ in the fit.⁵ To do this, we use error propagation to transform the covariance between the multipoles $P_\ell(k)$ and the AP parameters into the covariance between $P_\ell(k)$ and α_{AP} . We consider two versions of the data vector used to constrain α_{AP} : one using BAO information only, and one using better constraints on α_{AP} from voids [55, 56]. For the voids case, the α_{\parallel} and α_{\perp} covariances are scaled by a factor of approximately 4, corresponding to the improvement from BAO to void α_{AP} shown in Table 1 of [56]. This matches the factor of two improvement on Ω_m precision, from $\sigma_{\Omega_m} \sim 0.052$ from the anisotropic BAO AP information in the z_1 and z_3 bins, and the $\sigma_{\Omega_m} \sim 0.027$ constraint from [55, 56].

In addition to tests on the Nseries mocks, we also test our parameter recovery using noiseless data vectors as the input data. We consider two classes of noiseless mocks, EDE cosmologies and ΛCDM cosmologies. For the EDE cosmologies, we use the best-fit EDE model studied in [4] (originally from [57]) $h = 0.7219$, $\omega_b = 0.02253$, $\omega_{\text{cdm}} = 0.1306$, $A_s = 2.215 \times 10^{-9}$, $n_s = 0.9889$, $f_{\text{EDE}} = 0.122$, $\log_{10}(z_c) = 3.562$, and $\theta_{i,\text{scf}} = 2.83$. We consider a slightly different model from [4, 57] in that we set the neutrino mass to zero rather than the minimal mass. We generate the full nonlinear power spectrum using the EDE_CLASS_PT code⁶ [58], with $b_1 = 1.78$ and the remaining bias and counterterms set to their fiducial values: $b_2 = -0.12$, $b_{G_2} = -0.23$, $b_{\Gamma_3} = 0$, $c_0 = 0$, $c_2 = 30$, $c_4 = 0$, $\tilde{c} = 500$, $P_{\text{shot}} = 6669.63 (h^{-1} \text{ Mpc})^3$. We also consider 9 variations on this EDE cosmology,

⁵ In our companion paper [5], we also use uncalibrated BAO information from the isotropic distance scale, which considerably improves the Ω_m constraint beyond just using α_{AP} . However, the mock tests are all run in a single redshift bin because Nseries was only run for CMASS NGC. In a single bin, the only sound horizon free information on Ω_m comes from α_{AP} .

⁶ https://github.com/Michalychforever/EDE_class_pt

with varying h and all other parameters fixed; we fix Ω_m and ω_b so that changes in h are entirely propagated into changes in the baryon fraction. We consider variations in f_b between 0.123 and 0.195 (centered on the fiducial value of 0.147), corresponding to variations in h of 0.627 to 0.790 (fiducial value 0.722).

We also consider Λ CDM and w_0w_a CDM noiseless mocks using cosmologies drawn from the AbacusSummit suite [59]. We choose Abacus cosmologies spanning a wide range in f_b (from 0.138 to 0.176); the cosmological parameters are summarized in Table I. These mocks were generated with $b_1 = 1.99$, $b_2 = 0.24$, $b_{\mathcal{G}_2} = -0.22$, $b_{\Gamma_3} = 0.54$, $c_0 = 0$, $c_2 = 30$, $c_4 = 0$, $\tilde{c} = 0$, $a_0 = 0$, $a_2 = 0$, $P_{\text{shot}} = 0$ (i.e. shot noise fixed to the true value of $1/\bar{n} = 5000$ (h^{-1} Mpc) 3).

B. Template fits

As for the full-shape fit tests discussed above, we test the credible intervals inferred for f_b derived from the posterior when using the template based approach to fit either the Nseries mocks or synthetic data vectors. Here we only fit for the BAO amplitude and do not combine with the AP parameters, and so therefore only show credible intervals on f_b and not on h^{dens} . We sample the posterior with Cobaya [60, 61] and run until R-1=0.05; the faster likelihood evaluation time allows us to run to a smaller value of R-1 than the full-shape fits, but in both cases we test that the results are unchanged if we use a slightly higher value of R-1.

For the synthetic data vector fits, the default cosmological parameters are the fiducial BOSS cosmology, and the default nuisance parameters are $b_{\partial} = 0$ (pre-recon) or $b_{\partial} = 15$ (post-recon), $\Sigma_{xy} = 6 h^{-1}$ Mpc pre-recon or $\Sigma_{sm} = 15 h^{-1}$ Mpc post-recon, and $\Sigma_{fog} = 4 h^{-1}$ Mpc. We consider varying the derivative bias to $b_{\partial} = -10$ (5 post-recon) and $b_{\partial} = 10$ (25 post-recon); the smoothing scale to $\Sigma_{xy} = 3$ and $12 h^{-1}$ Mpc pre-recon ($\Sigma_{sm} = 8 h^{-1}$ Mpc and $\Sigma_{sm} = 24 h^{-1}$ Mpc post-recon); and the Finger-of-God damping to $\Sigma_{fog} = 0$ and $\Sigma_{fog} = 8 h^{-1}$ Mpc. We take the covariance matrix from the BOSS z_3 fit (combining both hemispheres), scaled to the combined volume of BOSS z_1 and z_3 . Since our model exactly matches the data for a single set of parameters, and we marginalize over all nuisance parameters, our fits are essentially tests of how sensitive we are to the prior, including projection effects that could potentially drive the marginalized constraints away from the best-fit.

We also test our sensitivity to the wiggle/no-wiggle split by generating a data vector with the smooth power spectrum generated in a different way from the EH98 fitting function. In this alternative approach, we follow the method of [62] and fit a smoothing spline to the linear correlation function in two windows at $70 h^{-1}$ Mpc and $250 h^{-1}$ Mpc, smoothly interpolating between the two to remove the BAO bump.

We then use several data vectors generated from differ-

ent cosmologies to test the sensitivity to the assumption of a fiducial, fixed template. First, we test that our results are robust to the change in cosmological parameters required for an Early Dark Energy fit to the CMB [4]. We generate a data vector from the best-fit EDE parameters to the CMB: $h = 0.7219$, $\omega_b = 0.02253$, $\omega_{cdm} = 0.1306$, $A_s = 2.215 \times 10^{-9}$, $n_s = 0.9889$, one massive neutrino with mass 0.06 eV, $f_{\text{EDE}} = 0.122$, $\log_{10}(z_c) = 3.562$, and $\theta_{i,scf} = 2.83$. We use the CLASSEDE⁷ code to create the $z = 0$ matter power spectrum. We also consider the impact of two other “extended” models that also affect the sound horizon and phase of BAO oscillations; a model changing $\Sigma_{m\nu}$ to 0.20 eV, and a model changing $N_{\text{eff}} = 3.82$ (both drawn from the Planck [1] extended-model chains with that value of N_{eff} or $\Sigma_{m\nu}$, allowing other parameters to shift to compensate; see Table II for parameters).

Finally, we consider the impact of uncertainty in the power spectrum template. We aim to keep our results model- and CMB-independent; we want to consider a wider range in cosmological parameters than that probed by the Planck Λ CDM fits. Therefore, we consider the range in cosmological parameters probed by the BOSS data themselves. We use the parameter constraints from the full-shape fits of [30].⁸ We create 10 test cosmologies drawn from MCMC chains fit to the BOSS power spectrum multipoles only (i.e. not including the real-space power spectrum Q_0 , BAO, or the bispectrum, which are part of their fiducial dataset), with free n_s .

IV. RESULTS OF MOCK TESTS

A. Full-shape fits

1. Fits to the Nseries mocks

The parameters of the true cosmology generally lie well within the $1\text{-}\sigma$ credible interval when fitting to the Nseries mocks, with the marginalised value of h lower than the truth by 0.13σ , f_b biased high by 0.30σ , and an 11.4% H_0 constraint, when using Ω_m information from the AP ratio from BOSS BAO. This is a relatively poor Ω_m constraint, with $\sigma_{\Omega_m} = 0.052$ (i.e. much of the cosmological information from post-reconstruction BAO is lost when marginalizing over the sound horizon and therefore limiting the available information to the AP ratio). We also consider adding constraints from the AP ratio measured using voids, which improves the precision on Ω_m by a factor of 2; this leads to a 0.19σ bias low on H_0 and an 8% H_0 measurement.

⁷ https://github.com/mwt5345/class_edc

⁸ Other full-shape fits have substantially similar errorbars when using similar datasets and cosmological parameters [39, 63, 64]; thus our results would be substantially similar if we sampled from chains from these results rather than from [30].

Name	h	ω_b	ω_{cdm}	A_s	n_s	α_s	N_{ur}	w_0	w_a
cosm131	0.7165	0.02237	0.1086	2.3146×10^{-9}	0.9649	0	2.0328	-1	0
cosm139	0.7164	0.02416	0.1128	2.1681×10^{-9}	0.9732	0	2.0327	-1	0
cosm130	0.6736	0.02237	0.1200	1.614×10^{-9}	0.9649	0	2.0328	-1	0
cosm159	0.5967	0.02206	0.1261	1.7977×10^{-9}	0.9673	0	2.0328	-1.082	-0.392
cosm167	0.7050	0.02248	0.1400	1.7321×10^{-9}	0.9715	-0.017	2.889	-1	0
cosm168	0.6070	0.02157	0.1084	2.5378×10^{-9}	0.9275	0.016	1.1911	-1	0
cosm172	0.6800	0.02232	0.1161	1.8904×10^{-9}	0.9628	0.038	1.9049	-1	0
cosm177	0.6820	0.02239	0.1344	2.0641×10^{-9}	1.002	0.007	2.8643	-0.757	-0.443
cosm169	0.6474	0.02189	0.1222	1.8067×10^{-9}	0.9898	0.038	1.9109	-1	0
cosm181	0.5745	0.02169	0.1112	2.0651×10^{-9}	0.9336	-0.013	1.4059	-0.910	0.350

TABLE I. AbacusSummit [59] cosmologies chosen to test recovery of γ_B in full-shape fits. We choose a wide range of input values of the baryon fraction, beyond testing the recovery of γ_B for the single fixed true cosmology of the Nseries mocks. In addition to the Λ CDM parameters, the running α_s , the number of ultrarelativistic species N_{ur} (with a single massive neutrino), and the dark energy equation of state parameters w_0 and w_a are also varied.

Name	h	ω_b	ω_{cdm}	A_s	n_s
Cosmology 0	0.6912	0.02237	0.1210	2.715×10^{-9}	0.9719
Cosmology 1	0.7074	0.02237	0.1472	2.683×10^{-9}	0.8391
Cosmology 2	0.6826	0.02237	0.1184	2.678×10^{-9}	0.9762
Cosmology 3	0.688	0.02237	0.1266	2.889×10^{-9}	1.001
Cosmology 4	0.7097	0.02237	0.1207	2.76×10^{-9}	0.9788
Cosmology 5	0.6879	0.02237	0.1200	2.875×10^{-9}	1.009
Cosmology 6	0.6744	0.02237	0.1308	2.943×10^{-9}	0.8072
Cosmology 7	0.6923	0.02237	0.1282	2.556×10^{-9}	0.9033
Cosmology 8	0.7019	0.02237	0.1236	2.993×10^{-9}	0.9459
Cosmology 9	0.6957	0.02237	0.1336	2.875×10^{-9}	0.8835
$N_{eff} = 3.82$	0.72024	0.02291	0.13110	2.168×10^{-9}	0.98974
$\Sigma_{m\nu} = 0.20$ eV	0.67248	0.02259	0.11557	2.159×10^{-9}	0.96965

TABLE II. Cosmologies chosen to test the template fits: parameters for 10 cosmologies drawn from the full-shape fits of [27] to test the sensitivity of γ_B to the choice of template cosmology.

We show a triangle plot for the posterior from a fit to Nseries in Fig. 5. γ_B and h^{dens} are primarily degenerate with cosmological parameters rather than galaxy biases, though recall that many nuisance parameters are marginalized analytically and hence not shown on Fig. 5. Of the galaxy biases, we see the strongest degeneracies with b_2 , in line with its contributions to the nonlinear BAO shift [24, 65–67]. The strongest degeneracies are with Ω_m , σ_8 , h , and n_s . As explained below, these degeneracies arise from the approximation that only the baryon fraction affects the amplitude of the baryon signature. In reality, there are weak dependencies on other parameters, principally Ω_m and h (Fig. 1). The BAO amplitude is least degenerate with the primordial power spectrum amplitude A_s ; this is reasonable because the BAO feature is the difference between the wiggle and no-wiggle power spectrum and thus should not depend on power spectrum amplitude. In contrast, σ_8 mixes the primordial amplitude with Ω_m and n_s , since it is the $z = 0$ amplitude of the small-scale power spectrum. Hence it acquires a degeneracy with the BAO amplitude due to its degeneracies with Ω_m and n_s . Finally, the n_s - γ_B degeneracy comes primarily from the stronger degeneracies

between Ω_m and γ_B , and n_s and Ω_m (coming from the impact of Ω_m on the power spectrum shape).

2. Degeneracies between the baryon fraction and $\Omega_m h^2$

The largest contribution to the degeneracies is the trend between $\Omega_m h^2$ and the power spectrum peak or trough height, shown in Fig. 5 of [6]. In other words, the heights of the peaks depend primarily on the baryon fraction, but have an important secondary dependence on $\Omega_m h^2$. This comes primarily from the impact of baryons on the growth rate (which also leads to the baryonic suppression of the power spectrum shape) [68, 69]. Cold dark matter, which is not coupled to the photon-baryon oscillations, begins to grow after matter-radiation equality, whereas baryonic perturbations are suppressed until the acoustic oscillations end at the drag epoch. Hence, if $\Omega_m h^2$ is larger, equality occurs earlier, the CDM has more time to grow while the baryons are oscillating, and the BAO amplitude is suppressed. There are also cosmological dependencies through the Silk damping scale and the time-variation of the sound speed (leading to a time-varying oscillation which translates into a time-varying amplitude) [68], though the latter depends only on ω_b and is thus well-constrained given our assumed ω_b constraint.

We show the $\Omega_m h^2$ - γ_B degeneracy in Fig. 6. The left panel shows the ratio of the linear power spectrum to the Eisenstein & Hu [6] fit for two different cosmologies which have been adjusted to have the same baryon fraction, $\gamma_B = 0.158$. Despite the match in γ_B , the BAO wiggles clearly have different amplitude. The cosmology with higher $\Omega_m h^2$ has less prominent BAO wiggles, matching the expected trend. The right panel shows that the degeneracy is present either when using $T_c(k)$ or $T_0(k)$ to split the transfer functions, showing that the degeneracy comes from the BAO wiggles themselves and not the baryonic shape change. However, using $T_c(k)$ brings in 20% stronger constraints on γ_B from the baryonic shape change, which leads to slightly less degeneracy between

Mock	Truth		BAO only			Add voids		
	h	f_b	h	$n\sigma$	f_b	$n\sigma$	h	$n\sigma$
Nseries	0.7	0.164	$0.689^{+0.083}_{-0.074}$	-0.13	$0.172^{+0.031}_{-0.027}$	0.30	$0.689^{+0.057}_{-0.051}$	-0.19
z_3 covariance	0.7	0.164	$0.694^{+0.116}_{-0.093}$	-0.05	$0.168^{+0.034}_{-0.032}$	0.13	$0.698^{+0.080}_{-0.071}$	-0.03
z_3 -NGC covariance	0.7	0.164	$0.704^{+0.149}_{-0.113}$	0.04	$0.159^{+0.039}_{-0.035}$	-0.13	$0.694^{+0.108}_{-0.078}$	-0.06
z_3 -SGC covariance	0.7	0.164	$0.719^{+0.413}_{-0.186}$	0.10	$0.132^{+0.047}_{-0.087}$	-0.68	$0.778^{+0.291}_{-0.189}$	0.41
z_3 -NGC + SGC	0.7	0.164	$0.706^{+0.129}_{-0.099}$	0.06	$0.151^{+0.034}_{-0.029}$	-0.38	$0.715^{+0.092}_{-0.078}$	0.19
Nseries + Q_0	0.7	0.164	$0.698^{+0.081}_{-0.069}$	-0.02	$0.168^{+0.029}_{-0.026}$	0.15	$0.694^{+0.060}_{-0.054}$	-0.11
[27] counterterm prior	0.7	0.164	$0.694^{+0.096}_{-0.072}$	-0.07	$0.167^{+0.031}_{-0.027}$	0.11	$0.691^{+0.075}_{-0.054}$	-0.16
2× bias prior	0.7	0.164	$0.704^{+0.084}_{-0.078}$	0.05	$0.166^{+0.032}_{-0.026}$	0.07	$0.698^{+0.068}_{-0.056}$	-0.04
2× [27] c.t. prior	0.7	0.164	$0.727^{+0.093}_{-0.087}$	0.36	$0.152^{+0.034}_{-0.026}$	-0.39	$0.730^{+0.075}_{-0.072}$	0.59
EDE	0.722	0.147	$0.754^{+0.114}_{-0.098}$	0.43	$0.132^{+0.038}_{-0.031}$	-0.48	$0.745^{+0.099}_{-0.077}$	0.45
Scale covariance by 10× volume	0.722	0.147	$0.745^{+0.033}_{-0.035}$	0.31	$0.138^{+0.014}_{-0.011}$	-0.29	$0.739^{+0.033}_{-0.029}$	0.33
[27] counterterm prior	0.722	0.147	$0.761^{+0.110}_{-0.090}$	0.53	$0.125^{+0.032}_{-0.026}$	-0.71	$0.761^{+0.092}_{-0.078}$	0.76
[27] counterterm prior + scale cov. by 10× vol.	0.722	0.147	$0.740^{+0.035}_{-0.036}$	0.24	$0.139^{+0.014}_{-0.013}$	-0.26	$0.736^{+0.035}_{-0.032}$	0.27

TABLE III. Parameter recovery tests for Nseries mocks (first block) and noiseless early dark energy (EDE) theory vector (second block). Two data combinations are shown for each test: both use f_b from the BAO amplitude and an $\Omega_b h^2$ prior with a BBN-like width. “BAO only” uses Ω_m constraints from the Alcock-Paczynski ratio (D_A/D_H) from BAO only, and “Add voids” includes tighter AP ratio constraints from voids. $n\sigma$ deviations are in units of the Nseries errorbar, using the appropriate upper or lower errorbar, except for the cases with increased covariance matrix (z_3 , z_3 -NGC, z_3 -SGC, z_3 -NGC + SGC), where the errorbar from that fit is used.

$\Omega_m h^2$ and γ_B . Hence we prefer to use $T_c(k)$ rather than $T_0(k)$ to split the transfer function.

These cosmological parameter degeneracies motivate our further consideration of template-style fits, where the cosmological dependence of the broadband is fixed and marginalized over with other nuisance parameters. The template fits thus assume that *only* the baryon fraction affects the split between transfer functions, since all other cosmological parameters are fixed. As shown in [68] and described above, the largest additional dependence comes from baryonic suppression of perturbations and the growth rate; at fixed ω_b , the Silk damping scale is only weakly dependent on $\Omega_m h^2$, and the time-dependence of the sound speed, frequency, and thus amplitude only depends on ω_b . Thus, the template fit assumes that matter growth from equality to decoupling matches that in the best-fit Λ CDM model. One might worry that this assumption limits the applicability of our method to extended models such as Early Dark Energy. However, the early growth history has been constrained by measurements of the early Integrated Sachs-Wolfe (ISW) effect [70–73], in which the Λ CDM early-ISW amplitude is allowed to vary freely. In the ISW effect [74, 75], time-varying gravitational potentials contribute to the CMB anisotropies; since potentials are constant in matter domination, the time variation either happens at early times, in the transition from radiation to matter domination, or at late times, when dark energy becomes non-negligible. The early ISW effect is thus a direct probe of the growth rate at the transition from radiation to matter domination, exactly overlapping the epoch from equality to drag that affects the BAO amplitude. Ref. [73] shows that the early ISW amplitude is constrained within 3% and agrees within 1σ of the Λ CDM prediction. This drives $\Omega_{cdm} h^2$ higher in Early Dark Energy fits to the CMB; if the non-EDE param-

eters were fixed to their Λ CDM values, the early ISW amplitude would be over-predicted by 20%. These strong constraints on the early growth history therefore suggest that a template-based approach is reasonable.

3. Nuisance parameter priors

The dependence on the priors applied to nuisance parameters [e.g. 39, 76–80] are a significant concern in this analysis. The three AbacusSummit Λ CDM noiseless theory vectors (cosm131, cosm139, and cosm130) show significant biases of 0.3–0.5 σ on f_b and h , even though they are generated from the same theory that we use for the fits and thus the true cosmology has $\chi^2 = 0$. One option is to instead perform a frequentist analysis and determine the maximum a posteriori (MAP) point and profile likelihoods. However, this option has several disadvantages: lack of suitable tools compared to tools available for Bayesian analysis (although see Procoli [81] and PROSPECT [82], which were released during the preparation of this manuscript); inability to interpret the frequentist results in a Bayesian framework; and losing the advantages of the analytic marginalization over b_{Γ_3} , c_0 , c_2 , c_4 , \tilde{c} , P_{shot} , a_0 and a_2 , which adds 8 extra nuisance parameters and leads to a corresponding increase in the difficulty of the minimization problem.

Part of the difficulty arises from skewed marginalized posteriors (Fig. 7). We mitigate the effect of the skewed posteriors by choosing more robust statistics: we quote the maximum of the marginalized posterior, rather than the mean or the median. We quote the (generally asymmetric) 68% highest-density interval as the errorbars (identical to the M-HPD statistic in [83]). The shifts between the mean, median, and maximum are especially dramatic for the noiseless theory vector tests; we find

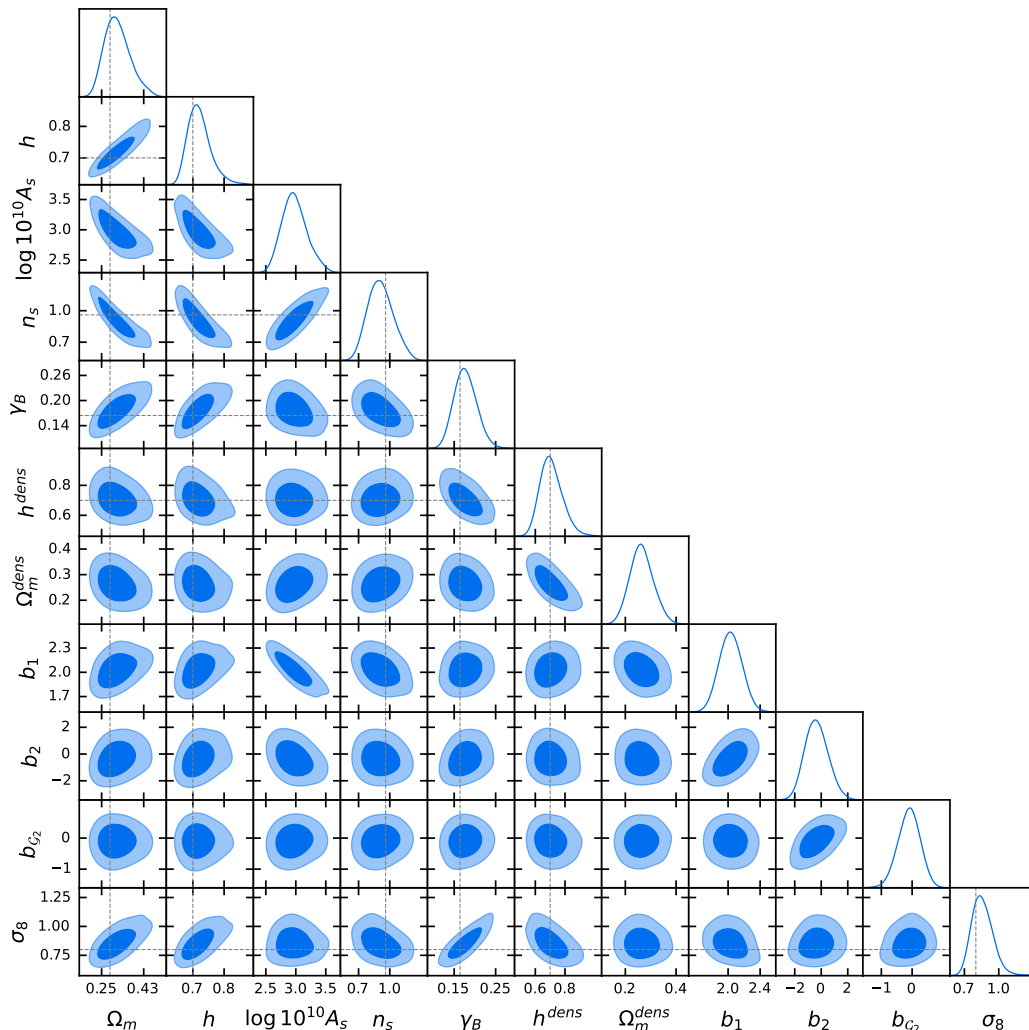


FIG. 5. Parameter constraints for the full-shape plus BAO amplitude model fitted to the mean of the 84 Nseries mocks, using the covariance for the BOSS z_3 NGC region, scaled to the entire BOSS volume. The data vector consists of the power spectrum monopole, quadrupole, and hexadecapole at $0.01 < k < 0.2 h \text{ Mpc}^{-1}$, combined with the ratio of the BAO scaling parameters, $\alpha_{\perp}/\alpha_{\parallel}$ and a Gaussian prior on ω_b with a width equal to current BBN constraints. We vary the standard Λ CDM parameters as well as two extra parameters, h^{dens} and Ω_m^{dens} , which only affect the BAO amplitude and the Alcock-Paczynski parameters. From these varied parameters we derive the BAO amplitude estimate γ_B . The galaxy biases b_1 , b_2 , and b_{G_2} are sampled in the MCMC chain, whereas b_{Γ_3} , the counterterms, and the stochastic parameters are marginalized analytically and hence not shown.

that h is biased high by $0.5\text{--}0.6\sigma$ when using the mean or median for the three Λ CDM theory vectors, but only 0.3σ when using the maximum. The EDE noiseless theory vector has even larger biases, with biases of $0.8\text{--}0.9\sigma$ for the mean and median, but only 0.5σ for the maximum. In contrast, the posteriors are less skewed for Nseries, with biases of 0.12σ high for the mean, 0.03σ high for the median, and 0.13σ low for the maximum. This result emphasizes the importance of using a wide variety of test cases, rather than one N -body mock run with a single cosmology. If the data prefers different parameters from that mock, the prior effects may be different, and the data may be biased in a different way than

the mock.

We also find that shrinking the priors on the counterterms and stochastic parameters improves parameter recovery when fitting the EDE theory vector. Since early dark energy leads to notable changes in the power spectrum compared to Λ CDM (see Fig. 5 in [4]), parameter biases in the EDE test could indicate model misspecification. Indeed, we find biases on h of 0.53σ and 0.76σ when using the same counterterm and stochastic term prior as [27] (for the “BAO only” and “add voids” cases, respectively). However, shrinking the covariance by a factor of 10 (corresponding to 10 times more volume) leads to minimal biases on h (0.24σ and 0.27σ), implying that

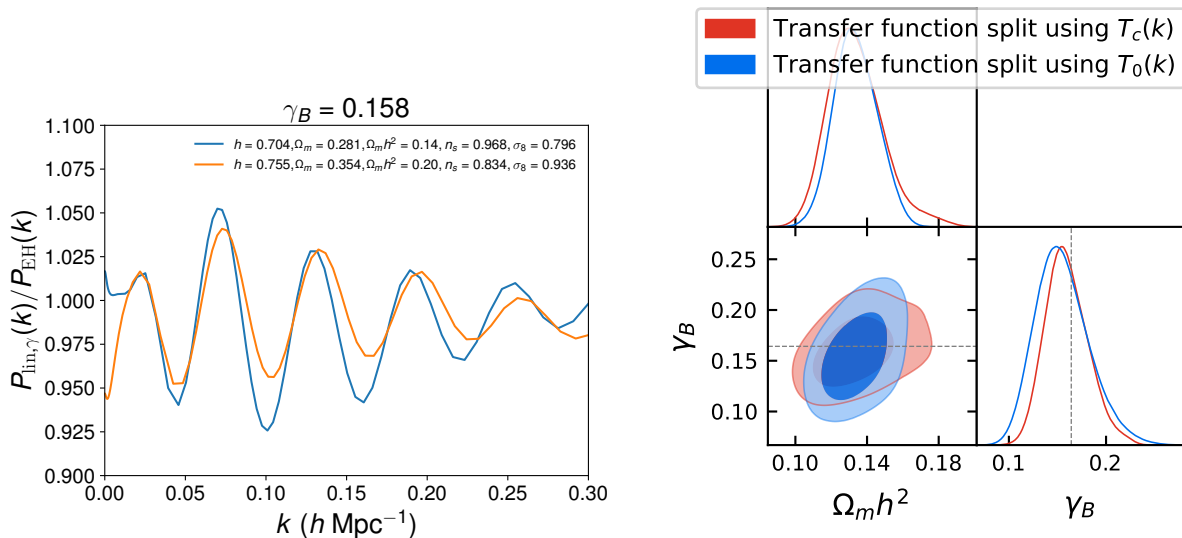


FIG. 6. *Left*: Comparison between two sets of parameters chosen along the Ω_m - γ_B degeneracy, adjusting both so that γ_B is the same ($\gamma_B = 0.158$). We plot the ratio between the linear power spectrum with adjusted BAO amplitude, $P_{\text{lin},\gamma}(k)$, and a smooth power spectrum consisting of the Eisenstein & Hu [6] fitting function plus a linear correction due to the change in shape of $P_{\text{lin},\gamma}$ in the second set where γ_B differs significantly from the true f_b . The BAO wiggles are notably larger for smaller $\Omega_m h^2$ despite the fact that γ_B is the same, leading to a degeneracy between $\Omega_b h^2$ and γ_B . *Right*: Using the CDM transfer function $T_c(k)$ (Eq. 17 in [6]) rather than the zero-baryon transfer function $T_0(k)$ (Eq. 29 in [6]) tightens constraints on γ_B by 20% by bringing in additional shape information, mitigating the $\Omega_m h^2$ - γ_B degeneracy.

the biases are due to prior effects, not model misspecification. We cannot shrink the covariance when running on data, but we can reduce the widths of priors, which also mitigates the dependence on the prior. We find that halving the counterterm and stochastic term priors leads to reduced biases of 0.43σ and 0.45σ on h , which are more robust to scaling the covariance down by a factor of 10 (dropping to 0.31σ and 0.33σ). Shrinking these priors does reduce the errors on h and f_b by $\sim 10\%$, raising the possibility that our errors are underestimated; however, we consider this a reasonable price to pay for reducing the biases on h and f_b .

Given the impact of the nuisance term priors, we test if parameter recovery is different when using covariances corresponding to each separate region, rather than to the combined BOSS volume. This is important because of the lack of realistic N -body mocks with full coverage of the BOSS region in all redshifts and hemispheres;⁹ hence we have only one data vector for Nseries (coming from a volume slightly larger than z_3 NGC) rather than the necessary four for a fully realistic test. If parameter recovery is less accurate when the covariance is larger, our

strategy of testing Nseries with a covariance re-scaled to the entire BOSS volume could underestimate parameter biases. When instead using a covariance scaled to the z_3 volume, or the z_3 NGC volume, we do find some notable shifts in the parameters, though all biases stay below 0.3σ . The considerably smaller z_3 -SGC has considerably larger biases, though these remain a relatively small fraction (0.4 – 0.55σ) of the much larger errorbars. However, combining multiple regions in the data should suppress the impact of large fluctuations in the SGC fits. We test this by comparing the results using the z_3 -scaled covariance to the combined z_3 NGC and SGC results. For the BAO-only case, the overall bias on h is similar, though the z_3 covariance is biased low and the NGC + SGC case is biased high. The baryon fraction results are somewhat less consistent, with NGC + SGC having a larger bias of almost 0.4σ . However, when adding the void AP information, the results on h are very similar, though the NGC+SGC combination does have a 7% larger errorbar.

We also test whether adding the real-space power spectrum estimate Q_0 improves our constraints. Q_0 is a linear combination of the monopole, quadrupole, and hexadecapole (equal to the $\mu = 0$ moment of the power spectrum) in which redshift-space distortions approximately cancel [32]. This allows Q_0 to be modelled to $k_{\text{max}} = 0.4 h \text{ Mpc}^{-1}$ in perturbation theory, in contrast to the $k_{\text{max}} = 0.2 h \text{ Mpc}^{-1}$ achievable for the multipoles. The higher k_{max} means that Q_0 contains more BAO wiggles and thus potentially offers a tighter constraint on the baryon fraction. We find that adding Q_0 offers 7–10%

⁹ The PATCHY approximate N -body mocks cover the entire BOSS footprint, but may not correctly describe the Universe on large scales. [46] find that they underestimate the BAO signal, with a larger damping than calculated from the Zel'dovich approximation and a larger damping than in the BOSS data. [84] find deviations between the Patchy mocks and their perturbative halo model at large scales.

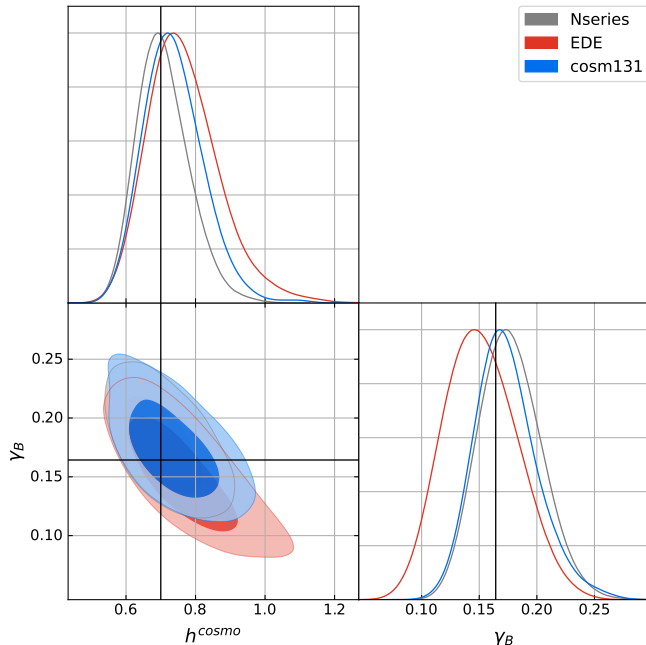


FIG. 7. Marginalized posteriors on h and γ_B from Nseries, EDE, and AbacusSummit cosm131 (a Λ CDM cosmology) tests. The cosm131 and particularly the EDE 1D posteriors are notably skewed; hence we use the maximum of the 1D posterior rather than the mean or median as a more robust statistic. The EDE and cosm131 posteriors are shifted so that their true cosmology coincides with the Nseries cosmology, $h = 0.7$ and $f_b = 0.164$ (solid black line).

tighter constraints on h , though only minimally stronger constraints on f_b . Due to the minimal statistical gains, we do not include Q_0 in our fiducial analysis.

We find similar results when doubling the bias or counterterm priors (matching the counterterm priors of [27]). Fitting to the Nseries mocks and doubling the bias priors leads to similarly tight constraints on h and f_b in the BAO only case, and 20% wider constraints on h when adding voids. The parameter biases in this case are very small, $< 0.1\sigma$. We also test doubling the counterterm prior of [27]. This leads to larger biases of $\sim 0.4\sigma$ on h and f_b , consistent with the argument that a larger counterterm prior leads to larger biases from prior effects. We therefore use our fiducial counterterm priors (half the width of [27]), since they lead to smaller parameter biases.

4. Fitting noiseless theory vectors

We compare the true and fitted values of h and f_b for the AbacusSummit and EDE noiseless theory vectors in Fig. 8. We find a consistent bias towards higher h and lower f_b . When using only the BAO AP ratio, the mean bias on h is 0.12σ (0.37σ) for AbacusSummit (EDE); the mean bias on f_b is -0.32σ (-0.38σ). When also adding the

voids AP ratio, the mean bias is 0.22σ (0.32σ). The AbacusSummit noiseless mock tests give significantly smaller biases on H_0 than the EDE noiseless mock tests. This is due to the inclusion of 3 w_0w_a cosmologies, in which the late-time change to the expansion history biases the AP measurement of Ω_m and leads to a bias towards smaller values of h , rather than the bias towards larger h seen in the other AbacusSummit mock tests and in the EDE tests. Excluding these three mock tests leads to a mean bias on h of 0.22σ (0.33σ) for the BAO AP ratio (voids) case.

The scatter about these biases is relatively tight, 0.2 – 0.4σ . The biases in the EDE and AbacusSummit tests are quite similar (excluding the w_0w_a cosmologies as mentioned above), all around 0.3 – 0.5σ . Thus, they could be entirely consistent with prior volume projection effects. Furthermore, the biases on Nseries have the opposite sign, making it difficult to tell whether our method is truly biased towards high h . At the current constraining power of the data, we regard these biases as negligible, and further point out that the combination of the full-shape and template fits offers a powerful consistency check with quite different systematics. For future data, we are encouraged by the results of the volume scaling test (particularly when restoring our counterterm prior to match that of [27]), which suggests that as the data gets more precise, the biases will become smaller. If the bias results from prior effects, we expect it to improve with the statistical error rather than remaining as a systematic floor.

B. Pre-reconstruction template fits

1. Fits to the Nseries mocks

We summarize the results of the pre-reconstruction template fits to the correlation function in Table IV. When fitting to the Nseries mocks, the marginalized constraint on γ_B slightly depends on the scaling of the covariance matrix; we see a 0.42σ bias on γ_B when using the covariance matrix from BOSS z_3 , but only a 0.09σ bias when scaling this covariance matrix to the entire BOSS volume. These results are quite similar to the full-shape fits to $P(k)$, with γ_B changing from 0.171 using full-shape fits to 0.176 using template fits, and the errorbar on the combined BOSS volume is nearly the same (0.027 vs. 0.029).

Our measurements of the BAO shifting parameters are very similar to those presented in [47] for α_\perp (they find 0.977 ± 0.002 , with a much smaller error since they scale the covariance matrix to the Nseries volume), but different for α_\parallel (they find 0.983 ± 0.0041). There are significant differences in the pipeline: they use a linear fit with $b_\partial = 0$ and fix the damping parameters; so it is perhaps not surprising that the more poorly constrained α_\parallel is different.

We show a triangle plot of parameter constraints in

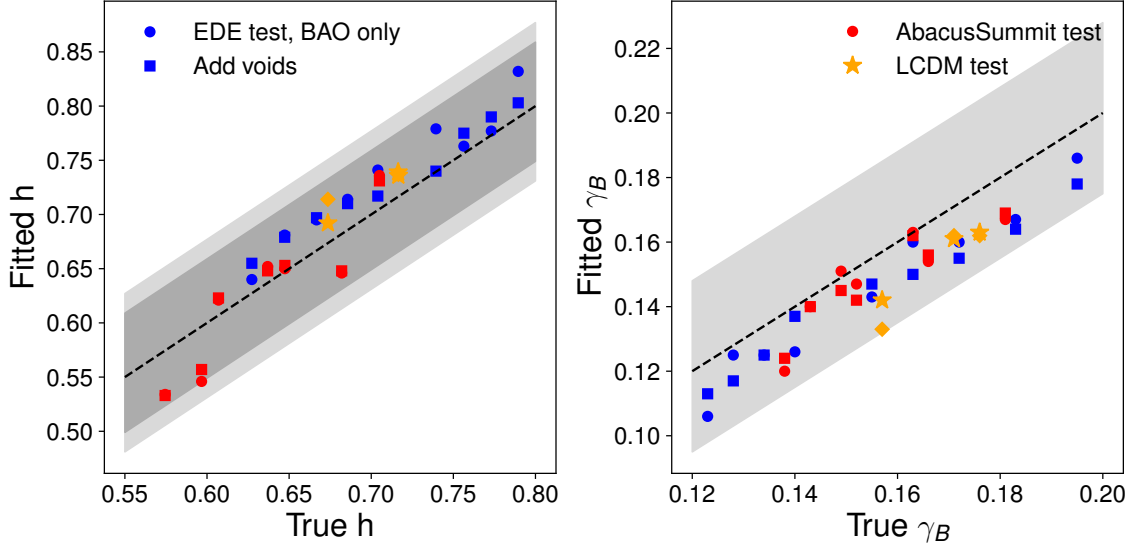


FIG. 8. Fitted and true h (left) and γ_B (right) for noiseless theory vector tests. Tests of EDE cosmology are shown in blue, either using Alcock-Paczynski constraints from BAO (circles) or stronger AP constraints from voids (squares, with half the Ω_m error of BAO AP). AbacusSummit tests are shown in red and orange; the 3 AbacusSummit theory vectors generated in a Λ CDM cosmology are orange stars and diamonds, whereas the other 7 AbacusSummit theory vectors are red. Errorbars are the h and γ_B constraints from the Nseries mock test with the covariance rescaled to the BOSS volume; the inner errorbands on the left panel are the errorbars when adding AP information from voids. While both the AbacusSummit and EDE tests are biased, they are both biased by a similar amount, and the Λ CDM tests are no less biased than the others (even though the best-fit model has $\chi^2 = 0$ by definition in the Λ CDM test). Moreover, all biases are a fraction of a σ , generally $< 0.5\sigma$.

Data	γ_{BAO}	σ_γ	f_b	$n\sigma$	α_\perp	σ_{α_\perp}	True	$n\sigma$	α_\parallel	$\sigma_{\alpha_\parallel}$	True	$n\sigma$
Nseries	0.176	0.038	0.164	0.42	0.979	0.021	0.979	-0.00	1.001	0.062	0.988	0.36
z_1+z_3 Cov.	0.167	0.029	0.164	0.09	0.979	0.013	0.979	0.03	1.000	0.036	0.988	0.35
Λ CDM	0.153	0.033	0.155	-0.06	0.998	0.020	1.000	-0.17	1.010	0.065	1.000	0.29
EDE	0.166	0.029	0.174	-0.29	1.017	0.017	1.019	-0.17	1.036	0.047	1.022	0.38
$b_\partial = -10$	0.158	0.033	0.155	0.09	0.996	0.022	1.000	-0.30	1.011	0.064	1.000	0.31
$b_\partial = 10$	0.154	0.033	0.155	-0.03	0.998	0.018	1.000	-0.19	1.008	0.058	1.000	0.23
$\Sigma_{xy} = 3$	0.149	0.030	0.155	-0.21	0.997	0.012	1.000	-0.23	1.007	0.030	1.000	0.20
$\Sigma_{xy} = 12$	0.190	0.052	0.155	1.22	0.992	0.075	1.000	-0.59	0.985	0.094	1.000	-0.41
$\Sigma_{\text{fog}} = 0$	0.156	0.031	0.155	0.03	0.996	0.020	1.000	-0.33	1.014	0.055	1.000	0.39
$\Sigma_{\text{fog}} = 8$	0.151	0.033	0.155	-0.14	0.998	0.022	1.000	-0.14	1.010	0.078	1.000	0.28
$\Sigma m_\nu = 0.2\text{eV}$	0.162	0.033	0.164	-0.05	1.001	0.019	1.000	0.11	1.017	0.057	1.000	0.48
$N_{\text{eff}} = 3.82$	0.152	0.031	0.149	0.11	0.990	0.019	0.994	-0.30	1.005	0.058	0.999	0.16
Spline P_{nw}	0.156	0.032	0.155	0.04	0.997	0.020	1.000	-0.20	1.016	0.062	1.000	0.43

TABLE IV. Template fits to the pre-reconstruction correlation function. The top row shows results on the Nseries mocks using the BOSS z_3 covariance matrix; the second row uses the same data vector but the covariance is scaled to match the combined z_1 and z_3 volume. Since we fit γ_B separately in the two redshift bins and then combine them, we use runs with the z_3 covariance to determine biases on γ_B , but compare to the errorbar from the scaled covariance runs. The next set shows results from input noiseless theory vectors with varying nuisance parameters, a different choice for how to split P_w and P_{nw} , and varying cosmologies (Early Dark Energy, larger neutrino mass, and N_{eff}).

Fig. 9. γ_B is not well correlated with the BAO shift parameters α_\parallel and α_\perp or the biases B_0 and B_2 . It is somewhat degenerate with the broadband shifting $q_{\parallel, BB}$, the derivative bias b_∂ and the smoothing scale Σ_{sm} . The degeneracy with b_∂ recalls the b_2 - γ_B degeneracy in the full-shape fits, and the b_2 contributions to the nonlinear BAO shift. The simple model that we use cannot generate nonlinear BAO shifts, since these come from one-loop terms. However, the $k^2 P_{\text{lin}}$ template, multiplied by

b_∂ , must have a different scale dependence from P_{lin} and therefore can change the amplitude of the BAO peak. Likewise, increasing the BAO damping Σ_{sm} suppresses the BAO peak, and therefore must be compensated by increasing γ_B , leading to a γ_B - Σ_{sm}^2 degeneracy.

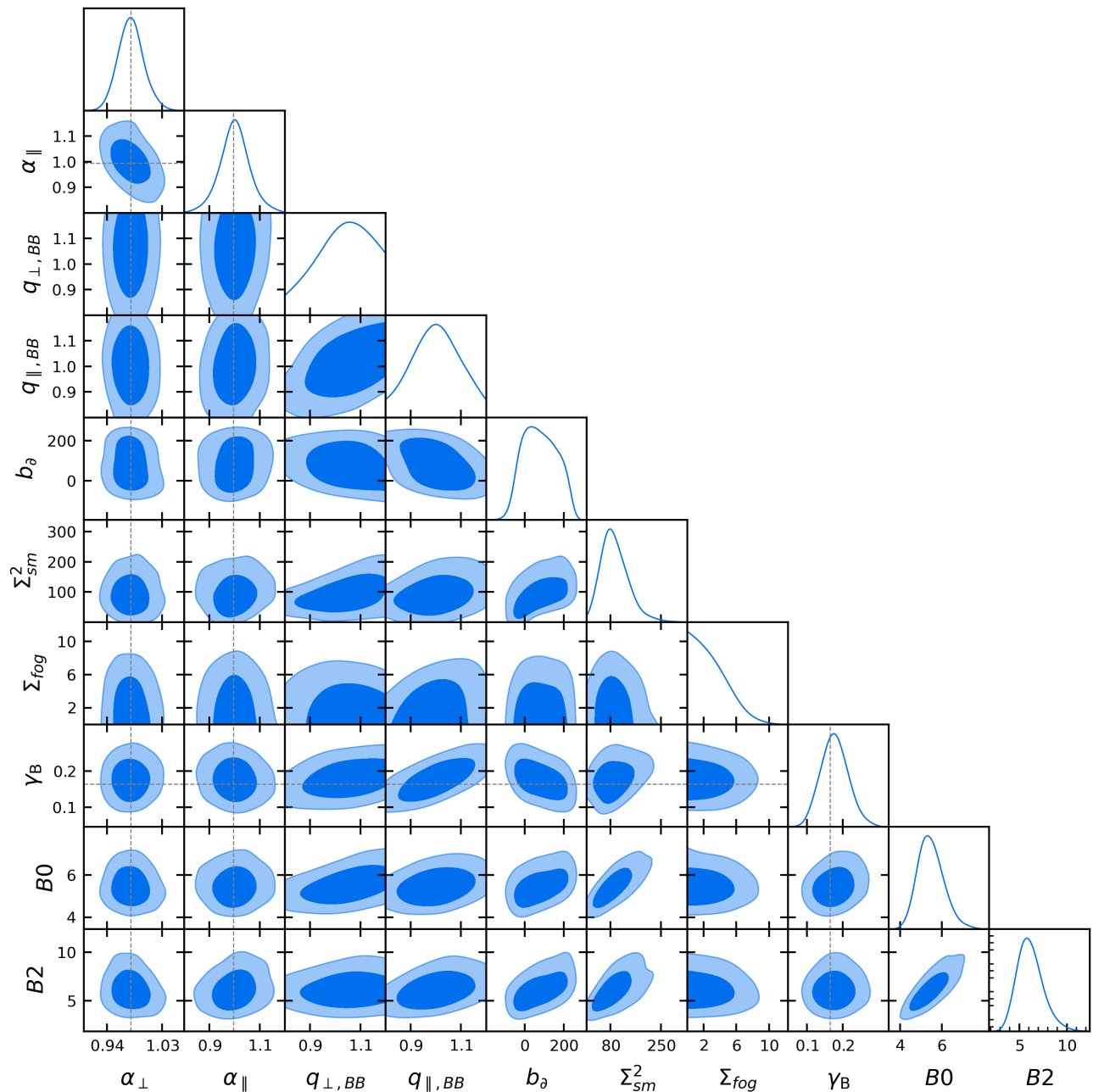


FIG. 9. Parameter constraints for the damped BAO template model fitted to the pre-reconstruction correlation function monopole and quadrupole at $50 < r < 150 h^{-1} \text{Mpc}$, averaged over the 84 Nseries mocks. We use the covariance for BOSS z_3 (combining NGC and SGC). The polynomial terms are marginalized analytically and hence not shown in this plot.

2. Robustness of the modeling

The amplitude of the baryon signature in the pre-reconstruction template fits is quite robust to extensions to ΛCDM , even as we always use the same fiducial ΛCDM model for the template. We find $< 0.3\sigma$ biases on γ_B when using an EDE cosmology with a different sound horizon as the input data, or when using a cosmology

with a higher neutrino mass or N_{eff} , inducing a phase shift in the BAO wiggles. The BAO scaling parameters α_{\parallel} and α_{\perp} are also recovered well ($< 0.3\sigma$ bias) in all cases except for α_{\parallel} when $\Sigma m_{\nu} = 0.2 \text{ eV}$, in which case the recovery is modestly worse, 0.5σ . This is similar to past results showing that the BAO scale is robust to changes in N_{eff} and Σm_{ν} [85].

We also show that the recovered baryon fraction and

shift parameters are robust to changing the true values of the nuisance parameters b_∂ , Σ_{xy} , and Σ_{fog} , except when the damping parameter Σ_{xy} becomes very large at $12 h^{-1} \text{Mpc}$. In this case, the BAO amplitude is highly suppressed and poorly detected. The bias on γ_B is still 0.67σ even if we measured it relative to the larger $\sigma_{\gamma_B} = 0.052$ from this fit, rather than $\sigma_{\gamma_B} = 0.029$ from the Nseries fit with scaled-down covariance. However, it isn't surprising that our model doesn't work well when the BAO shifts are so poorly constrained, and models with such a high damping parameter are robustly excluded by both the data and theoretical considerations anyway. Finally, we test the dependence of our model on inaccuracies in the [6] transfer function fits by replacing the smooth P_{nw} used to construct the mocks with a Fourier-transformed spline fit to two windows in the correlation function on either side of the BAO bump. This leads to negligible changes in the fitted parameters.

3. Fitting noiseless theory vectors

Finally, we test whether the baryon fraction is recovered well when changing the ΛCDM parameters of the input noiseless theory vector (Fig. 10). Here we find small but persistent systemic biases on γ_B (average $-0.36 \pm 0.15\sigma$), α_\perp (average $-0.19 \pm 0.13\sigma$) and α_\parallel (average $0.34 \pm 0.10\sigma$). These biases would be much larger if we only included a constant term in the monopole and not the quadrupole (matching our treatment of the post-reconstruction correlation function), -0.55σ , -0.46σ , and 0.61σ in γ_B , α_\perp and α_\parallel . This motivates the inclusion of the extra constant term in the quadrupole. Likewise, the biases would also be larger if we allowed a wider prior on b_∂ , -0.64σ , -0.33σ , and 0.46σ in γ_B , α_\perp and α_\parallel , if we allowed a flat prior on b_∂ between -1000 and 1000. However, shrinking the b_∂ prior too much leads to unacceptably large biases on Nseries; hence we choose a flat prior on b_∂ between -250 and 250 to balance these concerns.

C. Post-reconstruction template fits

1. Fits to the Nseries mocks

We recover the true values of γ_B , α_\parallel , α_\perp with biases $< 0.4\sigma$ when fitting to the mean of the 84 Nseries mocks (Table V). These results are much less dependent on the priors than the pre-reconstruction results, with shifts of $< 0.05\sigma$ in all parameters. We find good agreement between the pre and post-reconstruction results, particularly in the α parameters; as in the pre-reconstruction results, the bias that we measure on α_\parallel has opposite sign to [47].

If we used the linear BAO model of Ref. [42], rather than the Ref. [44] model, we would find a significant bias on γ_B on the Nseries mocks, with $\gamma_B = 0.189 \pm 0.035$

(0.71σ bias). This is largely due to the absence of the derivative bias, b_∂ , which adds power on small scales to partially emulate the effects of nonlinear structure formation. By adding a component $\propto k^2 P_{\text{lin}}$, which has a different weighting of the BAO oscillations, b_∂ can cause the amplitude of the BAO peak to change.

We place an informative prior on b_∂ , a Gaussian centered at 15 with a standard deviation of 5. This value of b_∂ is motivated by the best-fit values of b_∂ in the EFT1 model of ref. [44], $b_\partial \sim 15$.¹⁰ In this model, we find $\gamma_B = 0.171 \pm 0.030$, an 0.31σ offset from the truth (using the reduced errorbar from the fit with the covariance scaled to the full BOSS volume). This result is dependent on the b_∂ prior: if we do not impose any prior on b_∂ , we find $\gamma_B = 0.191 \pm 0.034$ and $b_\partial = -4.0 \pm 12.8$. The b_∂ prior allows us to recover an unbiased value of the baryon fraction, at the price of shifting the nuisance parameters ($\sim 1\sigma$ shifts in Σ_{fog} and Σ_{sm}) and a slightly worse fit ($\Delta\chi^2 = 3$). Essentially, the b_∂ prior is a simulation-based constraint on the impact of nonlinear structure formation on the baryon fraction.

We show a triangle plot of parameter constraints in Fig. 11. The degeneracies are similar to the pre-reconstruction case in Fig. 9, but generally less prominent. While γ_B appears to be much less degenerate with b_∂ in the post-reconstruction case, we note that this is largely due to the restrictive prior placed on b_∂ post-reconstruction.

2. Robustness of the modeling

We use a considerably more restricted set of broadband polynomials than the standard BAO method used in [18, 42]. Rather than the 6 polynomials used in that model (3 for each multipole), we use a single constant term for the monopole. We also vary four other physically motivated broadband terms¹¹: 2 shift parameters $q_{\parallel, BB}$ and $q_{\perp, BB}$, Σ_{fog} and b_∂ . The reason for this is the strong degeneracy between higher-order polynomials and the BAO amplitude, which can partially mimic the BAO bump and distort the size of the broadband that the BAO bump is compared with to constrain the BAO amplitude. Simultaneously fitting γ_B and the 6 polynomial terms leads to a nearly unconstrained $\gamma_B = 0.31 \pm 0.18$. Despite the weak constraint on γ_B , the BAO feature is still detected at high significance (8.3σ),¹² due to the highly non-Gaussian shape of the γ_B posterior. Most

¹⁰ This result depends mildly on redshift but not on linear bias, even over a large range in mean halo mass (Fig. 14 in [44]). This suggests that the γ_B measurement is insensitive to the details of the halo occupation distribution.

¹¹ Three of these parameters are truly free, while b_∂ is prior-dominated.

¹² Defined as the square-root in the difference of χ^2 between the best-fit model with $\gamma = 0$ (no BAO) and fixing $\gamma = 0.1643$.

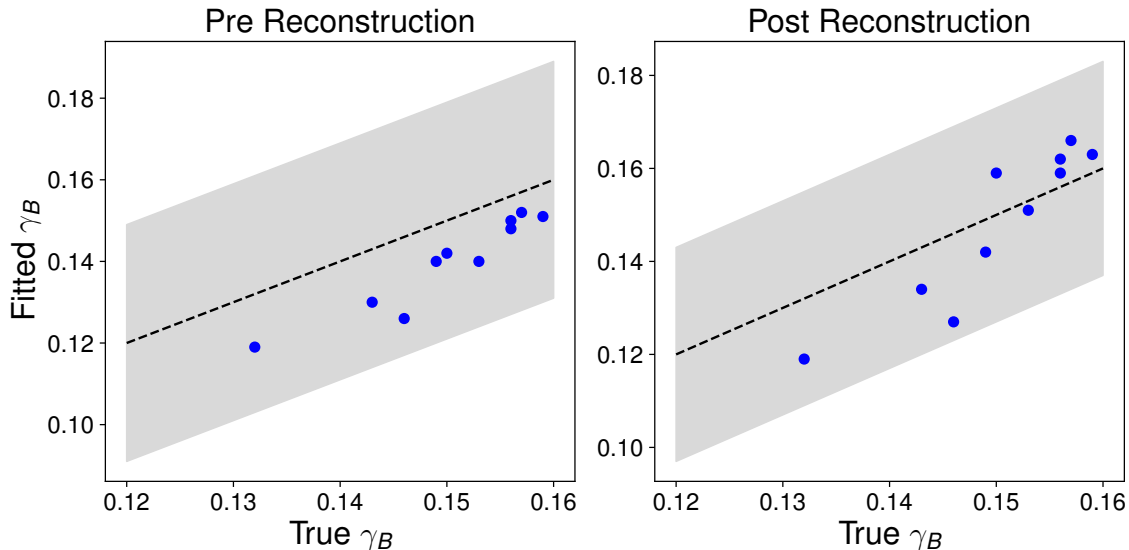


FIG. 10. Fitted and true γ_B for noiseless theory vector tests with varying Λ CDM parameters, both for pre-reconstruction template fits (*left*) and post-reconstruction (*right*). Gray errorbands are the 1σ errors from Nseries fit with the BOSS z_3 covariance scaled to the entire BOSS volume.

Data	γ_{BAO}	σ_γ	f_b	$n\sigma$	α_\perp	σ_{α_\perp}	True	$n\sigma$	α_\parallel	$\sigma_{\alpha_\parallel}$	True	$n\sigma$
Nseries	0.171	0.030	0.164	0.31	0.978	0.012	0.979	-0.09	0.995	0.025	0.988	0.43
z_1+z_3 Cov.	0.170	0.023	0.164	0.27	0.978	0.008	0.979	-0.12	0.994	0.016	0.988	0.42
Λ CDM	0.164	0.034	0.155	0.37	0.999	0.013	1.000	-0.12	1.002	0.026	1.000	0.10
EDE	0.178	0.031	0.174	0.19	1.019	0.010	1.019	0.02	1.023	0.021	1.022	0.09
$b_\partial = 5$	0.153	0.034	0.155	-0.10	0.998	0.015	1.000	-0.18	1.002	0.028	1.000	0.12
$b_\partial = 25$	0.176	0.036	0.155	0.89	1.000	0.012	1.000	-0.04	0.999	0.023	1.000	-0.04
$\Sigma_{\text{sm}} = 8$	0.157	0.032	0.155	0.10	0.999	0.012	1.000	-0.10	1.000	0.025	1.000	0.03
$\Sigma_{\text{sm}} = 24$	0.157	0.032	0.155	0.08	1.000	0.016	1.000	-0.05	1.001	0.029	1.000	0.07
$\Sigma_{\text{fog}} = 0$	0.163	0.034	0.155	0.34	0.999	0.013	1.000	-0.11	1.001	0.025	1.000	0.08
$\Sigma_{\text{fog}} = 8$	0.162	0.034	0.155	0.30	0.998	0.013	1.000	-0.21	1.002	0.026	1.000	0.12
$\Sigma m_\nu = 0.2\text{eV}$	0.166	0.031	0.164	0.09	1.003	0.012	1.000	0.44	1.005	0.023	1.000	0.35
$N_{\text{eff}} = 3.82$	0.157	0.033	0.149	0.36	0.992	0.013	0.994	-0.27	0.999	0.025	0.999	0.01
Spline P_{nw}	0.170	0.032	0.155	0.64	0.997	0.012	1.000	-0.36	0.999	0.022	1.000	-0.06

TABLE V. Template fits to the post-reconstruction correlation function. Format is the same as Table IV.

of the loss of constraining power comes from the $1/r^2$ term. We furthermore find that the other two polynomial terms are not favored in fits to data (i.e. they do not improve the goodness of fit by more than expected for adding extra degrees of freedom). However, we keep the constant term in the monopole to marginalize over the potential impact of observational systematics, which produce nearly constant changes in the monopole on the large scales that we fit ($r > 50 h^{-1}$ Mpc). This is shown in Fig. 6 in [18], which demonstrates that turning the stellar density weights off changes the monopole by an additive constant on large scales, and does not affect the quadrupole.¹³

As in the pre-reconstruction case, we find good recovery (generally $< 0.3\sigma$) of γ_B , α_\parallel and α_\perp for the beyond- Λ CDM models considered: early dark energy, massive neutrinos, and extra relativistic degrees of freedom. We also find that γ_B is insensitive to changes in the nuisance parameters, with the exception of b_∂ . Large values of b_∂ create a bias towards high γ_B . Given the b_∂ - γ_B degeneracy discussed before and noted for the pre-reconstruction case, this is not surprising.

¹³ Fig. 6 in [18] shows a large scale-dependent impact of seeing weights in the LOWZE3 region; however, this is $< 10\%$ of the

total BOSS area and the impact of seeing weights are negligible across the entire footprint.

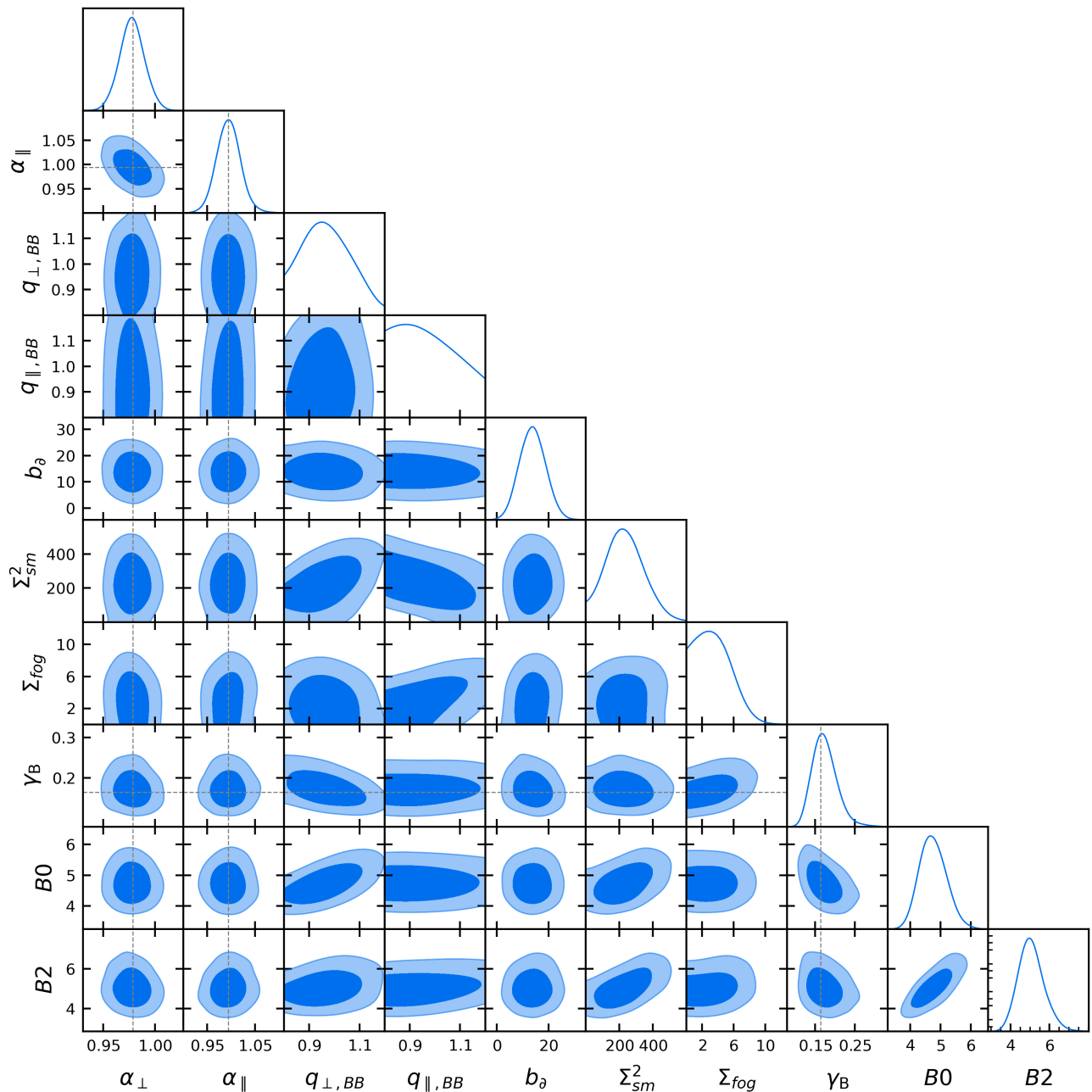


FIG. 11. Same as Fig. 9, but for the post-reconstruction correlation function averaged over the 84 Nseries mocks.

3. Fitting noiseless theory vectors

The post-reconstruction fits are less sensitive to changing the Λ CDM parameters than the pre-reconstruction fits (Fig. 10). We find a mean bias of -0.09σ and a standard deviation of 0.40σ across the ten cosmologies tested. Additionally, α_{\perp} and α_{\parallel} are considerably less biased than in the pre-reconstruction case, with biases of -0.12σ and 0.10σ , respectively. The considerably weaker dependence on the fiducial cosmology in the post-reconstruction case

may be due to the sharper BAO peak, which is easier to distinguish from the broadband and hence less degenerate with the cosmological parameters that affect its shape. The scatter when changing cosmologies is much larger if we instead scale the entire correlation function by α_{\parallel} and α_{\perp} (dropping the two extra broadband shift

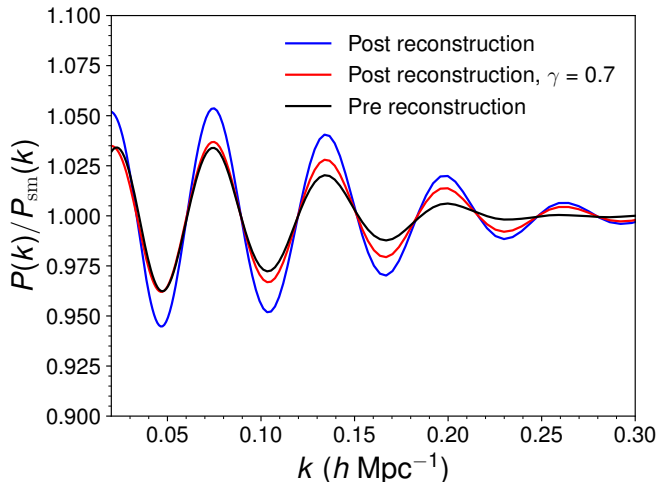


FIG. 12. The oscillatory portion of the power spectrum, $P(k)/P_{\text{nw}}(k)$, for a pre-reconstruction model, and a post-reconstruction model with the default γ_B and with $\gamma_B = 0.7$. The effects of reconstruction (or equivalently, reducing the BAO damping) and changing γ_B are distinct; reconstruction sharpens the higher- k peaks whereas γ_B affects all peaks equally. Therefore, reconstruction does not lead to tighter constraints on γ_B .

parameters), with a 0.74σ scatter in γ_B .¹⁴ While the baseline constraints on Nseries are very similar whether we use the standard two scaling parameters or the new method with four scaling parameters, we favor using four scaling parameters because it decouples γ_B from the broadband changing with the fiducial cosmology.

D. Summary of mock tests

We have demonstrated three separate methods to fit the amplitude of the baryon signature that recover similar results from Nseries mocks: $0.172^{+0.031}_{-0.027}$ for full-shape perturbative fitting to $P(k)$; 0.167 ± 0.029 for pre-reconstruction template fitting to $\xi(r)$; and 0.170 ± 0.023 for post-reconstruction template fitting, compared to the true value of $f_b = 0.164$. The constraining power of the post-reconstruction fits is slightly better, with a 20% reduction in the errorbar. However, this is largely attributable to the informative prior on b_θ ; if we instead

¹⁴ This can be mitigated by adding the ShapeFit parameter m [86] to marginalize over the impact of the fiducial cosmology. A relatively narrow prior on m between -0.1 and 0.1 encompasses the range in cosmological parameters constrained by the BOSS full shape fits, reducing the scatter in γ_B to 0.31σ without adding significant prior volume effects. However, in our fiducial method with 4 scaling parameters, adding m as an additional parameter does not reduce the scatter in γ_B when varying cosmology, and generally has minimal impact on the results. For simplicity (and due to the arbitrariness of the chosen priors in m to avoid prior effects), we therefore do not vary m in our baseline model.

place the same broad flat prior on b_θ that is used for the pre-reconstruction fits, $\sigma_{\gamma_B} = 0.026$. Hence, despite the sharper BAO peak post-reconstruction, the constraints on γ_B are not tighter. This is more readily appreciated in Fourier space, where we see that changing γ_B changes the amplitudes of all peaks, whereas reconstruction changes the damping scale and thus changes the relative peak heights (Fig. 12). Since γ_B is not very degenerate with the damping parameters, sharpening the BAO peaks therefore does not improve γ_B constraints much.

We also find that all methods are able to recover the correct baryon fraction if the true cosmology is an EDE cosmology rather than Λ CDM. When considering the best-fit EDE model to Planck from [4] as the truth, we find biases in f_b of -0.43σ , -0.29σ , and 0.19σ for full-shape, pre-reconstruction, and post-reconstruction fits, respectively. Moreover, in the full-shape case, we test parameter recovery on EDE cosmologies with varying f_b , and find biases $\sim 0.3\sigma$ that are similar to the biases seen if the true model is Λ CDM, and hence may be attributable to prior effects.

We place a systematic error of 0.013 on γ_B (equivalent to $\sim 0.5\sigma$) measured in all three methods, when combining all redshift bins. This roughly encapsulates the biases seen on the fits to Nseries; the effects of prior effects on the full-shape fits; and biases seen when varying the true cosmology and baryon fraction. We do not shift the central value of γ_B , since the Nseries tests are generally biased high whereas the varying cosmology (noiseless theory vector) tests are biased low, i.e. we do not trust the Nseries power spectrum at the level where we can use the fits to set shifts on recovered parameters.

V. BARYON FRACTION FROM BOSS DATA

A. BOSS data

We use the BOSS [16] galaxy catalogs released in the 12th Data Release (DR12) of SDSS [11, 87], part of the SDSS-III program [88]. BOSS galaxies are selected [89] from 5-band [90] SDSS imaging [91, 92] across 14,555 deg^2 observed using the BOSS spectrograph [93] on the SDSS telescope [92] with high redshift success rate [94]. BOSS contains 1.4 million galaxies, targeted in two regions of the sky (North Galactic Cap and South Galactic Cap) and with two distinct galaxy selections, LOWZ and CMASS. LOWZ and CMASS were then merged together into the “CMASSLOWZTOT” sample [89],¹⁵ and simple redshift cuts were used to define 3 bins: z_1 at $0.2 < z < 0.5$, z_2 at $0.4 < z < 0.6$, and z_3 at $0.5 < z < 0.75$.

To facilitate comparison with past results, we use pub-

¹⁵ Publicly available at data.sdss.org/sas/dr12/boss/lss.

Model	χ^2	γ_B	BAO significance ($n\sigma$)	α_\perp	α_\parallel
0.2 < z < 0.5					
Pre-Recon	38	0.156 ± 0.038	6.3	0.979 ± 0.021	1.051 ± 0.041
Post-Recon	40	0.175 ± 0.037	8.3	0.985 ± 0.012	1.021 ± 0.026
Full-Shape	210	$0.157^{+0.031}_{-0.033}$			
0.4 < z < 0.6					
Pre-Recon	43	0.156 ± 0.040	6.3	1.00 ± 0.026	1.022 ± 0.061
Post-Recon	25	0.162 ± 0.032	8.4	0.993 ± 0.011	0.986 ± 0.020
0.5 < z < 0.75					
Pre-Recon	29	0.177 ± 0.044	6.6	0.990 ± 0.024	0.964 ± 0.053
Post-Recon	31	0.204 ± 0.042	8.7	0.994 ± 0.012	0.953 ± 0.019
Full-Shape	188	$0.145^{+0.031}_{-0.032}$			
Combined					
Pre-Recon		0.153 ± 0.029			
Post-Recon		0.173 ± 0.029			
Full-Shape		0.154 ± 0.023			

TABLE VI. Results from fits to the BOSS pre-reconstruction and post-reconstruction correlation functions (using the template method) and unreconstructed power spectrum (using the full shape method). The template fits are split by redshift bin, and we show both γ_B and the Alcock-Paczynski parameters, which are jointly fit. We also show the combined results for γ_B , including all bins with the covariance computed from 1000 Patchy mocks. We have 28 (29) degrees of freedom for the pre- (post-) reconstruction fits, and 195 degrees of freedom (230 data points and 35 parameters) for the full-shape fits.

licly available correlation functions¹⁶ and power spectra.¹⁷ The correlation functions used for the template fits are measured with and without BAO reconstruction [17]. The BOSS team used the “Rec-Iso” convention (i.e. the quadrupole is suppressed after running reconstruction), with reconstruction implemented following the algorithm of [95]. The post-reconstruction correlation function is used for the fiducial BAO fitting result of BOSS, due to the increased signal-to-noise of the BAO peak and reduction in nonlinear systematics that shift the peak. The covariance matrix is measured from 1000 approximate MultiDark-Patchy mocks [48, 96], created using fast, approximate N -body simulations and cut to the BOSS sky area and redshift cuts. For the pre-reconstruction correlation functions, we measure the correlation functions and power spectra ourselves from the available pair-counts of the DR12 catalogs and Patchy mocks.¹⁸ We use the correlation function monopole (ξ_0) and quadrupole (ξ_2) measured in 20 bins of width $5 h^{-1}$ Mpc between $50 h^{-1}$ Mpc and $150 h^{-1}$ Mpc. Following [18], for the post-reconstruction fits, we average χ^2 over fits to data with five different choices of bin center separated by $1 h^{-1}$ Mpc (i.e. data starts at 50, 51, 52, 53, and $54 h^{-1}$ Mpc). For the pre-reconstruction fits, we

use a single bin center with no offset.

For the full-shape fits, we use the publicly available power spectra of [27], measured using a window-free quadratic estimator [31]. While these power spectra are slightly different from those released by the BOSS collaboration (which are convolved with the survey window), we use the new window-free measurements for compatibility with the full-shape pipeline of [27],¹⁹ which did not exist until after the BOSS data were released. We use the power spectrum monopole (P_0), quadrupole (P_2) and hexadecapole (P_4) measured between $k = 0.01 h \text{ Mpc}^{-1}$ and $k = 0.20 h \text{ Mpc}^{-1}$ in bins of $\Delta k = 0.005 h \text{ Mpc}^{-1}$. Unlike the correlation functions, the power spectrum measurements are split by Galactic cap, since the number density and galaxy selection is slightly different between the two Galactic caps, potentially leading to different best-fit values of the galaxy bias parameters. This change in the nuisance parameters is more relevant for full-shape fitting, which requires accurate modelling of the nuisances to extract cosmological information from the shape of the galaxy power spectrum. Furthermore, the power spectra were only measured for the non-overlapping redshift bins at $0.2 < z < 0.5$ and $0.5 < z < 0.75$, reducing the need to estimate the covariance between all three redshift bins. This would be quite noisy due to the large size of the combined data vector, which is comparable to the number of mocks available.

Covariance matrices are again computed from 1000 Patchy mocks with matching survey geometry. By default, we combine the power spectrum measurements with the post-reconstruction Alcock-Paczynski parameters and directly fit cosmological parameters to the

¹⁶ https://github.com/ashleyjross/BAOfit/tree/master/exampledata/Ross_2016_COMBINEDDR12

¹⁷ <https://github.com/oliverphilcox/Spectra-Without-Windows>

¹⁸ We found poor agreement with the pre-reconstruction BAO fits in Table 6 of [18] (even when using their method and code), if we used the publicly available correlation functions and covariance matrices of [97]. Re-measuring the correlation function did not change the results much, whereas re-measuring the covariance matrix led to much better agreement, though it was still not perfect.

¹⁹ https://github.com/oliverphilcox/full_shape_likelihoods

combined dataset. There is a nontrivial covariance between the post-reconstruction AP parameters and the pre-reconstruction power spectrum; we also use the 1000 Patchy mocks to measure this covariance. Unlike in [27], we use the consensus (Fourier space [46] plus configuration space [18]) AP parameters released by the BOSS team, in which NGC and SGC are combined. This allows us to measure both the covariance between P_ℓ , α_\parallel and α_\perp , and between P_ℓ and $F_{\text{AP}} \equiv D_M/D_H$ (which is required for our explicitly sound horizon independent measurements).

In both cases we account for the bias when inverting a noisy covariance matrix by using the Gaussian approximation prescription of Ref. [98], which updates the Ref. [99] treatment used in Ref. [18] and Ref. [27].

B. Results

Our results are summarized in Table VI. We show both the individual bin results and the combination of all three bins, with the proper covariance computed from mocks. The pre-reconstruction combined γ_B is smaller than γ_B in any of the individual bins. This is because we impose a flat prior on H_0 when combining the bins, which is not a flat prior on f_b . We apply this prior because it is appropriate for an H_0 measurement, and because the full-shape fits already use a flat H_0 prior rather than a flat f_b prior.

We show contours of constant posterior levels in Figs. 13, 14, 15, for the data fit with the full shape model and pre- and post-reconstruction template fits. We compare the clustering signal to the best-fit models in Figs. 16, 17, 18, 19. While the post-reconstruction quadrupoles in the second and third redshift bins look like poor fits, the significance of the deviation is overstated in these plots due to the strong correlations between bins. In particular, for the second bin, the quadrupole has $\chi^2 = 8.9$ with 15 data points (i.e. the model fits the data very well). The seemingly highly anomalous run of high points in the quadrupole between 65 and 100 h^{-1} Mpc in the third redshift bin only has $\chi^2 = 8$ over 8 data points (though it would have $\chi^2 = 19$ if the covariance were diagonal). Overall, the worst-fit bin (pre-reconstruction $0.4 < z < 0.6$) has a p -value of 0.035. We conclude that the model fits the data well.

We find γ_B agrees well between the pre-reconstruction and post-reconstruction fits, with offsets of 0.5σ , 0.15σ , and 0.61σ . This is similar to the agreement between pre- and post-reconstruction α_\parallel and α_\perp , either as determined by our fits or by those of [18]. Our constraints on the AP parameters agree well with [18]: the central values agree with [18] to within 0.3σ , although some of the errorbars are different ($\sim 30\%$ tighter constraints on post-reconstruction α_\perp and 50% looser constraints on pre-reconstruction α_\parallel). The reasons for these differences are explored in detail in Appendix B. The smaller errorbar on post-reconstruction α_\perp is primarily due to a

change in the power spectrum template used to fit the BAO.²⁰ The larger error on pre-reconstruction α_\parallel in z_2 and z_3 comes from a variety of sources, with similar contributions from freeing the damping parameters, defining α_\parallel so that it only shifts the oscillatory component of the transfer function, rather than the entire power spectrum, and the updates in the BAO templates.

We use a considerably more restricted set of polynomials than [18], but we find no evidence that our model needs any more polynomial terms. For the post-reconstruction correlation function, adding the $1/r$ and $1/r^2$ polynomials (and the constant term to the quadrupole) improves χ^2 by 2 (3, 4) for the first (second, third) redshift bins. Accounting for the additional 5 free parameters leads to $\Delta\text{AIC} = -8$ (-7, -6) using the Akaike Information Criterion, i.e. the default model with the single constant term in the monopole is favored. Likewise, we find improvements in χ^2 of 4 (0, 1) for the three bins in the pre-reconstruction fits, yielding $\Delta\text{AIC} = -4$ (-8, -7).

We find good agreement between pre-reconstruction, post-reconstruction, and full shape results in the first redshift bin, but the agreement is less good in the third bin, in particular with an offset of 0.059 between the post-reconstruction and full-shape results.

We compare the observed discrepancies between pre-reconstruction, post-reconstruction and full shape to the discrepancies measured in the 84 Nseries mocks. The volume of each mock is similar to the volume of each redshift bin, and thus the differences from the mocks can be compared to the differences observed in all bins. We find 43, 67 and 32 (52%, 81%, and 39%) of the mocks have a larger absolute value difference between the pre and post-reconstruction fits than the differences in data of 0.019, 0.006, and 0.027 for the three redshift bins. Hence these differences are totally in line with the expected scatter from the mocks. Likewise, we find 80 (28) (96%, 34%) of the 20 mocks have larger absolute differences between the pre-reconstruction and full-shape fits than the 0.002 and 0.032 observed. Finally, we find 48 (5) (58%, 6%) of the 20 mocks have larger absolute differences between post-reconstruction and full-shape than the 0.018 and 0.059 observed. While the difference between post-reconstruction and full-shape fits in the $0.5 < z < 0.75$ is large, it is not out of line with the differences observed in mocks.

As mentioned above, we find some differences in the derived credible regions between data and mocks. Most notably, the template fit credible regions are somewhat larger than the expected 0.038 (pre-recon) or 0.030 (post-recon). The full-shape fits in individual redshift bins have

²⁰ We thank Ashley Ross for finding this discrepancy between the current version of the LSSAnalysis code and the pipeline used for BOSS, which corresponds to this commit: <https://github.com/ashleyjross/LSSAnalysis/commit/6ab0faa9f4ce9ec740fe66e871c7e2500fd720f>.

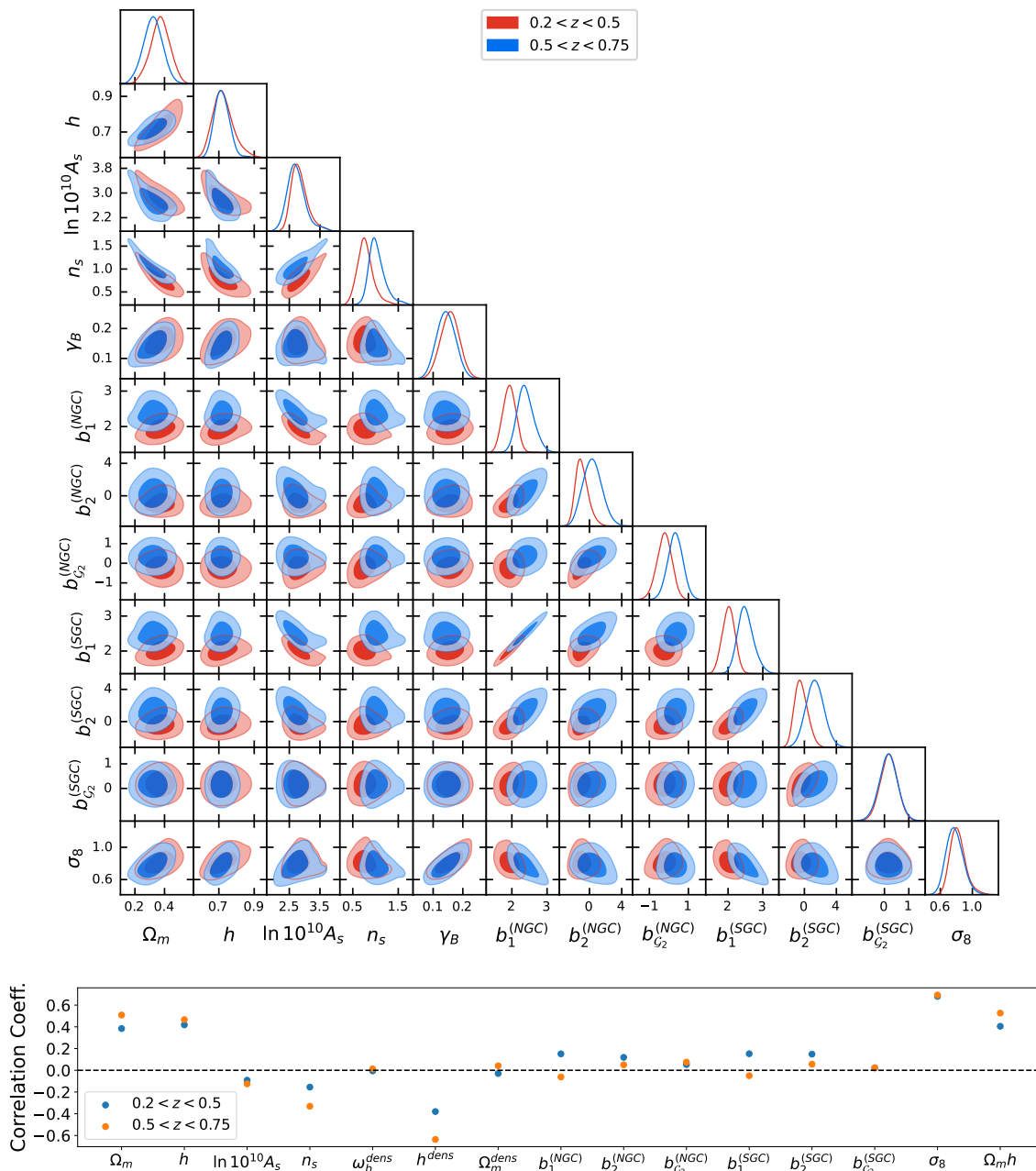


FIG. 13. Parameter constraints on BOSS data, using the full-shape method and comparing the two bins, $0.2 < z < 0.5$ and $0.5 < z < 0.75$. The bottom panel shows correlation coefficients between the parameter γ_B and the other parameters of the model; the strongest degeneracies are with the cosmological parameters.

similar errors between data and mocks (0.032), but as shown in our companion paper [5], the error on the combined fit is considerably smaller on data (0.021) than in mocks using the combined covariance (0.029). We individually fit the 84 Nseries mocks with a covariance matrix scaled to the entire BOSS volume. We find a mean error of 0.0285; 6 (5) mocks (7%, 6%) have a lower (upper) error smaller than the observed combined error of 0.021. For the pre-reconstruction template fits, we find 38 (23, 7) (46%, 28%, 8%) of the mocks have larger errors than

observed. For the post-reconstruction, template fits, 10 (29, 3) (12%, 35%, 3.6%) have larger errorbars than observed.

VI. DISCUSSION AND CONCLUSIONS

We have developed a model to constrain the baryon fraction using the amplitude of the baryon signal by splitting the transfer function into components arising

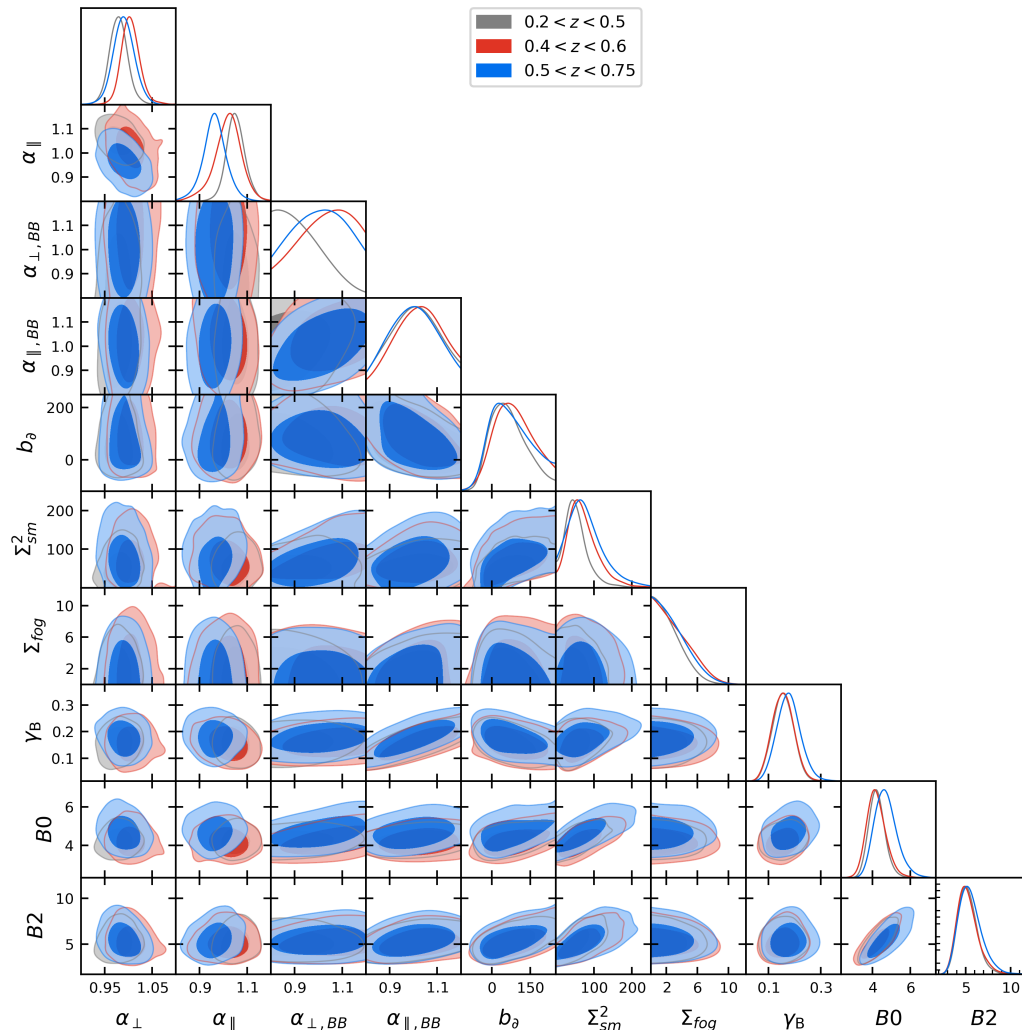


FIG. 14. Parameter constraints on BOSS data, from the pre-reconstruction template fits in three bins.

from cold dark matter and baryons. We describe the transfer function split and apply it to both full-shape and template-based BAO models in Section II. In Sections III and IV, we describe the results of testing our model on the mean of the 84 Nseries mocks, as well as noiseless theory vectors generated in early dark energy (EDE) or Λ CDM cosmology. On this extensive series of mock tests, we find biases on the recovered baryon fraction of $< 0.3\sigma$ for the full-shape and post-reconstruction fits, and $< 0.4\sigma$ for the pre-reconstruction fits compared to the errors derived fitting the BOSS data. When fitting for an explicitly sound horizon independent Hubble constant, in combination with the physical baryon abundance $\Omega_b h^2$ and the matter density Ω_m from geometrical probes (excluding isotropic BAO distance information that requires a calibrated value of the sound horizon), we find biases of less than $< 0.2\sigma$. To test that the results are independent of the sound horizon, we fit for the baryon fraction using an early dark energy cosmology

as the truth, which has true $H_0 = 72.19 \text{ km s}^{-1} \text{ Mpc}^{-1}$ and sound horizon $r_s = 138 \text{ Mpc}$ [57]. We find credible regions with biases of 0.4σ (0.3σ , 0.2σ) on the baryon fraction for full shape, pre-reconstruction, and post-reconstruction fits. We also tested that we recovered the correct cosmology when varying the input f_b within both EDE and Λ CDM cosmologies. We find an average bias of $1.67 \text{ km s}^{-1} \text{ Mpc}^{-1}$ on H_0 in the Λ CDM cosmologies (or those with a running spectral index or extra ultrarelativistic species), and $1.8 \text{ km s}^{-1} \text{ Mpc}^{-1}$ on the EDE cosmologies (i.e. our recovered values of H_0 are biased high from the truth).

When fitting to data, we find consistent values of the baryon fraction between our three methods, with discrepancies consistent with the scatter seen in mocks. When combining all redshift bins, we find $f_b = 0.153 \pm 0.029$ for pre-reconstruction template fits, $f_b = 0.173 \pm 0.027$ for the post-reconstruction template fits, and $f_b = 0.154 \pm 0.022$ for the full-shape fits. We estimate the system-

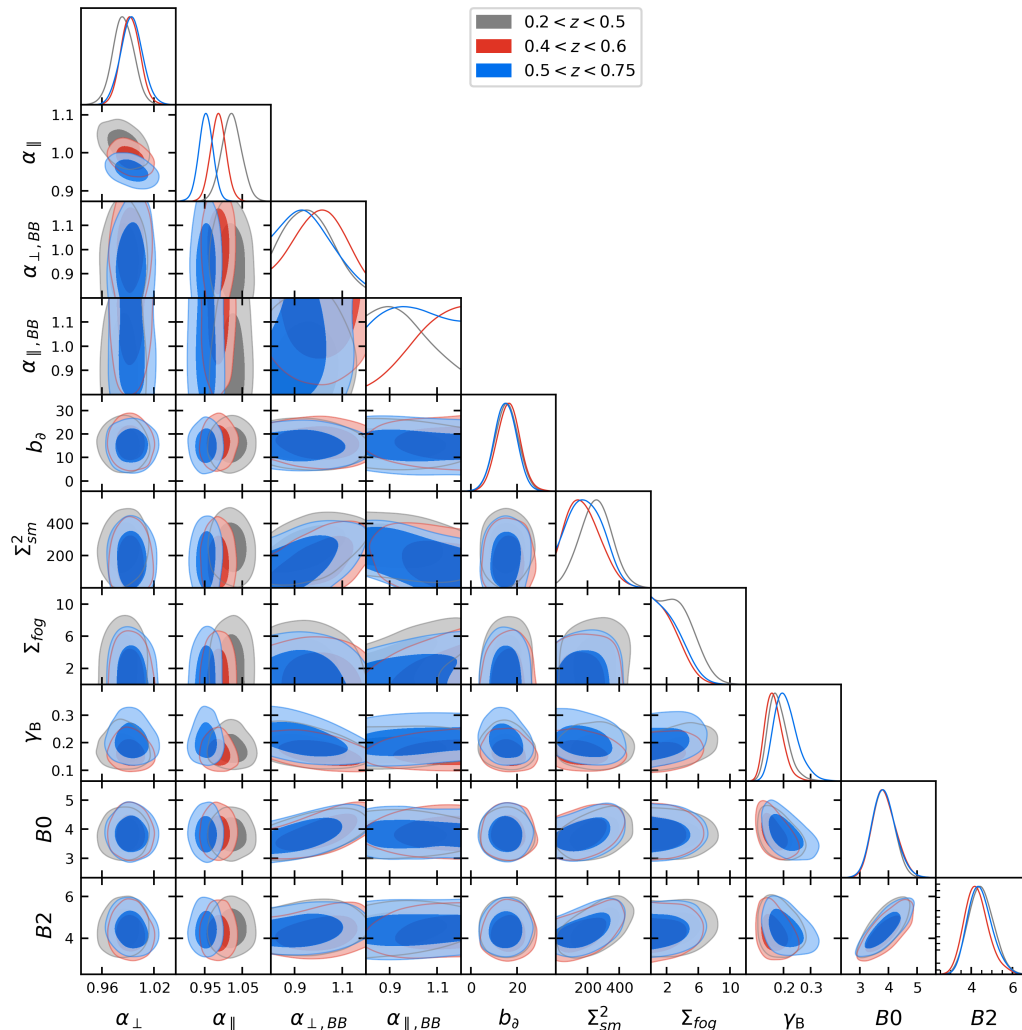


FIG. 15. Parameter constraints on BOSS data, from the post-reconstruction template fits in three bins.

atic error as 0.013 for all three methods following the findings summarized in Sec. IV D. The baryon fraction differs between Λ CDM and Early Dark Energy fits to the cosmic microwave background, due to the higher cold dark matter density required in the EDE cosmology. The higher matter density is required to match the observed imprint of the early ISW effect, which is modified due to the altered growth history around recombination from early dark energy [73]. Using Planck TTTEEE and lensing, BAO, Type Ia supernovae, RSD, and SHOES, $f_b = 0.1599 \pm 0.0015$ in Λ CDM and $f_b = 0.1504 \pm 0.0040$ in EDE [4]. Our measurement of the baryon fraction is consistent with both constraints; indeed, it will require an order-of-magnitude improvement on the baryon fraction measured from the BAO to differentiate between the models (Fig. 20).

Each of our three fitting methods has its own benefits and drawbacks. The full-shape fitting method is by far the most computationally expensive, with many

more free parameters and a considerably more complicated model than the template-fit BAO models considered. However, it offers considerably more flexibility than the template-fit models, with a full set of nonlinear and bias parameters and variations in cosmological parameters. It allows us to consider cases where the early growth history deviates from that given in the template cosmology, changing the relationship between γ_B and the baryon fraction in a way that depends on $\Omega_m h^2$. On the other hand, the model is quite sensitive to the choice of prior on nuisance parameters, leading to biases after marginalization even when the data under consideration is a noiseless theory model, and hence the best-fit has $\chi^2 = 0$. In contrast, the template-fit methods are much cheaper to evaluate and quicker to interpret. However, the effects of nonlinearity and higher-order bias are represented only in an ad hoc way, with a k^2 -dependent bias parameterized by b_δ . Since the prior on b_δ is informative in the post-reconstruction case, it would be preferable to

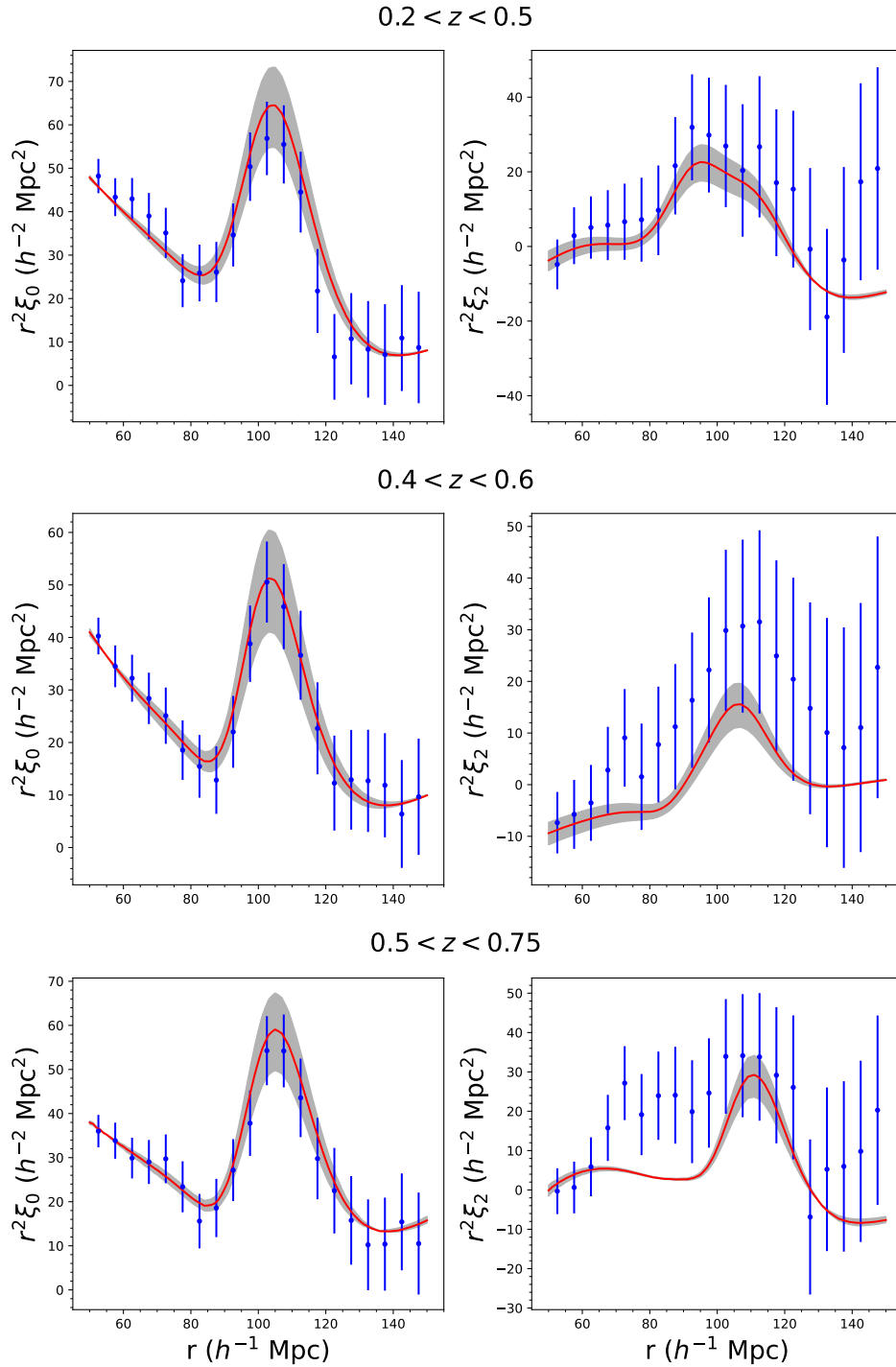


FIG. 16. BOSS post-reconstruction data and best fit model. Gray shaded line shows the impact of changing γ_B by 1σ from its best fit value.

have a more complete model of bias and nonlinearity. Biases resulting from prior marginalization effects are less prevalent than in the full-shape case due to the smaller number of nuisance parameters, but prior choice is no less important. Last, the BAO peak is sharper in the post-reconstruction case and it is thus potentially possi-

ble to extract more information about the BAO amplitude than in the pre-reconstruction or full-shape cases; however, our fits suggest that this extra information is modest, reducing the uncertainty on the baryon fraction by 7% on data and 20% on mocks. Nevertheless, we prefer to use the post-reconstruction template fits

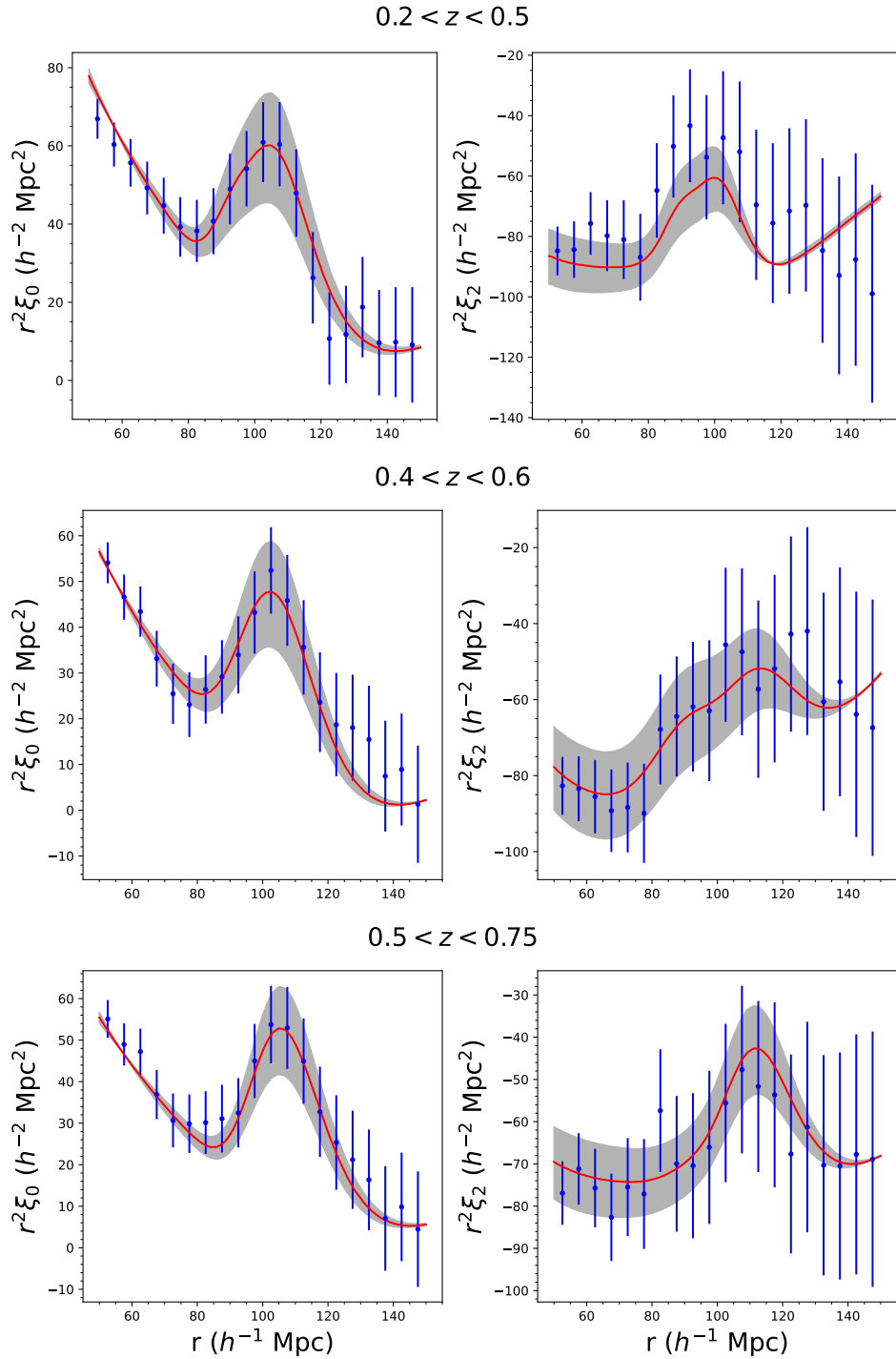


FIG. 17. Same as Fig. 16, but for the pre-reconstruction data.

rather than pre-reconstruction, since reconstruction removes nonlinear peak-shifting that could bias the BAO amplitude.

A. Future potential of this method

In light of the Hubble tension, constraints on H_0 from spectroscopic galaxy surveys have been an intense focus of interest [12]. The tightest constraints achieve $\sigma_{H_0} \sim 0.4 \text{ km s}^{-1} \text{ Mpc}^{-1}$ [11, 12, 100, 101] by combining BAO with precise measurements of r_d (depending on ω_b)

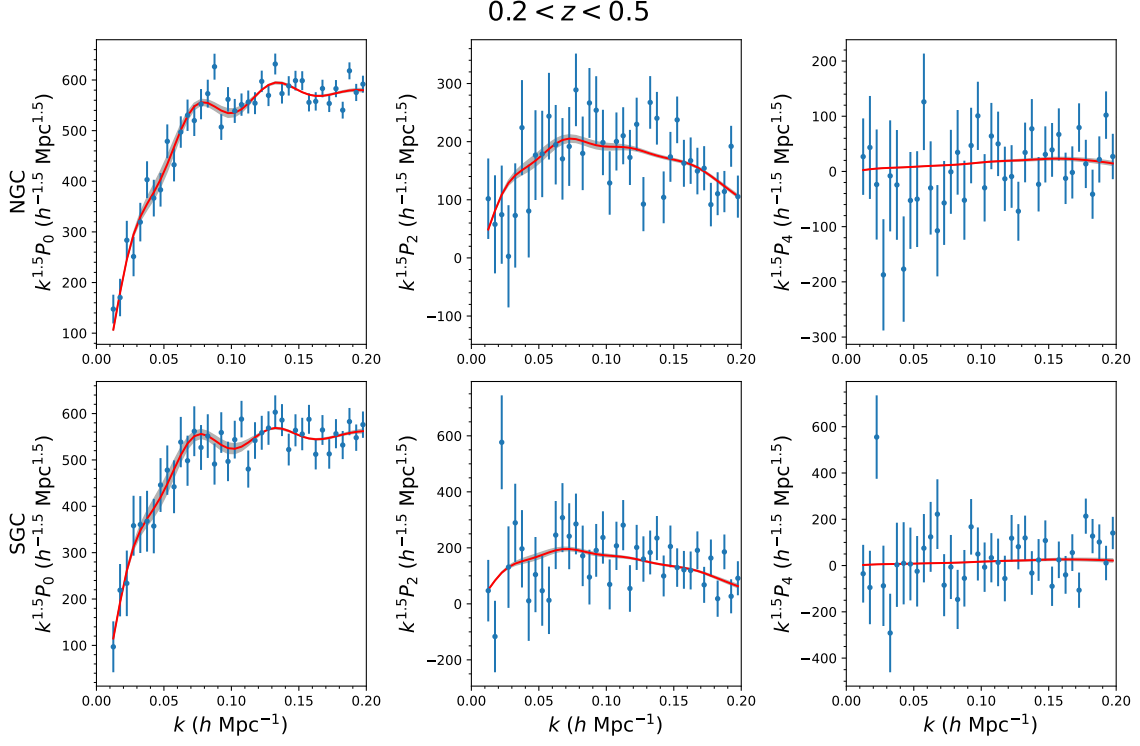


FIG. 18. Comparison of power spectrum data, best-fit model (red) and 1σ range in γ_B (shaded), for the first redshift bin.

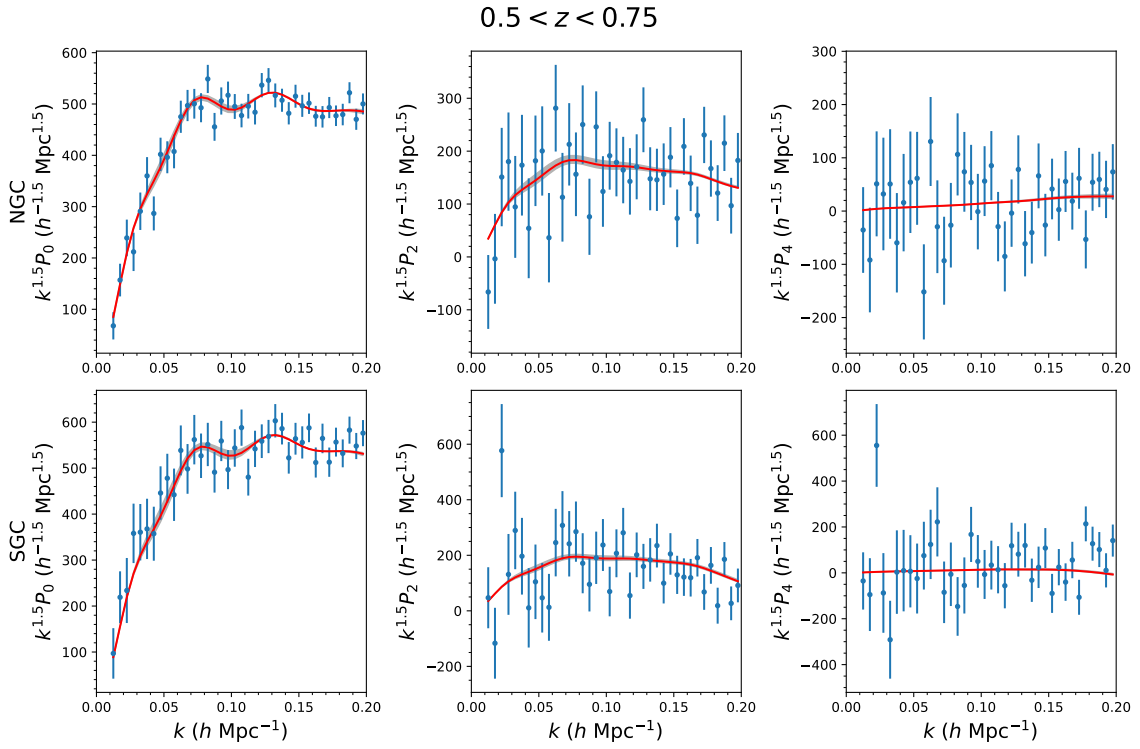


FIG. 19. Comparison of power spectrum data, best-fit model (red) and 1σ range in γ_B (shaded), for the second redshift bin.

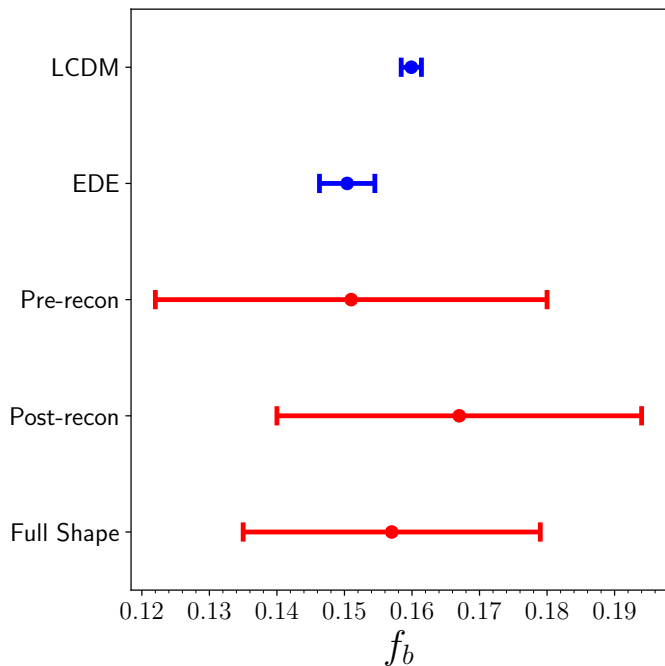


FIG. 20. Comparison of our f_b measurement (red), using the three fitting methods, to Λ CDM models fit to Planck and Early Dark Energy f_b models fit to the combination of Planck, BAO, supernovae, SH0ES, and RSD.

and Ω_m from Planck. However, this measurement cannot test for systematics in the CMB dataset or changes due to modified early-time physics. Excluding Planck information and calibrating r_d with ω_b from BBN leads to $\sigma_{H_0} \sim 1.0 \text{ km s}^{-1} \text{ Mpc}^{-1}$ [102–104]. Full-shape fits bring extra information from the shape of the matter power spectrum, and lead to similar values of H_0 with a slightly more accurate measurement ($\sigma_{H_0} \sim 0.8 \text{ km s}^{-1} \text{ Mpc}^{-1}$) if a Planck prior on n_s is used [29, 30, 33, 64, 105–111]. In the absence of such a prior, the constraining power is similar to BAO + BBN; the additional shape information does not contribute much to shrinking the H_0 error.

All of these probes assume Λ CDM at recombination, either in the fits to Planck or in the extrapolation from the ω_b value at BBN to the sound horizon at the drag epoch. Changes to early-time physics (most notably EDE, but also additional relativistic degrees of freedom, or varying electron mass [112]) can modify the relationship between ω_b and r_d . Hence, Ref. [113] proposed a sound horizon independent measurement of H_0 , based on the equality scale, which depends on $\Omega_m h^2$, and additional probes of Ω_m such as supernovae or weak lensing. Ref. [113] used large-scale structure information from CMB lensing, and additional work applied this method to the galaxy power spectrum [114–116]. The implementation of this method used a perturbative Λ CDM fit to the BOSS power spectrum, adding an extra isotropic BAO scaling parameter to explicitly marginalize over the sound horizon and decouple it from the rest

of the cosmological parameters. When combining the BOSS power spectrum with Pantheon supernovae and CMB lensing, [115] obtain $H_0 = 64.8_{-2.5}^{+2.2} \text{ km s}^{-1} \text{ Mpc}^{-1}$. Without the BOSS power spectrum, ACT and Planck CMB lensing and Pantheon+ alone give a similar result, $H_0 = 64.9 \pm 2.8 \text{ km s}^{-1} \text{ Mpc}^{-1}$ [117]. However, Ref. [118] point out that early dark energy also alters the shape of the power spectrum by changing the early expansion history (see also [119]). Therefore, the sound horizon marginalized constraints on H_0 , when analyzed in an early dark energy cosmology, shift towards higher values of H_0 by $\Delta H_0 = 3.8(4.9) \text{ km s}^{-1} \text{ Mpc}^{-1}$ (depending on whether Ω_m is constrained from supernovae or uncalibrated BAO and CMB), and the error nearly doubles. Similar shifts are seen in a cosmology with extra relativistic degrees of freedom, ΔN_{eff} . On the other hand, if the sound horizon is modified via a time-varying electron mass, only the time of recombination is affected, not the early growth history, and the constraints on H_0 are unchanged.

The approach of Ref. [120] is similar. Restricting their dataset to galaxy surveys only, plus a BBN prior on ω_b , they combine uncalibrated BAO with constraints on the power spectrum shape from the ShapeFit compression [86, 121], interpreted with Λ CDM, to obtain $H_0 = 70.1_{-2.1}^{+1.9} \text{ km s}^{-1} \text{ Mpc}^{-1}$. This result is similarly model dependent. Allowing for a wide prior on n_s , freeing the neutrino mass, or adding ΔN_{eff} broadens the constraint to $\sigma_{H_0} = 2.5 (3.2, 2.5) \text{ km s}^{-1} \text{ Mpc}^{-1}$, while leaving the central value largely unchanged except for $\nu\Lambda$ CDM, which increases H_0 to $73.3 \text{ km s}^{-1} \text{ Mpc}^{-1}$. Last, Ref. [122] focus on measuring only the turnover scale, rather than the entire shape of the power spectrum, and linking it to $\Omega_m h^2$ and therefore H_0 with supernovae or uncalibrated BAO; they obtain $H_0 = 72.9_{-8.6}^{+10.0} \text{ km s}^{-1} \text{ Mpc}^{-1}$ from eBOSS quasars when combining with BAO. Since they only use the equality scale (which is close to the maximum scale of the survey) rather than the shape of the power spectrum, they obtain larger errorbars.

Our method probes different, more simple physics than the methods above, and currently yields a larger error on H_0 than Refs. [115] or [120], with $\sigma_{H_0} = 5.4 \text{ km s}^{-1} \text{ Mpc}^{-1}$ from BOSS data alone. These errors are dominated by uncertainty on f_b and do not improve much with better measurements of Ω_m . However, our method is complementary in other ways and, in particular, is less model-dependent than the results of [115, 118].

There will be a bias in our recovered H_0 if the model does not have enough freedom to fit the true shape of the underlying baryon or CDM transfer functions, if there are strong prior dependencies on the parameters of those shapes biasing the model, or if the posterior is biased away from the true matter-radiation equality scale (i.e. finds the wrong $\Omega_m h^2$). The latter changes the time when CDM fluctuations can start to grow while baryon perturbations are frozen until decoupling, changing the amplitude of the BAO as discussed in Ref. [6]. We find that if the universe truly followed an EDE cosmology,

but we fit only Λ CDM models, our H_0 constraint would be biased high by $2 \text{ km s}^{-1} \text{ Mpc}^{-1}$. This may be due to limitations in the modelling, but is also consistent with the shifts seen in Λ CDM noiseless theory vectors, which are due entirely to prior effects as the true cosmology has a best-fit $\chi^2 = 0$ by definition, in this case.

In a related test, [118] fixed their data and changed the theory model from Λ CDM to EDE, when fitting a full EFT model, finding an increase in H_0 by a larger amount, $4\text{--}5 \text{ km s}^{-1} \text{ Mpc}^{-1}$. For the tests we have performed for all of the three methods used, presented in Tables III, IV & V, we find smaller changes in H_0 ($\sim 2 \text{ km s}^{-1} \text{ Mpc}^{-1}$) at a level below the statistical error, which is approximately $\Delta H_0 \pm 5 \text{ km s}^{-1} \text{ Mpc}^{-1}$.

Moreover, the BAO amplitude information, which dominates our measurement of the baryon signature, is independent of the ShapeFit compression of [120]. ShapeFit allows for the broad-band power spectrum shape to deviate from a template linear power spectrum, parameterized by m , which gives the width of a tanh function modulated power law that multiplies the template power spectrum. Our measurement primarily picks up the effect of changes in the BAO amplitude, which is explicitly not included in the broad-band shape information of ShapeFit.²¹

Ongoing and future spectroscopic surveys will radically improve our measurement of the BAO feature. DESI covers an effective volume of 60 Gpc^3 [123],²² nearly an order-of-magnitude larger than BOSS at 7.8 Gpc^3 [11]. We show in Table III that increasing the volume by a factor of 10 improves f_b constraints by $\sqrt{10}$. Our method will continue to be dominated by the f_b uncertainty rather than Ω_m , implying that DESI will allow us to reach a precision of $2 \text{ km s}^{-1} \text{ Mpc}^{-1}$: sufficient to differentiate SH0ES and CMB/LSS measurements at 3σ if our results agree with one or the other. The effective volume of Euclid is slightly larger, 81 Gpc^3 [125].²³ This yields an H_0 precision of $1.3 \text{ km s}^{-1} \text{ Mpc}^{-1}$ from the combination of Euclid and DESI, nearing the current precision of the SH0ES measurement ($1 \text{ km s}^{-1} \text{ Mpc}^{-1}$). The high-

precision redshift sample of SphereX [126] will also cover a similar effective volume to DESI and Euclid, though at lower redshift. While the survey strategy has not yet been defined, the Roman space telescope high latitude survey could also achieve a high-precision baryon fraction measurement, with [127] presenting a survey strategy that achieves an effective volume of 30 Gpc^3 . Further into the future, Stage 5 spectroscopic surveys [128] such as MegaMapper [129] or MSE [130] will achieve similar or tighter precision at even higher redshifts. At the same time, H_0 measurements using r_d or full-shape information will also continue to improve, with H_0 errors expected to be $< 0.5 \text{ km s}^{-1} \text{ Mpc}^{-1}$ [116, 131]. The very high precision of future surveys allow for exquisite tests of consistency and model-independence between different H_0 probes in large-scale structure, which should be highly informative about new physics solutions to the H_0 tension.

ACKNOWLEDGMENTS

We thank Ashley Ross and Mariana Vargas Magana for useful conversations and for helping to dig out old data.

AK was supported as a CITA National Fellow by the Natural Sciences and Engineering Research Council of Canada (NSERC), funding reference #DIS-2022-568580.

WP acknowledges support from the Natural Sciences and Engineering Research Council of Canada (NSERC), [funding reference number RGPIN-2019-03908] and from the Canadian Space Agency.

Research at Perimeter Institute is supported in part by the Government of Canada through the Department of Innovation, Science and Economic Development Canada and by the Province of Ontario through the Ministry of Colleges and Universities.

This research was enabled in part by support provided by Compute Ontario (computeontario.ca) and the Digital Research Alliance of Canada (alliancecan.ca).

[1] Planck Collaboration, N. Aghanim, Y. Akrami, M. Ashdown, J. Aumont, C. Baccigalupi et al., *Planck 2018 results. VI. Cosmological parameters*, *A&A* **641** (2020) A6 [1807.06209].

[2] A.G. Riess, W. Yuan, L.M. Macri, D. Scolnic, D. Brout, S. Casertano et al., *A Comprehensive*

Measurement of the Local Value of the Hubble Constant with $1 \text{ km s}^{-1} \text{ Mpc}^{-1}$ Uncertainty from the Hubble Space Telescope and the SH0ES Team, *ApJ* **934** (2022) L7 [2112.04510].

[3] R.J. Cooke, M. Pettini, K.M. Nollett and R. Jorgenson, *The Primordial Deuterium Abundance of the Most Metal-poor Damped Lyman- α System*, *ApJ* **830** (2016) 148 [1607.03900].

[4] J.C. Hill, E. McDonough, M.W. Toomey and S. Alexander, *Early dark energy does not restore cosmological concordance*, *Phys. Rev. D* **102** (2020) 043507 [2003.07355].

[5] Krolewski, Alex and Percival, Will J. and Woodfinden, Alex, *A new method to determine H_0 from cosmological energy-density measurements*, in prep., .

[6] D.J. Eisenstein and W. Hu, *Baryonic Features in the*

²¹ Fig. 5 shows that we do receive some degeneracy-breaking power from the shape of the power spectrum, but this only modestly improves our γ_B and thus H_0 constraints.

²² Note that the forecasts presented in Section 6 of this paper supersede the older forecasts of [124].

²³ Calculated from their Table 3 and Eq. 90 using $P_0 = 10000 h^{-3} \text{ Mpc}^3$.

- Matter Transfer Function, *ApJ* **496** (1998) 605 [[astro-ph/9709112](#)].
- [7] W.J. Percival, C.M. Baugh, J. Bland-Hawthorn, T. Bridges, R. Cannon, S. Cole et al., *The 2dF Galaxy Redshift Survey: the power spectrum and the matter content of the Universe*, *MNRAS* **327** (2001) 1297 [[astro-ph/0105252](#)].
- [8] S. Cole, W.J. Percival, J.A. Peacock, P. Norberg, C.M. Baugh, C.S. Frenk et al., *The 2dF Galaxy Redshift Survey: power-spectrum analysis of the final data set and cosmological implications*, *MNRAS* **362** (2005) 505 [[astro-ph/0501174](#)].
- [9] D.J. Eisenstein, I. Zehavi, D.W. Hogg, R. Scoccimarro, M.R. Blanton, R.C. Nichol et al., *Detection of the Baryon Acoustic Peak in the Large-Scale Correlation Function of SDSS Luminous Red Galaxies*, *ApJ* **633** (2005) 560 [[astro-ph/0501171](#)].
- [10] *The clustering of galaxies in the SDSS-III Baryon Oscillation Spectroscopic Survey: baryon acoustic oscillations in the Data Release 9 spectroscopic galaxy sample*, *MNRAS* **427** (2012) 3435 [[1203.6594](#)].
- [11] S. Alam, M. Ata, S. Bailey, F. Beutler, D. Bizyaev, J.A. Blazek et al., *The clustering of galaxies in the completed SDSS-III Baryon Oscillation Spectroscopic Survey: cosmological analysis of the DR12 galaxy sample*, *MNRAS* **470** (2017) 2617 [[1607.03155](#)].
- [12] S. Alam, M. Aubert, S. Avila, C. Balland, J.E. Bautista, M.A. Bershadsky et al., *Completed SDSS-IV extended Baryon Oscillation Spectroscopic Survey: Cosmological implications from two decades of spectroscopic surveys at the Apache Point Observatory*, *Phys. Rev. D* **103** (2021) 083533 [[2007.08991](#)].
- [13] C. Alcock and B. Paczynski, *An evolution free test for non-zero cosmological constant*, *Nature* **281** (1979) 358.
- [14] G. Lavaux and B.D. Wandelt, *Precision cosmography with stacked voids*, *ApJ* **754** (2012) 109 [[1110.0345](#)].
- [15] D.G. York, J. Adelman, J. Anderson, John E., S.F. Anderson, J. Annis, N.A. Bahcall et al., *The Sloan Digital Sky Survey: Technical Summary*, *AJ* **120** (2000) 1579 [[astro-ph/0006396](#)].
- [16] K.S. Dawson, D.J. Schlegel, C.P. Ahn, S.F. Anderson, É. Aubourg, S. Bailey et al., *The Baryon Oscillation Spectroscopic Survey of SDSS-III*, *AJ* **145** (2013) 10 [[1208.0022](#)].
- [17] D.J. Eisenstein, H.-J. Seo, E. Sirko and D.N. Spergel, *Improving Cosmological Distance Measurements by Reconstruction of the Baryon Acoustic Peak*, *ApJ* **664** (2007) 675 [[astro-ph/0604362](#)].
- [18] A.J. Ross, F. Beutler, C.-H. Chuang, M. Pellejero-Ibanez, H.-J. Seo, M. Vargas-Magaña et al., *The clustering of galaxies in the completed SDSS-III Baryon Oscillation Spectroscopic Survey: observational systematics and baryon acoustic oscillations in the correlation function*, *MNRAS* **464** (2017) 1168 [[1607.03145](#)].
- [19] J. Lesgourgues, *The Cosmic Linear Anisotropy Solving System (CLASS) I: Overview*, *arXiv e-prints* (2011) [arXiv:1104.2932](#) [[1104.2932](#)].
- [20] A. Lewis, A. Challinor and A. Lasenby, *Efficient computation of CMB anisotropies in closed FRW models*, *ApJ* **538** (2000) 473 [[astro-ph/9911177](#)].
- [21] C. Howlett, A. Lewis, A. Hall and A. Challinor, *CMB power spectrum parameter degeneracies in the era of precision cosmology*, *J. Cosmology Astropart. Phys.* **1204** (2012) 027 [[1201.3654](#)].
- [22] R. Barkana and A. Loeb, *Scale-dependent bias of galaxies from baryonic acoustic oscillations*, *MNRAS* **415** (2011) 3113 [[1009.1393](#)].
- [23] F. Schmidt, *Effect of relative velocity and density perturbations between baryons and dark matter on the clustering of galaxies*, *Phys. Rev. D* **94** (2016) 063508 [[1602.09059](#)].
- [24] S.-F. Chen, C. Howlett, M. White, P. McDonald, A.J. Ross, H.-J. Seo et al., *Baryon Acoustic Oscillation Theory and Modelling Systematics for the DESI 2024 results*, *arXiv e-prints* (2024) [arXiv:2402.14070](#) [[2402.14070](#)].
- [25] D. Baumann, A. Nicolis, L. Senatore and M. Zaldarriaga, *Cosmological non-linearities as an effective fluid*, *J. Cosmology Astropart. Phys.* **2012** (2012) 051 [[1004.2488](#)].
- [26] J.J.M. Carrasco, M.P. Hertzberg and L. Senatore, *The effective field theory of cosmological large scale structures*, *Journal of High Energy Physics* **2012** (2012) 82 [[1206.2926](#)].
- [27] O.H.E. Philcox and M.M. Ivanov, *BOSS DR12 full-shape cosmology: Λ CDM constraints from the large-scale galaxy power spectrum and bispectrum monopole*, *Phys. Rev. D* **105** (2022) 043517 [[2112.04515](#)].
- [28] A. Chudaykin, M.M. Ivanov, O.H.E. Philcox and M. Simonović, *Nonlinear perturbation theory extension of the Boltzmann code CLASS*, *Phys. Rev. D* **102** (2020) 063533 [[2004.10607](#)].
- [29] M.M. Ivanov, M. Simonović and M. Zaldarriaga, *Cosmological parameters from the BOSS galaxy power spectrum*, *J. Cosmology Astropart. Phys.* **2020** (2020) 042 [[1909.05277](#)].
- [30] O.H.E. Philcox, M.M. Ivanov, M. Simonović and M. Zaldarriaga, *Combining full-shape and BAO analyses of galaxy power spectra: a 1.6% CMB-independent constraint on H_0* , *J. Cosmology Astropart. Phys.* **2020** (2020) 032 [[2002.04035](#)].
- [31] O.H.E. Philcox, *Cosmology without window functions: Quadratic estimators for the galaxy power spectrum*, *Phys. Rev. D* **103** (2021) 103504 [[2012.09389](#)].
- [32] M.M. Ivanov, O.H.E. Philcox, M. Simonović, M. Zaldarriaga, T. Nishimichi and M. Takada, *Cosmological constraints without nonlinear redshift-space distortions*, *Phys. Rev. D* **105** (2022) 043531 [[2110.00006](#)].
- [33] S.-F. Chen, Z. Vlah, E. Castorina and M. White, *Redshift-space distortions in Lagrangian perturbation theory*, *J. Cosmology Astropart. Phys.* **2021** (2021) 100 [[2012.04636](#)].
- [34] G. D'Amico, L. Senatore and P. Zhang, *Limits on w CDM from the EFTofLSS with the PyBird code*, *J. Cosmology Astropart. Phys.* **2021** (2021) 006 [[2003.07956](#)].
- [35] T. Nishimichi, G. D'Amico, M.M. Ivanov, L. Senatore, M. Simonović, M. Takada et al., *Blinded challenge for precision cosmology with large-scale structure: Results from effective field theory for the redshift-space galaxy power spectrum*, *Phys. Rev. D* **102** (2020) 123541 [[2003.08277](#)].
- [36] D. Blas, M. Garny, M.M. Ivanov and S. Sibiryakov, *Time-sliced perturbation theory II: baryon acoustic*

- oscillations and infrared resummation*, *J. Cosmology Astropart. Phys.* **2016** (2016) 028 [1605.02149].
- [37] M.M. Ivanov, O.H.E. Philcox, T. Nishimichi, M. Simonović, M. Takada and M. Zaldarriaga, *Precision analysis of the redshift-space galaxy bispectrum*, *Phys. Rev. D* **105** (2022) 063512 [2110.10161].
- [38] G. D’Amico, Y. Donath, L. Senatore and P. Zhang, *Limits on Clustering and Smooth Quintessence from the EFTofLSS*, *arXiv e-prints* (2020) arXiv:2012.07554 [2012.07554].
- [39] T. Simon, P. Zhang, V. Poulin and T.L. Smith, *Consistency of effective field theory analyses of the BOSS power spectrum*, *Phys. Rev. D* **107** (2023) 123530 [2208.05929].
- [40] G. D’Amico, L. Senatore, P. Zhang and T. Nishimichi, *Taming redshift-space distortion effects in the EFTofLSS and its application to data*, *arXiv e-prints* (2021) arXiv:2110.00016 [2110.00016].
- [41] O.H.E. Philcox, M.M. Ivanov, M. Zaldarriaga, M. Simonović and M. Schmittfull, *Fewer mocks and less noise: Reducing the dimensionality of cosmological observables with subspace projections*, *Phys. Rev. D* **103** (2021) 043508 [2009.03311].
- [42] H.-J. Seo, F. Beutler, A.J. Ross and S. Saito, *Modeling the reconstructed BAO in Fourier space*, *MNRAS* **460** (2016) 2453 [1511.00663].
- [43] N. Kaiser, *Clustering in real space and in redshift space*, *MNRAS* **227** (1987) 1.
- [44] Z. Ding, H.-J. Seo, Z. Vlah, Y. Feng, M. Schmittfull and F. Beutler, *Theoretical systematics of Future Baryon Acoustic Oscillation Surveys*, *MNRAS* **479** (2018) 1021 [1708.01297].
- [45] W.E. Ballinger, J.A. Peacock and A.F. Heavens, *Measuring the cosmological constant with redshift surveys*, *MNRAS* **282** (1996) 877 [astro-ph/9605017].
- [46] F. Beutler, H.-J. Seo, A.J. Ross, P. McDonald, S. Saito, A.S. Bolton et al., *The clustering of galaxies in the completed SDSS-III Baryon Oscillation Spectroscopic Survey: baryon acoustic oscillations in the Fourier space*, *MNRAS* **464** (2017) 3409 [1607.03149].
- [47] H. Gil-Marín, J.E. Bautista, R. Paviot, M. Vargas-Magaña, S. de la Torre, S. Fromenteau et al., *The Completed SDSS-IV extended Baryon Oscillation Spectroscopic Survey: measurement of the BAO and growth rate of structure of the luminous red galaxy sample from the anisotropic power spectrum between redshifts 0.6 and 1.0*, *MNRAS* **498** (2020) 2492 [2007.08994].
- [48] F.-S. Kitaura, S. Rodríguez-Torres, C.-H. Chuang, C. Zhao, F. Prada, H. Gil-Marín et al., *The clustering of galaxies in the SDSS-III Baryon Oscillation Spectroscopic Survey: mock galaxy catalogues for the BOSS Final Data Release*, *MNRAS* **456** (2016) 4156 [1509.06400].
- [49] M. White, J.L. Tinker and C.K. McBride, *Mock galaxy catalogues using the quick particle mesh method*, *MNRAS* **437** (2014) 2594 [1309.5532].
- [50] A.J. Cuesta, M. Vargas-Magaña, F. Beutler, A.S. Bolton, J.R. Brownstein, D.J. Eisenstein et al., *The clustering of galaxies in the SDSS-III Baryon Oscillation Spectroscopic Survey: baryon acoustic oscillations in the correlation function of LOWZ and CMASS galaxies in Data Release 12*, *MNRAS* **457** (2016) 1770 [1509.06371].
- [51] T. Brinckmann and J. Lesgourgues, *MontePython 3: boosted MCMC sampler and other features*, **1804.07261**.
- [52] B. Audren, J. Lesgourgues, K. Benabed and S. Prunet, *Conservative Constraints on Early Cosmology: an illustration of the Monte Python cosmological parameter inference code*, *JCAP* **1302** (2013) 001 [1210.7183].
- [53] A. Gelman and D.B. Rubin, *Inference from iterative simulation using multiple sequences*, *Statistical Science* **7** (1992) 457.
- [54] A. Lewis, *GetDist: a Python package for analysing Monte Carlo samples*, **1910.13970**.
- [55] A. Woodfinden, S. Nadathur, W.J. Percival, S. Radinovic, E. Massara and H.A. Winther, *Measurements of cosmic expansion and growth rate of structure from voids in the Sloan Digital Sky Survey between redshift 0.07 and 1.0*, *MNRAS* **516** (2022) 4307 [2205.06258].
- [56] A. Woodfinden, W.J. Percival, S. Nadathur, H.A. Winther, T.S. Fraser, E. Massara et al., *Cosmological measurements from void-galaxy and galaxy-galaxy clustering in the Sloan Digital Sky Survey*, *MNRAS* **523** (2023) 6360 [2303.06143].
- [57] T.L. Smith, V. Poulin and M.A. Amin, *Oscillating scalar fields and the Hubble tension: A resolution with novel signatures*, *Phys. Rev. D* **101** (2020) 063523 [1908.06995].
- [58] M.M. Ivanov, E. McDonough, J.C. Hill, M. Simonović, M.W. Toomey, S. Alexander et al., *Constraining early dark energy with large-scale structure*, *Phys. Rev. D* **102** (2020) 103502 [2006.11235].
- [59] N.A. Maksimova, L.H. Garrison, D.J. Eisenstein, B. Hadzhiyska, S. Bose and T.P. Satterthwaite, *AbacusSummit: a massive set of high-accuracy, high-resolution N-body simulations*, *Monthly Notices of the Royal Astronomical Society* **508** (2021) 4017 [https://academic.oup.com/mnras/article-pdf/508/3/4017/408].
- [60] J. Torrado and A. Lewis, *Cobaya: code for Bayesian analysis of hierarchical physical models*, *J. Cosmology Astropart. Phys.* **2021** (2021) 057 [2005.05290].
- [61] J. Torrado and A. Lewis, “Cobaya: Bayesian analysis in cosmology.” Astrophysics Source Code Library, record ascl:1910.019, Oct., 2019.
- [62] J.L. Bernal, T.L. Smith, K.K. Boddy and M. Kamionkowski, *Robustness of baryon acoustic oscillation constraints for early-Universe modifications of Λ CDM cosmology*, *Phys. Rev. D* **102** (2020) 123515 [2004.07263].
- [63] S.-F. Chen, Z. Vlah and M. White, *A new analysis of galaxy 2-point functions in the BOSS survey, including full-shape information and post-reconstruction BAO*, *J. Cosmology Astropart. Phys.* **2022** (2022) 008 [2110.05530].
- [64] G. d’Amico, J. Gleyzes, N. Kokron, K. Markovic, L. Senatore, P. Zhang et al., *The cosmological analysis of the SDSS/BOSS data from the Effective Field Theory of Large-Scale Structure*, *J. Cosmology Astropart. Phys.* **2020** (2020) 005 [1909.05271].
- [65] M. Crocce and R. Scoccimarro, *Nonlinear evolution of baryon acoustic oscillations*, *Phys. Rev. D* **77** (2008) 023533 [0704.2783].

- [66] N. Padmanabhan and M. White, *Calibrating the baryon oscillation ruler for matter and halos*, *Phys. Rev. D* **80** (2009) 063508 [0906.1198].
- [67] B.D. Sherwin and M. Zaldarriaga, *Shift of the baryon acoustic oscillation scale: A simple physical picture*, *Phys. Rev. D* **85** (2012) 103523 [1202.3998].
- [68] W. Hu and N. Sugiyama, *Small-Scale Cosmological Perturbations: an Analytic Approach*, *ApJ* **471** (1996) 542 [astro-ph/9510117].
- [69] P. Meszaros, *The behaviour of point masses in an expanding cosmological substratum.*, *A&A* **37** (1974) 225.
- [70] Z. Hou, R. Keisler, L. Knox, M. Millea and C. Reichardt, *How massless neutrinos affect the cosmic microwave background damping tail*, *Phys. Rev. D* **87** (2013) 083008 [1104.2333].
- [71] G. Cabass, M. Gerbino, E. Giusarma, A. Melchiorri, L. Pagano and L. Salvati, *Constraints on the early and late integrated Sachs-Wolfe effects from the Planck 2015 cosmic microwave background anisotropies in the angular power spectra*, *Phys. Rev. D* **92** (2015) 063534 [1507.07586].
- [72] J.A. Kable, G.E. Addison and C.L. Bennett, *Deconstructing the Planck TT Power Spectrum to Constrain Deviations from Λ CDM*, *ApJ* **905** (2020) 164 [2008.01785].
- [73] S. Vagnozzi, *Consistency tests of Λ CDM from the early integrated Sachs-Wolfe effect: Implications for early-time new physics and the Hubble tension*, *Phys. Rev. D* **104** (2021) 063524 [2105.10425].
- [74] R.K. Sachs and A.M. Wolfe, *Perturbations of a Cosmological Model and Angular Variations of the Microwave Background*, *ApJ* **147** (1967) 73.
- [75] M.J. Rees and D.W. Sciama, *Large-scale Density Inhomogeneities in the Universe*, *Nature* **217** (1968) 511.
- [76] J. Hamann, *Evidence for extra radiation? Profile likelihood versus Bayesian posterior*, *J. Cosmology Astropart. Phys.* **2012** (2012) 021 [1110.4271].
- [77] Planck Collaboration, P.A.R. Ade, N. Aghanim, M. Arnaud, M. Ashdown, J. Aumont et al., *Planck intermediate results. XVI. Profile likelihoods for cosmological parameters*, *A&A* **566** (2014) A54 [1311.1657].
- [78] T.L. Smith, V. Poulin, J.L. Bernal, K.K. Boddy, M. Kamionkowski and R. Murgia, *Early dark energy is not excluded by current large-scale structure data*, *Phys. Rev. D* **103** (2021) 123542 [2009.10740].
- [79] L. Herold, E.G.M. Ferreira and E. Komatsu, *New Constraint on Early Dark Energy from Planck and BOSS Data Using the Profile Likelihood*, *ApJ* **929** (2022) L16 [2112.12140].
- [80] E. Brinch Holm, L. Herold, S. Hannestad, A. Nygaard and T. Tram, *Discovering a new well: Decaying dark matter with profile likelihoods*, *arXiv e-prints* (2022) arXiv:2211.01935 [2211.01935].
- [81] T. Karwal, Y. Patel, A. Bartlett, V. Poulin, T.L. Smith and D.N. Pfeffer, *Procoli: Profiles of cosmological likelihoods*, *arXiv e-prints* (2024) arXiv:2401.14225 [2401.14225].
- [82] E. Brinch Holm, A. Nygaard, J. Dakin, S. Hannestad and T. Tram, *PROSPECT: A profile likelihood code for frequentist cosmological parameter inference*, *arXiv e-prints* (2023) arXiv:2312.02972 [2312.02972].
- [83] C. Heymans, T. Tröster, M. Asgari, C. Blake, H. Hildebrandt, B. Joachimi et al., *KiDS-1000 Cosmology: Multi-probe weak gravitational lensing and spectroscopic galaxy clustering constraints*, *A&A* **646** (2021) A140 [2007.15632].
- [84] B. Yu, U. Seljak, Y. Li and S. Singh, *RSD measurements from BOSS galaxy power spectrum using the halo perturbation theory model*, *J. Cosmology Astropart. Phys.* **2023** (2023) 057 [2211.16794].
- [85] K. Thepsuriya and A. Lewis, *Accuracy of cosmological parameters using the baryon acoustic scale*, *J. Cosmology Astropart. Phys.* **2015** (2015) 034 [1409.5066].
- [86] S. Brieden, H. Gil-Marín and L. Verde, *ShapeFit: extracting the power spectrum shape information in galaxy surveys beyond BAO and RSD*, *J. Cosmology Astropart. Phys.* **2021** (2021) 054 [2106.07641].
- [87] S. Alam, F.D. Albareti, C. Allende Prieto, F. Anders, S.F. Anderson, T. Anderton et al., *The Eleventh and Twelfth Data Releases of the Sloan Digital Sky Survey: Final Data from SDSS-III*, *ApJS* **219** (2015) 12 [1501.00963].
- [88] D.J. Eisenstein, D.H. Weinberg, E. Agol, H. Aihara, C. Allende Prieto, S.F. Anderson et al., *SDSS-III: Massive Spectroscopic Surveys of the Distant Universe, the Milky Way, and Extra-Solar Planetary Systems*, *AJ* **142** (2011) 72 [1101.1529].
- [89] B. Reid, S. Ho, N. Padmanabhan, W.J. Percival, J. Tinker, R. Tojeiro et al., *SDSS-III Baryon Oscillation Spectroscopic Survey Data Release 12: galaxy target selection and large-scale structure catalogues*, *MNRAS* **455** (2016) 1553 [1509.06529].
- [90] M. Fukugita, T. Ichikawa, J.E. Gunn, M. Doi, K. Shimasaku and D.P. Schneider, *The Sloan Digital Sky Survey Photometric System*, *AJ* **111** (1996) 1748.
- [91] J.E. Gunn, M. Carr, C. Rockosi, M. Sekiguchi, K. Berry, B. Elms et al., *The Sloan Digital Sky Survey Photometric Camera*, *AJ* **116** (1998) 3040 [astro-ph/9809085].
- [92] J.E. Gunn, W.A. Siegmund, E.J. Mannery, R.E. Owen, C.L. Hull, R.F. Leger et al., *The 2.5 m Telescope of the Sloan Digital Sky Survey*, *AJ* **131** (2006) 2332 [astro-ph/0602326].
- [93] S.A. Smee, J.E. Gunn, A. Uomoto, N. Roe, D. Schlegel, C.M. Rockosi et al., *The Multi-object, Fiber-fed Spectrographs for the Sloan Digital Sky Survey and the Baryon Oscillation Spectroscopic Survey*, *AJ* **146** (2013) 32 [1208.2233].
- [94] A.S. Bolton, D.J. Schlegel, É. Aubourg, S. Bailey, V. Bhardwaj, J.R. Brownstein et al., *Spectral Classification and Redshift Measurement for the SDSS-III Baryon Oscillation Spectroscopic Survey*, *AJ* **144** (2012) 144 [1207.7326].
- [95] N. Padmanabhan, X. Xu, D.J. Eisenstein, R. Scalzo, A.J. Cuesta, K.T. Mehta et al., *A 2 per cent distance to $z = 0.35$ by reconstructing baryon acoustic oscillations - I. Methods and application to the Sloan Digital Sky Survey*, *MNRAS* **427** (2012) 2132 [1202.0090].
- [96] S.A. Rodríguez-Torres, C.-H. Chuang, F. Prada, H. Guo, A. Klypin, P. Behroozi et al., *The clustering of galaxies in the SDSS-III Baryon Oscillation Spectroscopic Survey: modelling the clustering and halo*

- occupation distribution of BOSS CMASS galaxies in the Final Data Release, *MNRAS* **460** (2016) 1173 [1509.06404].
- [97] S. Satpathy, S. Alam, S. Ho, M. White, N.A. Bahcall, F. Beutler et al., *The clustering of galaxies in the completed SDSS-III Baryon Oscillation Spectroscopic Survey: on the measurement of growth rate using galaxy correlation functions*, *MNRAS* **469** (2017) 1369 [1607.03148].
- [98] W.J. Percival, O. Friedrich, E. Sellentin and A. Heavens, *Matching Bayesian and frequentist coverage probabilities when using an approximate data covariance matrix*, *MNRAS* **510** (2022) 3207 [2108.10402].
- [99] J. Hartlap, P. Simon and P. Schneider, *Why your model parameter confidences might be too optimistic. Unbiased estimation of the inverse covariance matrix*, *A&A* **464** (2007) 399 [astro-ph/0608064].
- [100] A. Cuceu, J. Farr, P. Lemos and A. Font-Ribera, *Baryon Acoustic Oscillations and the Hubble constant: past, present and future*, *J. Cosmology Astropart. Phys.* **2019** (2019) 044 [1906.11628].
- [101] M. Blomqvist, H. du Mas des Bourboux, N.G. Busca, V. de Sainte Agathe, J. Rich, C. Balland et al., *Baryon acoustic oscillations from the cross-correlation of Ly α absorption and quasars in eBOSS DR14*, *A&A* **629** (2019) A86 [1904.03430].
- [102] Y. Wang, L. Xu and G.-B. Zhao, *A Measurement of the Hubble Constant Using Galaxy Redshift Surveys*, *ApJ* **849** (2017) 84 [1706.09149].
- [103] N. Schöneberg, J. Lesgourgues and D.C. Hooper, *The BAO+BBN take on the Hubble tension*, *J. Cosmology Astropart. Phys.* **2019** (2019) 029 [1907.11594].
- [104] N. Schöneberg, L. Verde, H. Gil-Marín and S. Brieden, *BAO+BBN revisited - growing the Hubble tension with a 0.7 km/s/Mpc constraint*, *J. Cosmology Astropart. Phys.* **2022** (2022) 039 [2209.14330].
- [105] T. Colas, G. d'Amico, L. Senatore, P. Zhang and F. Beutler, *Efficient cosmological analysis of the SDSS/BOSS data from the Effective Field Theory of Large-Scale Structure*, *J. Cosmology Astropart. Phys.* **2020** (2020) 001 [1909.07951].
- [106] T. Tröster, A.G. Sánchez, M. Asgari, C. Blake, M. Crocce, C. Heymans et al., *Cosmology from large-scale structure. Constraining Λ CDM with BOSS*, *A&A* **633** (2020) L10 [1909.11006].
- [107] D. Wadekar, M.M. Ivanov and R. Scoccimarro, *Cosmological constraints from BOSS with analytic covariance matrices*, *Phys. Rev. D* **102** (2020) 123521 [2009.00622].
- [108] G. D'Amico, L. Senatore, P. Zhang and H. Zheng, *The Hubble tension in light of the Full-Shape analysis of Large-Scale Structure data*, *J. Cosmology Astropart. Phys.* **2021** (2021) 072 [2006.12420].
- [109] G. D'Amico, Y. Donath, M. Lewandowski, L. Senatore and P. Zhang, *The BOSS bispectrum analysis at one loop from the Effective Field Theory of Large-Scale Structure*, *arXiv e-prints* (2022) arXiv:2206.08327 [2206.08327].
- [110] P. Zhang, G. D'Amico, L. Senatore, C. Zhao and Y. Cai, *BOSS Correlation Function analysis from the Effective Field Theory of Large-Scale Structure*, *J. Cosmology Astropart. Phys.* **2022** (2022) 036 [2110.07539].
- [111] M.M. Ivanov, O.H.E. Philcox, G. Cabass, T. Nishimichi, M. Simonović and M. Zaldarriaga, *Cosmology with the galaxy bispectrum multipoles: Optimal estimation and application to BOSS data*, *Phys. Rev. D* **107** (2023) 083515 [2302.04414].
- [112] N. Schöneberg, G.F. Abellán, A.P. Sánchez, S.J. Witte, V. Poulin and J. Lesgourgues, *The H_0 Olympics: A fair ranking of proposed models*, *Phys. Rep.* **984** (2022) 1 [2107.10291].
- [113] E.J. Baxter and B.D. Sherwin, *Determining the Hubble constant without the sound horizon scale: measurements from CMB lensing*, *MNRAS* **501** (2021) 1823 [2007.04007].
- [114] O.H.E. Philcox, B.D. Sherwin, G.S. Farren and E.J. Baxter, *Determining the Hubble constant without the sound horizon: Measurements from galaxy surveys*, *Phys. Rev. D* **103** (2021) 023538 [2008.08084].
- [115] O.H.E. Philcox, G.S. Farren, B.D. Sherwin, E.J. Baxter and D.J. Brout, *Determining the Hubble constant without the sound horizon: A 3.6 % constraint on H_0 from galaxy surveys, CMB lensing, and supernovae*, *Phys. Rev. D* **106** (2022) 063530 [2204.02984].
- [116] G.S. Farren, O.H.E. Philcox and B.D. Sherwin, *Determining the Hubble constant without the sound horizon: Perspectives with future galaxy surveys*, *Phys. Rev. D* **105** (2022) 063503 [2112.10749].
- [117] M.S. Madhavacheril, F.J. Qu, B.D. Sherwin, N. MacCrann, Y. Li, I. Abril-Cabezas et al., *The Atacama Cosmology Telescope: DR6 Gravitational Lensing Map and Cosmological Parameters*, *ApJ* **962** (2024) 113 [2304.05203].
- [118] T.L. Smith, V. Poulin and T. Simon, *Assessing the robustness of sound horizon-free determinations of the Hubble constant*, *Phys. Rev. D* **108** (2023) 103525 [2208.12992].
- [119] J.A. Kable and V. Miranda, *Sound Horizon Independent Constraints on Early Dark Energy: The Role of Supernova Data*, *arXiv e-prints* (2024) arXiv:2403.11916 [2403.11916].
- [120] S. Brieden, H. Gil-Marín and L. Verde, *A tale of two (or more) h 's*, *J. Cosmology Astropart. Phys.* **2023** (2023) 023 [2212.04522].
- [121] S. Brieden, H. Gil-Marín and L. Verde, *Model-agnostic interpretation of 10 billion years of cosmic evolution traced by BOSS and eBOSS data*, *J. Cosmology Astropart. Phys.* **2022** (2022) 024 [2204.11868].
- [122] B. Bahr-Kalus, D. Parkinson and E.-M. Mueller, *Measurement of the matter-radiation equality scale using the extended baryon oscillation spectroscopic survey quasar sample*, *MNRAS* **524** (2023) 2463 [2302.07484].
- [123] A.G. Adame, J. Aguilar, S. Ahlen, S. Alam, G. Aldering, D.M. Alexander et al., *Validation of the Scientific Program for the Dark Energy Spectroscopic Instrument*, *AJ* **167** (2024) 62 [2306.06307].
- [124] DESI Collaboration, A. Aghamousa, J. Aguilar, S. Ahlen, S. Alam, L.E. Allen et al., *The DESI Experiment Part I: Science, Targeting, and Survey Design*, *arXiv e-prints* (2016) arXiv:1611.00036 [1611.00036].
- [125] Euclid Collaboration, A. Blanchard, S. Camera, C. Carbone, V.F. Cardone, S. Casas et al., *Euclid preparation. VII. Forecast validation for Euclid*

- cosmological probes*, *A&A* **642** (2020) A191 [1910.09273].
- [126] O. Doré, J. Bock, M. Ashby, P. Capak, A. Cooray, R. de Putter et al., *Cosmology with the SPHEREX All-Sky Spectral Survey*, *arXiv e-prints* (2014) arXiv:1412.4872 [1412.4872].
- [127] T. Eifler, H. Miyatake, E. Krause, C. Heinrich, V. Miranda, C. Hirata et al., *Cosmology with the Roman Space Telescope - multiprobe strategies*, *MNRAS* **507** (2021) 1746 [2004.05271].
- [128] D.J. Schlegel, S. Ferraro, G. Aldering, C. Baltay, S. BenZvi, R. Besuner et al., *A Spectroscopic Road Map for Cosmic Frontier: DESI, DESI-II, Stage-5*, *arXiv e-prints* (2022) arXiv:2209.03585 [2209.03585].
- [129] D.J. Schlegel, J.A. Kollmeier, G. Aldering, S. Bailey, C. Baltay, C. Bebek et al., *The MegaMapper: A Stage-5 Spectroscopic Instrument Concept for the Study of Inflation and Dark Energy*, *arXiv e-prints* (2022) arXiv:2209.04322 [2209.04322].
- [130] W.J. Percival, C. Yèche, M. Bilicki, A. Font-Ribera, N.P. Hathi, C. Howlett et al., *Cosmology with the MaunaKea Spectroscopic Explorer*, *arXiv e-prints* (2019) arXiv:1903.03158 [1903.03158].
- [131] M.M. Ivanov and O.H.E. Philcox, *Measuring H_0 with Spectroscopic Surveys*, *arXiv e-prints* (2023) arXiv:2305.07977 [2305.07977].

Appendix A: Results on fits to f_b -varying noiseless theory vectors

Here we show the credible regions of h and f_b for the tests with varying true f_b , either using Abacus-

Summit cosmologies or using EDE cosmologies, in Tables VII, VIII and IX. These are plotted in Figs. 8 and 10.

Appendix B: Differences between our BAO fits and the BOSS DR12 correlation function fits

We present a detailed comparison of our results and those of the BOSS team [18] in Table X. Overall, we find that our model fits the correlation functions just as well as the model used in BOSS, with shifts in the AP parameters of $< 0.2\sigma$ post-reconstruction and $< 0.45\sigma$ pre-reconstruction. Our errorbars are 20–30% tighter post-reconstruction; similar for pre-reconstruction α_{\perp} , and up to 50% larger for pre-reconstruction α_{\parallel} . For the post-reconstruction fits, this change in errorbars is largely driven by the updated templates; running the BOSS analysis code with the updated templates yields similar errorbars to our baseline constraints and all other choices. For pre-reconstruction z_2 and z_3 , the relatively large downward shifts of 0.36σ and 0.45σ in α_{\perp} are driven by our choice to vary the damping parameters, γ_B , and the broadband shift parameters, which lead to 0.23σ and 0.38σ shifts, respectively. The large increase in pre-reconstruction α_{\parallel} errorbars comes from a variety of sources.

Mock	Truth		BAO only			Add voids		
	h	f_b	h	$n\sigma$	f_b	$n\sigma$	h	$n\sigma$
cosm131	0.717	0.171	$0.740^{+0.093}_{-0.080}$	0.31	$0.158^{+0.026}_{-0.022}$	-0.42	$0.734^{+0.068}_{-0.057}$	0.33
cosm139	0.716	0.176	$0.743^{+0.090}_{-0.081}$	0.36	$0.164^{+0.025}_{-0.025}$	-0.39	$0.739^{+0.068}_{-0.054}$	0.45
cosm130	0.674	0.157	$0.691^{+0.093}_{-0.077}$	0.23	$0.142^{+0.032}_{-0.028}$	-0.48	$0.689^{+0.078}_{-0.063}$	0.29
cosm159	0.597	0.149	$0.551^{+0.065}_{-0.057}$	-0.55	$0.148^{+0.032}_{-0.031}$	-0.03	$0.554^{+0.068}_{-0.068}$	-0.75
cosm167	0.705	0.138	$0.731^{+0.098}_{-0.083}$	0.35	$0.124^{+0.026}_{-0.026}$	-0.45	$0.736^{+0.068}_{-0.075}$	0.61
cosm168	0.607	0.166	$0.619^{+0.062}_{-0.057}$	0.16	$0.159^{+0.022}_{-0.025}$	-0.23	$0.617^{+0.051}_{-0.041}$	0.20
cosm172	0.637	0.181	$0.647^{+0.074}_{-0.060}$	0.14	$0.169^{+0.027}_{-0.025}$	-0.39	$0.650^{+0.056}_{-0.044}$	0.25
cosm177	0.682	0.143	$0.649^{+0.081}_{-0.065}$	-0.40	$0.139^{+0.029}_{-0.025}$	-0.13	$0.649^{+0.068}_{-0.060}$	-0.58
cosm169	0.647	0.152	$0.653^{+0.083}_{-0.068}$	0.08	$0.143^{+0.031}_{-0.026}$	-0.29	$0.655^{+0.063}_{-0.057}$	0.16
cosm181	0.575	0.163	$0.536^{+0.057}_{-0.048}$	-0.47	$0.159^{+0.030}_{-0.028}$	-0.13	$0.535^{+0.053}_{-0.042}$	-0.70
EDE001	0.790	0.123	$0.815^{+0.135}_{-0.104}$	0.34	$0.111^{+0.026}_{-0.026}$	-0.39	$0.803^{+0.116}_{-0.086}$	0.25
EDE002	0.773	0.128	$0.797^{+0.125}_{-0.102}$	0.32	$0.119^{+0.026}_{-0.027}$	-0.29	$0.791^{+0.101}_{-0.084}$	0.35
EDE003	0.756	0.134	$0.778^{+0.122}_{-0.098}$	0.30	$0.121^{+0.030}_{-0.027}$	-0.42	$0.760^{+0.104}_{-0.072}$	0.08
EDE004	0.739	0.140	$0.773^{+0.108}_{-0.098}$	0.46	$0.128^{+0.030}_{-0.028}$	-0.39	$0.766^{+0.101}_{-0.078}$	0.53
EDE006	0.704	0.155	$0.743^{+0.102}_{-0.087}$	0.53	$0.138^{+0.033}_{-0.029}$	-0.55	$0.733^{+0.090}_{-0.077}$	0.57
EDE007	0.686	0.163	$0.721^{+0.095}_{-0.077}$	0.47	$0.146^{+0.031}_{-0.027}$	-0.55	$0.706^{+0.086}_{-0.066}$	0.39
EDE008	0.667	0.172	$0.706^{+0.095}_{-0.075}$	0.53	$0.150^{+0.035}_{-0.029}$	-0.71	$0.689^{+0.080}_{-0.060}$	0.43
EDE009	0.647	0.183	$0.677^{+0.092}_{-0.077}$	0.41	$0.166^{+0.040}_{-0.036}$	-0.55	$0.668^{+0.077}_{-0.057}$	0.41
EDE010	0.627	0.195	$0.653^{+0.090}_{-0.065}$	0.35	$0.177^{+0.036}_{-0.033}$	-0.58	$0.643^{+0.078}_{-0.057}$	0.31

TABLE VII. Full-shape fit parameter recovery tests for noiseless theory vectors with varying f_b in w_0w_a CDM cosmologies drawn from AbacusSummit (first block); and noiseless theory vectors with varying f_b and all other parameters fixed to the EDE cosmology (second block). The format is the same as Table III.

Data	γ_{BAO}	σ_γ	f_b	$n\sigma$	α_\perp	σ_{α_\perp}	True	$n\sigma$	α_\parallel	$\sigma_{\alpha_\parallel}$	True	$n\sigma$
Cos. 0	0.148	0.026	0.156	-0.29	0.986	0.014	0.988	-0.16	1.003	0.041	0.991	0.32
Cos. 1	0.119	0.025	0.132	-0.45	0.988	0.018	0.993	-0.40	1.000	0.057	0.982	0.50
Cos. 2	0.151	0.026	0.159	-0.26	0.992	0.015	0.995	-0.22	1.010	0.044	0.997	0.34
Cos. 3	0.142	0.023	0.150	-0.27	0.993	0.013	0.996	-0.22	1.003	0.038	0.994	0.27
Cos. 4	0.150	0.026	0.156	-0.22	0.966	0.013	0.968	-0.17	0.984	0.036	0.978	0.17
Cos. 5	0.152	0.024	0.157	-0.18	0.988	0.013	0.990	-0.19	1.004	0.038	0.993	0.29
Cos. 6	0.126	0.023	0.146	-0.70	1.010	0.016	1.015	-0.35	1.022	0.048	1.004	0.52
Cos. 7	0.140	0.026	0.149	-0.30	0.990	0.017	0.993	-0.23	1.003	0.050	0.991	0.34
Cos. 8	0.140	0.024	0.153	-0.45	0.976	0.013	0.979	-0.24	0.993	0.035	0.984	0.26
Cos. 9	0.130	0.022	0.143	-0.48	0.990	0.015	0.994	-0.30	1.001	0.043	0.989	0.35

TABLE VIII. Template fits to noiseless theory vectors for the pre-reconstruction correlation function, using ten Λ CDM noiseless theory vectors with varying parameters, all fit with the same fixed-cosmology template.

Data	γ_{BAO}	σ_γ	f_b	$n\sigma$	α_\perp	σ_{α_\perp}	True	$n\sigma$	α_\parallel	$\sigma_{\alpha_\parallel}$	True	$n\sigma$
Cos. 0	0.159	0.025	0.156	0.12	0.987	0.010	0.988	-0.06	0.992	0.022	0.991	0.07
Cos. 1	0.119	0.019	0.132	-0.58	0.991	0.013	0.993	-0.26	0.983	0.028	0.982	0.10
Cos. 2	0.163	0.026	0.159	0.18	0.994	0.010	0.995	-0.13	0.999	0.020	0.997	0.09
Cos. 3	0.159	0.025	0.150	0.37	0.996	0.010	0.996	-0.02	0.994	0.022	0.994	0.03
Cos. 4	0.162	0.024	0.156	0.24	0.967	0.010	0.968	-0.10	0.981	0.019	0.978	0.19
Cos. 5	0.166	0.026	0.157	0.41	0.990	0.010	0.990	-0.05	0.994	0.020	0.993	0.06
Cos. 6	0.127	0.018	0.146	-0.84	1.013	0.011	1.015	-0.23	1.007	0.023	1.004	0.19
Cos. 7	0.142	0.023	0.149	-0.29	0.992	0.012	0.993	-0.06	0.992	0.023	0.991	0.07
Cos. 8	0.151	0.021	0.153	-0.10	0.978	0.009	0.979	-0.09	0.985	0.019	0.984	0.11
Cos. 9	0.134	0.020	0.143	-0.39	0.992	0.011	0.994	-0.22	0.991	0.022	0.989	0.12

TABLE IX. Template fits to noiseless theory vectors for the post-reconstruction correlation function, with the same format as Table VIII.

Redshift bin and model	χ^2	γ_B	α_\perp	α_\parallel
z1				
Pre-Recon	38	0.156 ± 0.038	0.979 ± 0.021	1.051 ± 0.041
Pre-Recon, add $1/r$ and $1/r^2$	34		0.974 ± 0.018	1.057 ± 0.035
Pre-Recon, add $1/r$ and $1/r^2$, fix Σ , γ_B , q_\parallel , q_\perp	49		0.972 ± 0.024	1.047 ± 0.060
Ross et al. (2017) + updated templates	36		0.983 ± 0.020	1.053 ± 0.038
Ross et al. (2017)	37		0.983 ± 0.022	1.051 ± 0.037
Post-Recon	40	0.175 ± 0.037	0.985 ± 0.012	1.021 ± 0.026
Post-recon, add $1/r$ and $1/r^2$	38		0.982 ± 0.012	1.026 ± 0.027
Post-recon, add $1/r$ and $1/r^2$, fix Σ , γ_B , q_\parallel , q_\perp	39		0.983 ± 0.012	1.027 ± 0.026
Ross. et al. (2017) + updated templates	39		0.984 ± 0.013	1.026 ± 0.027
Ross et al. (2017)	42		0.988 ± 0.015	1.022 ± 0.027
z2				
Pre-Recon	43	0.156 ± 0.040	1.00 ± 0.026	1.022 ± 0.061
Pre-Recon, add $1/r$ and $1/r^2$	43		1.001 ± 0.018	1.019 ± 0.050
Pre-Recon, add $1/r$ and $1/r^2$, fix Σ , γ_B , q_\parallel , q_\perp	45		1.006 ± 0.022	1.027 ± 0.054
Ross et al. (2017) + updated templates	42		1.007 ± 0.020	1.021 ± 0.048
Ross et al. (2017)	42		1.008 ± 0.022	1.024 ± 0.042
Post-Recon	25	0.162 ± 0.032	0.993 ± 0.011	0.986 ± 0.020
Post-Recon, add $1/r$ and $1/r^2$	22		0.992 ± 0.011	0.987 ± 0.020
Post-recon, add $1/r$ and $1/r^2$, fix Σ , γ_B , q_\parallel , q_\perp	26		0.992 ± 0.011	0.988 ± 0.022
Ross et al. (2017) + updated templates	24		0.994 ± 0.012	0.988 ± 0.021
Ross et al. (2017)	30		0.994 ± 0.014	0.984 ± 0.023
z3				
Pre-Recon	29	0.177 ± 0.044	0.990 ± 0.024	0.964 ± 0.053
Pre-Recon, add $1/r$ and $1/r^2$	28		0.991 ± 0.023	0.960 ± 0.056
Pre-Recon, add $1/r$ and $1/r^2$, fix Σ , γ_B , q_\parallel , q_\perp	33		0.999 ± 0.025	0.961 ± 0.046
Ross et al. (2017) + updated templates	28		0.997 ± 0.023	0.958 ± 0.042
Ross et al. (2017)	28		1.001 ± 0.024	0.953 ± 0.035
Post-Recon	31	0.204 ± 0.042	0.994 ± 0.012	0.953 ± 0.019
Post-Recon, add $1/r$ and $1/r^2$	27		0.993 ± 0.013	0.955 ± 0.019
Post-Recon, add $1/r$ and $1/r^2$, fix Σ , γ_B , q_\parallel , q_\perp	30		0.992 ± 0.013	0.957 ± 0.023
Ross et al. (2017) + updated templates	28		0.995 ± 0.014	0.957 ± 0.021
Ross et al. (2017)	32		0.995 ± 0.016	0.958 ± 0.023

TABLE X. Differences between our template-fitting results on the AP parameters and the BOSS results from Ross et al. (2017) [18]. Within each redshift bin and pre or post-recon block, the top line is our baseline result and the bottom line is the one from Ross et al. (2017). We then vary our method by adding polynomials $1/r$ and $1/r^2$ to the monopole and quadrupole; fixing the extra parameters that we allow to vary (damping, γ_B , and broadband shifts); and then comparing to re-running the publicly available BOSS code with updated templates. γ_B is only varied in our baseline fits and the line below it, and hence not shown for other cases; for the case with the $1/r$ and $1/r^2$ terms, we do not show the γ_B constraint as it is very poor due to degeneracies with the polynomial parameters.